Neda Negahbani

Optimization of inverted hexagonal lipid phase preparation by rapid solvent exchange

Master's Thesis

Graz University of Technology

Supervisor:Univ.-Prof. Dipl-Ing. Dr.techn. Georg Pabst

Institute of Materials Physics

With cooperation with
Institute of Molecular Biosciences
Biophysics Division

Graz, June 2016

Statutory Declaration

I declare that I have authored this thesis independently, that I have not used other than the declared sources/resources, and that I have explicitly marked all material which has been quoted either literally or by content from the used sources.

Graz, _____ _____

Date Signature

Eidesstattliche Erklärung[1]

Ich erkläre an Eides statt, dass ich die vorliegende Arbeit selbstständig verfasst, andere als die angegebenen Quellen/Hilfsmittel nicht benutzt, und die den benutzten Quellen wörtlich und inhaltlich entnommenen Stellen als solche kenntlich gemacht habe.

Graz, am _____ _____

Datum Unterschrift

[1] Beschluss der Curricula-Kommission für Bachelor-, Master- und Diplomstudien vom 10.11.2008; Genehmigung des Senates am 1.12.2008

Dedication

I dedicate this thesis to my parents who are two lights of wisdom in my life. I am so grateful for their endless love and support. This work would not be finished without their encourage and faith about my ability. Also, I dedicate this work to my brothers for their kind supports and advice.

Acknowledgement

First of all, I want to acknowledge my thesis advisor Prof. Georg Pabst who gave me this chance to work in his wonderful research group. I have learned more from him not only about physics but also about the successful team working and management. Work with my friends in this team made unforgettable moments full of science and happiness for me. Also, I appreciate the Austrian Science Fund FWF for their financial support of my project.

At the end, I say thank you to my family and friends for their support and encourage and everyone who helped me go a step further during this project.

Abstract

We have tried for the first time to make the inverted hexagonal structure (H_{II}) of different lipid mixtures by the rapid solvent exchange (RSE) method. In this process, a host lipid was mixed with lipids composed of different carbon chain lengths.The host and guest lipids were dissolved separately in the organic solvent before mixing together. The organic solvent was removed during RSE process of producing an organic-solvent-free mixture of the host and guest lipids. Each sample was investigated by the small angle X-ray scattering (SAXS) at different temperatures. We have found the lattice parameter and spontaneous curvature of samples by in-house Matlab codes. Our results showed this approach can yield to make the net H_{II} lipid structures. Therefore, using the RSE can help to make lipid mixture in H_{II} phase in a timely fashion. Also, for each examined bilayer forming lipid, the spontaneous curvature of the pure monolayer structure was found by the extrapolation. According to our results, there is no correlation between spontaneous curvature and the lipids carbon chain length.

Zusammenfassung

Im Rahmen dieser Arbeit wurde erstmals versucht, eine invertierte hexagonale Struktur (H_{II}) aus verschiedenen Lipid-Mischungen mit der Rapid-Solvent-Exchange (RSE) Methode herzustellen. Bei diesem Prozess wurde ein Host-Lipid mit Lipiden verschiedener Kohlenstoff-Kettenlängen gemischt. Die Host- und Guest-Lipide wurden getrennt im organischen Lösungsmittel aufgelöst. Das organische Lösungsmittel wurde während des RSE-Prozesses durch die Erzeugung einer von organischen Lösungsmitteln freien Mischung von Host- und Guest-Lipiden entfernt. Jede Probe wurde mit Kleinwinkel-Röntgen-Streuung (SAXS) bei verschiedenen Temperaturen untersucht. Gitterparameter und spontane Krümmung der Proben wurden mit eigenen Matlab-Codes berechnet. Unsere Ergebnisse zeigten, dass dieser Ansatz verwendet werden kann, um H_{II}-Lipid-Strukturen herzustellen. Daher kann die Benutzung von RSE eine Hilfe sein, um Lipid-Mischungen von H_{II} Phasen in kurzer Zeit herzustellen. Weiters wurde für jedes untersuchte Doppelschicht-bildende Lipid die spontane Krümmung der reinen Monolayer-Struktur durch Extrapolation erhalten. Laut unseren Ergebnissen gibt es für Phosphocholine keinen Zusammenhang zwischen spontaner Krümmung und Länge der Lipid-Kohlenstoff-Ketten.

Contents

List of Figures

1 Introduction

This chapter describes some basic biological information which is necessary to understand the topic of this thesis. Different kinds of lipids and their chemical structures are important for analyzing the cell membrane structure. Also, you can find description of cell membrane and mathematical estimation of its structure in this chapter.

1.1 Lipids

Lipids are the building blocks of the organic membranes. They have a vital role in living cells. Lipid molecules can carry fatty acid, oil, hormones and some special vitamins which are soluble only in oil such as vitamin D. Each lipid consists of two main parts: a head and a tail. Heads are hydrophilic and tails are the hydrophobic part of lipids consisting of hydrocarbon chains. There are different methods to classify the lipids. One of these methods is related to head group function of lipids. According to this approach, there are three main lipids: phospholipids, sterols and triglycerides. [22, 23]

1.1.1 Phospholipids

Phospholipids make up the main component of the membrane's structure. This kind of lipids tends to make bilayer structures. Approximately half of the lipids belong to this class.

DOPE

DOPE is one of the neutral phospholipids which is normally found in the outer membrane of nerves and bacteria [53]. 1, 2-dioleoyl-sn-glycero-3-phosphoethanolamine is the complete chemical name of this lipid and it consists of two mono-unsaturated hydrocarbon chains.

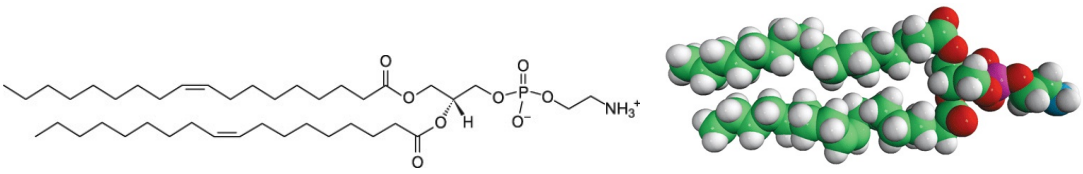

Figure 1.1: Chemical structure of DOPE. [4]

DMPC

The complete chemical name of this lipid is 1,2-dimyristoyl-sn-glycero-3-phosphocholine which consists of saturated hydrocarbon chains.

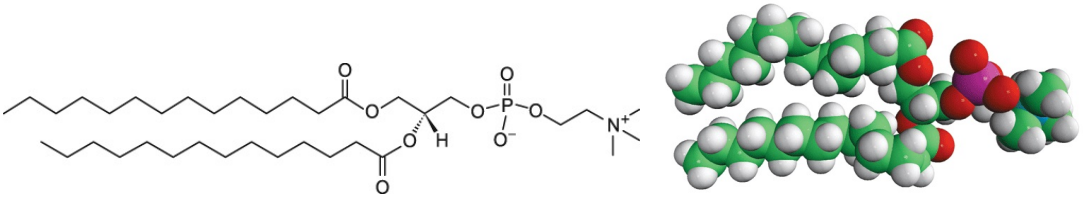

Figure 1.2: Chemical structure of DMPC. [4]

DPPC

The chemical name of this lipid is 1,2-dipalmitoyl-sn-glycero-3-phosphocholine which consists of saturated hydrocarbon chains. This lipid same as other PC lipids can find mostly in the animal cell membrane.

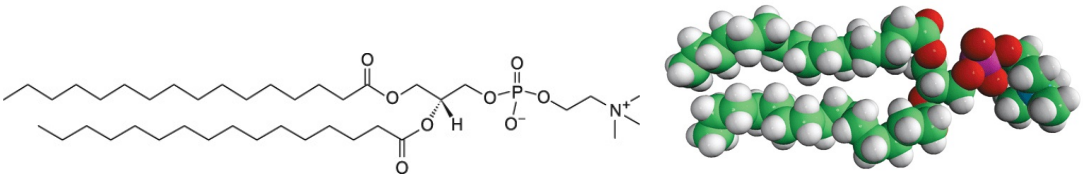

Figure 1.3: Chemical structure of DPPC. [4]

DSPC

The chemical name of this lipid is 1,2-distearoyl-sn-glycero-3-phosphocholine which consists of saturated hydrocarbon chains. Same as other PC lipids DSPC can be found mostly in the animal cell membrane.

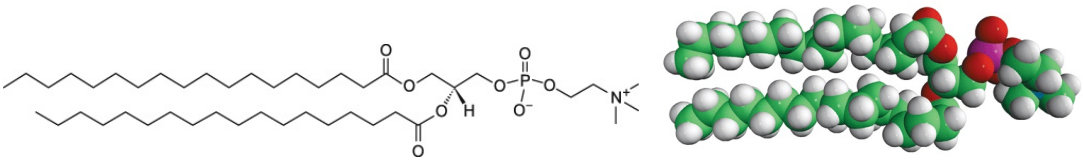

Figure 1.4: Chemical structure of DSPC. [4]

Sphingomyelin(SM)

This kind of phospholipids is based on sphingosine and consists of unsaturated hydrocarbon chains. SM is found mostly in outer part of the animal membrane especially in nerve cell and red blood cell.

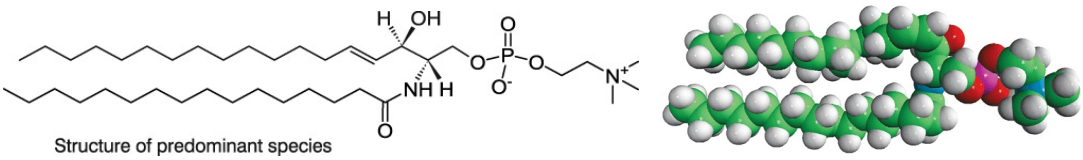

Figure 1.5: Palmitoyl Sphingomyelin. [4]

Ceramide

N-(hexanoyl)-sphing-4-enine or ceramide consists of sphingosine and fatty acid. It consists of saturated hydrocarbon chains.

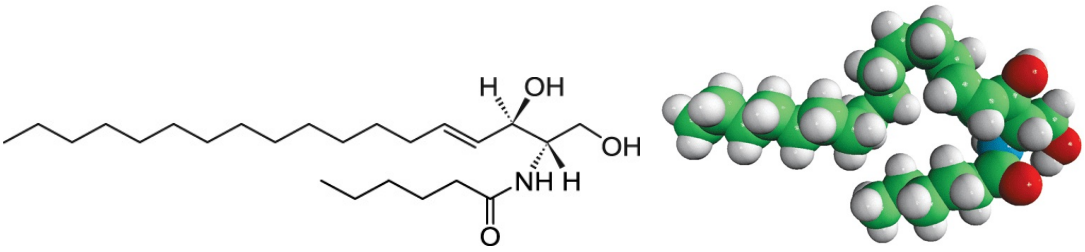

Figure 1.6: C16 : 0 Ceramide. [4]

1.1.2 Steroids

These lipids consist of 3 cyclohexane rings and 1 cyclopentane ring. Therefore, they have the completely different feature in comparison to other lipids classes. The most notable sterol lipid is cholesterols.

1.1.3 Triglycerides

Triglycerides contain three fatty acid chains and form the major part of fat stored in the human body.

1.2 Cell membrane

Every cell is enclosed by a membrane. The membrane is composed of many lipids which order to form bilayers. In living cell membranes there are also proteins and cholesterol molecules in mixture with lipids. According to osmotic force, membranes control the incoming and outgoing material from the cell.

1.3 Lipid shape

The shape of lipids is an important element which determines their properties. In order to find the shape of each lipid we should consider the packing parameter (p)

$$P = \frac{v}{a.l} \tag{1.1}$$

where v is the molecular volume, a is the cross section area of the head group and l is the length of hydrocarbon's chain of lipid. If $P = 1$ then the lipid shape is cylindrical and its aggregate has bilayer lamellar structure. If $P > 1$ the lipid shape is inverted cone that means the head group is small and the tail is bulky. Inverted micelles and inverted hexagonal structures are the expected aggregate shape in this case. If $P < 1$ the lipid has a normal cone shape that means this lipid consist of a big head and skinny tail. In this case, the aggregate structure will be micelles (for $p < \frac{1}{3}$) or normal hexagonal shapes. The schematic information can be finding in Figure 1.7 . [1,4]

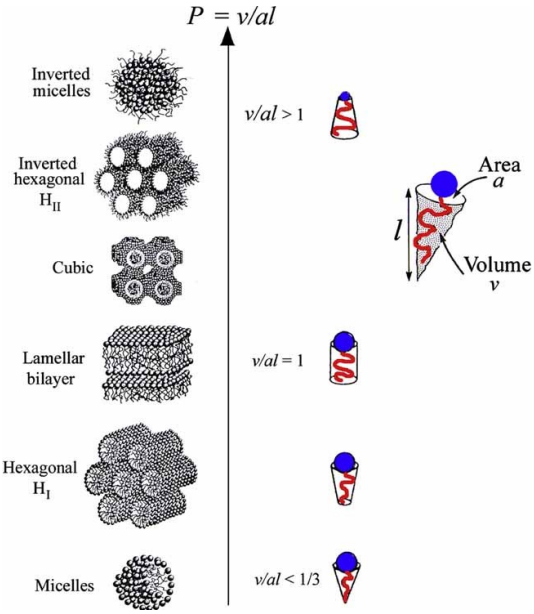

Figure 1.7: Packing parameter and lipids Properties related to that. [1]

1.4 Spontaneous curvature of lipid

The membrane has a soft biostructure thus, it is important to know how bending forces change the structure. For the first time, Wolfgang Helfrich created a formula for elastic bending energy of the surface that caused

change in surface's shape [27]. See equations (1.2) and (1.3)

$$dE_{surface} = \left[\frac{\kappa}{2}(\frac{1}{R_1} + \frac{1}{R_2} + \frac{\kappa_G}{R_1 R_2})^2\right] dA \tag{1.2}$$

$$E_{surface} = \oint_S dE_{surface} = E_\kappa + E_{\kappa G} \tag{1.3}$$

where $E_{surface}$ is the elastic bending energy of surface, κ is normal bending modulus,R_1 andR_2 are principal radii of curvature, κ_G is Gaussian curvature modulus and A is the area.

It is necessary to know the mathematical background about the surface to have a better understanding of these formulas. The cross section of each surface consists of two perpendicular principle surfaces (c_1, c_2) that each of these surfaces belongs to the sphere with a certain radius. We consider these radii as the principle radii. Figure 1.8 illustrates an inverse relation between principle surface and principle radius which define the exact shape of the main structure. The Gaussian curvature modulus κ_G is important to give the topological information about the surface. There is a relation between the energy of interface and Gaussian curvature proportional to $4\pi(1-g)$.(See equation(1.4))

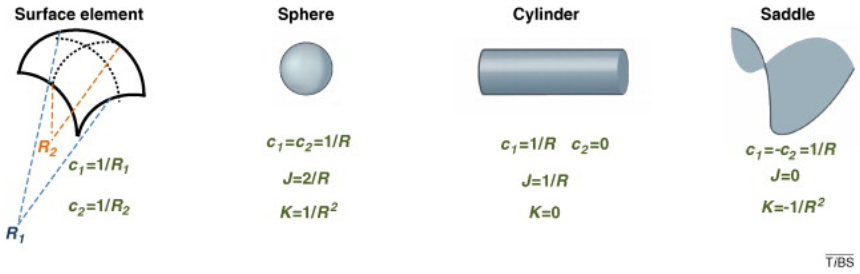

Figure 1.8: Schematic principle radii R_1 and R_2. [2]

$$E_{\kappa G} = \kappa_G \oint_S \frac{1}{R_1 R_2} dA = \kappa_G 4\pi(1-g) \tag{1.4}$$

where g is the genus number and refers to topological complexity in shape. You can find more information about g in Figure 1.9. If two symmetric lipid monolayers should be near each other in a bilayer structure, this bilayer has

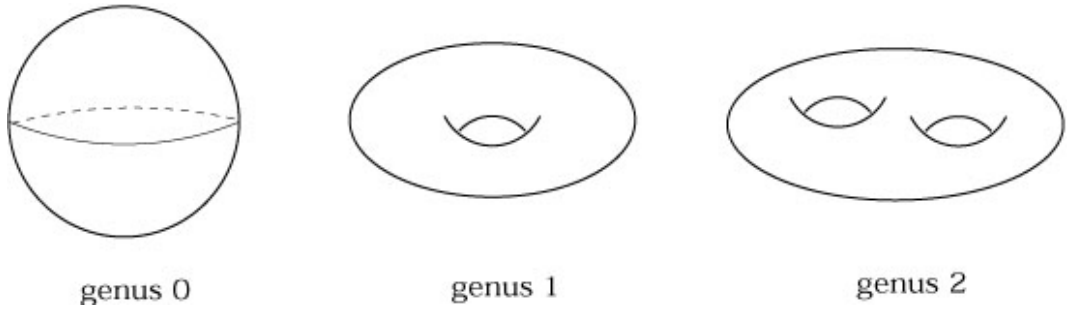

Figure 1.9: The schematic information for different genus number. [3]

no curve and its spontaneous curvature is zero. But if two monolayers are chemically different, their bilayer tends to be curvy and this curve is related to the infinite spontaneous curvature as $C_0 = R_0^{-1}$ [27]. In this case, we have a change in bending energy of the system as equation 1.5.

$$dE_{surface} = \left[\frac{\kappa}{2}\left(\frac{1}{R_1} + \frac{1}{R_2} - \frac{2}{R_0}\right)^2 + \frac{\kappa_G}{R_1 R_2}\right] dA \tag{1.5}$$

1.5 Rapid solvent exchange (RSE)

There are many different methods to make artificial membranes. One of the newest ones is called rapid solvent exchange method or RSE. This method was invented by Buboltz and Feigenson [30]. This approach is based on applying vacuum, temperature and vortexing on a solution of lipid and organic solvent in the aqua buffer. The first step is to dissolve lipids in the organic solvents such as cholorform and methanol that can fully dissolve the lipid stock. The next step is mixing the lipid stock with aqueous buffer because the aqua environment is necessary to make lipid structures. The final step is to inject this mixture of lipid stock and water into the test tube and place in RSE apparatus. In RSE apparatus, the test tube is connected to the vacuum pump, vortex, and heating gun. The vortex increases the mixing rate of lipids in water, the heating gun prepares the suitable temperature for evaporating the organic solvent and remove it completely from the sample, vacuum pump takes the evaporated organic solvent out of the test tube and the inert gas flow like as argon helps to trapping the evaporating organic

solvent by the vacuum pump and keep the inside pressure constant [31].

In this case forming a vesicle takes about one minute. On the other hand, the quality of vesicles is so high with the maximum mixing of lipids.

1.5.1 Historical evolution of RSE

Invention

In 1999 Buboltz and Feigenson published an article about a novel strategy of making liposome. They called their technique the rapid solvent exchange or RSE. They claimed in this method there was no more solid state mode in order to make free solvent lipid mixture but there was a direct transfer between the organic solvent and aqua buffer in lipid mixture. The name of this method came from this advantage. In that time they worked on determining the maximum solubility of cholesterol in the multi phospholipids bilayers. They found increasing of monohydrated of pure cholesterol crystals during their studies. That seems this problem appeared after going to the solid phase during the free-solvent process. Thus they invented RSE for making homogeneous structures of lipid's mixtures in the aqua buffer.

Their RSE apparatus consisted of a vacuum manifold which was connected to 10 ml or 50 ml FEP Teflon Oak Ridge tubes on top of the apparatus and vortex device placed at the bottom of the teflon tube. This kind of tube had the minimum probability of lipid adsorption during RSE. The lipid solution stock was injected into the teflon tube with a Hamiltonian syringe. Standard vacuum pressure considered as 23 torr for 23°C (room temperature). The mechanical vacuum pump had an adjustable inlet valve to handling the vacuum connection. For sample preparation at higher temperatures, the higher pressures were used and in this case the test tube covered with the forced-air jacket which was connected to the heat gun. In additional, the vacuum pressure should be aligned a bit more than the vapor pressure of water. During this process, the teflon tube consist of water as a buffer was placed on the vortex device. Then the vortex was turned on and caused the buffer find the cylindrical shell form after that the vacuum pump was opened and the solution of lipid in organic solvent was injected in to the test tube with a Hamiltonian syringe through the narrow needle which fixed in tube head coverage. As soon as organic solvent solution came into the test tube environment, it experienced the vacuum and the vaporization

process started at this moment, along with some evaporation cooling. On the other hand, because of low distance between the injection aperture and under vortex aqua (about 1 cm), organic solvent droplets immediately touched the water. Because water carried the heat gun temperatures then the temperature of organic solvent droplets increased and this completed evaporation process. The cylindrical shell form of aqua buffer under vortex increased the contact surface between water and organic solvent drops and vortexing helped the pushing vapor to the vacuum pump. Then the organic solvent very quickly and efficiently was removed from the system.

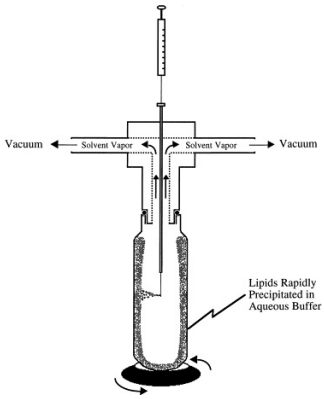

Figure 1.10: Schematic picture of RSE process in the first invention [30].

The standard time for RSE process was defined as one minute after injection also a second after injection more than 99.99% of organic solvent was removed and even after 30 seconds the sample was completely free of organic solvent.

Kinetical optimization

In 2009 Buboltz published a new article about the improvement the RSE technique [31]. At first, they removed injection part of RSE device (the needle in the top of the test tube). Then the lipid organic solvent solution was mixed directly before placing the test tube in the RSE apparatus. This improvement increased the sample preparation time by a factor of 3 faster than before because it was not necessary to clean the needle after making each sample.

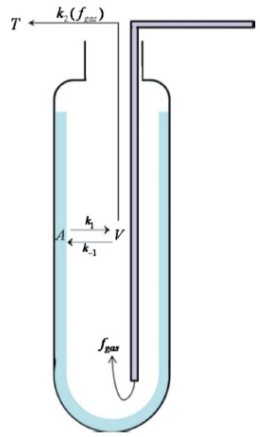

Figure 1.11: Kinetic process during RSE defined by Buboltz. [31]

Another important development was kinetic optimization. In this case, a simple two-step kinetic model was defined for each residual organic solvent present. They considered three situations for residual solvent related to its position: (A) solvent dissolved within the aqueous phase, (V) headspace solvent vapor (in an exchange with aqua phase), and (T) trapped solvent removed from the sample tube and trapped by vacuum.(See figure 1.11) The exchange between A and V is described with two coefficients k_1 and k_{-1} which are proportional to the interfacial area between A and V. The trap-transfer coefficient was defined as k_2 which is related to transfer from V to T.k_2 depends on tube-neck diameter, the gradient of pressure along the tube-to-trap path and constant of solvent diffusion in the vapor phase. They added the controllable inert gas flow (f_{gas}) near the vortexing sample in to the test tube. It caused the organic solvent vapor quickly become trapped into the vacuum after sweeping from the surface of vortexing sample. In this case, k_2 depended on inert gas flow but k_1 and k_{-1} are constant parameter independent from f_{gas}.

Controllable elements

In 2015 A.A. Rieder published an article about new optimization in RSE method [24]. The improvements included, some changes in the RSE device allowing for control over the vortex speed, evaporation speed and temperature during the process. In this case, the test tube with buffer or pure

water was preheated to the same temperature as RSE temperature for some minutes. The RSE device also was preheated to favorable temperature by heat gun. Lipid organic solvent solution was injected into the test tube containing buffer just before putting in RSE apparatus. The vortex speed was adjustable and also the vacuum speed could be aligned on the evaporation pressure between buffer and the organic solvent (minimum pressure) and after opening the vacuum valve pressure starts from this minimum (Automatically method) or manually adjust during RSE on this pressure (manually method). In the last step of RSE process, after closing the vacuum valve and vortex, the system was purged with Argon for one second. They found imputing mechanical energy during vortexing and evacuation speed in parallel to lipid concentration and the organic solvent to buffer ratio had an important impact on RSE results. For instant decreasing the vortex speed and increasing the evacuation times to some minutes during increasing lipid solvent concentration caused achieving to the highest number of MLVs.

1.5.2 Why RSE?

Thin film technique and lyophilization are known as the standard former methods to mixing lipids and preparing membranes. These methods consist of some dehydration process. During dehydration, especially for the mixture of different lipids, the probability of phase separation in solid phases increases, because all of the lipids do not dehydration dehydrate to the same degree. Therefore it is not easy to rehydrate the sample homogeneously again. This effect has been seen dramatically in lipid mixtures containing high concentrations of cholesterol. [31, 54]The other disadvantage of these approaches is that they are time-consuming processes.

RSE is a very fast method to make samples because lipids pass quickly from organic solvent to aqua buffer. The lipid preparation time is on the order of minutes. The other advantage of this method is controlling of temperature, evacuation and pressure in order to reach the maximal solubility of lipids in the aqua buffer. RSE does not consist of any dehydration process which can cause a decrease in the phase transition probability and lipid demixing effect. Finally, it is easy to establish a RSE apparatus in every lab.

2 Methods

Now a day there is a motivation to study about cell membrane. Finding a better treatment, cure or diagnosis methods when confronted with illnesses are the broad motivation of these studies. During this kind of research sometimes necessary to utilize artificial membranes. Since the biological membrane consists of a mixture of different lipids, optimizing the preparation lipid mixtures is necessary. In this chapter, the use of RSE is outlined as a model membrane preparation method.

2.1 Sample preparation

Our experiments were based on the RSE approach which was optimized by Rieder et al. [24]

Phospholipids were purchased from Avanti Polar Lipids (Alabaster, AL) and used without any further purification. For each sample, lipid powders were dissolved to a 30 $\frac{mg}{ml}$ concentration in Chloroform/Methanol [9:1].

In our experiment, lipid guests were mixed with the host DOPE. For each sample, two lipid stock solutions were required; one guest stock solution and one host stock solution.

Before initiation the RSE preparation, ultra pure (18mOhm) water was put in the test tube and preheated in the oven for four minutes. The preheating temperature was the same as the RSE temperature. The RSE temperature should be higher than the guest molecule melting temperature to increase the lipid mixing probability and avoiding of coexisting phase combination. The volume of water and volume of stock solution are brought together at a 1:1 ratio.

After preheating the water, the appropriate volumes of lipid stock solutions were added to the water test tube. Note, the test tube should be immediately introduced to the RSE apparatus.

The test tube was put on a pre-heated vortex apparatus with the speed

of approximately 1800 rpm. The connection between the test tube and RSE apparatus was sealed with an o-ring. After fixing the test tube in position, the vacuum pump was turned on and the vacuum valve was opened. Before starting the experiment, the vacuum pump was adjusted on minimum pressure, which should be between the vapor pressure of water and the organic solvent to ensure the organic solvent removal without changing in water amount (see figure 2.2). After 5 minutes, the vacuum pump and the vortex were turned off, and the system was open to a flow of Argon. The test tube was removed from the apparatus and the sample preparation was finished.

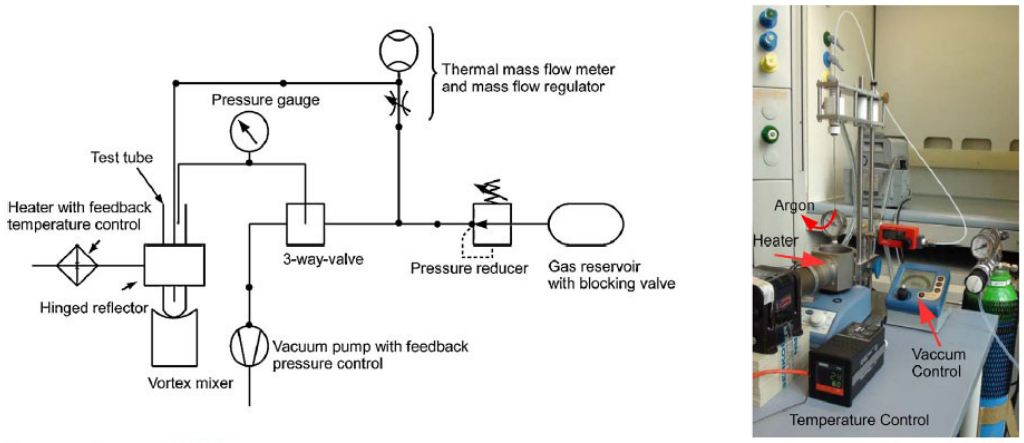

Figure 2.1: RSE apparatus structure [24].

The vapor pressure can be found from the Thermo physical Databank of materials [32]. During RSE, the temperature should be more than a lipid melting point if we have the mixture of lipids the RSE temperature should be more than the melting point of guest lipid. Thus, for finding the suitable minimum pressure, it is necessary to find the relation between pressure and temperature (Eqn. 2.1).

$$p = e^{A*ln(T)+\frac{B}{T}+C+DT^2} \tag{2.1}$$

where p is evaporation pressure of the water and organic solvent molecules, T is temperature and A, B, C, D are coefficients of the KDB Correlation Equation 2.1. These coefficients are available for each substance in the Korean databank [32].

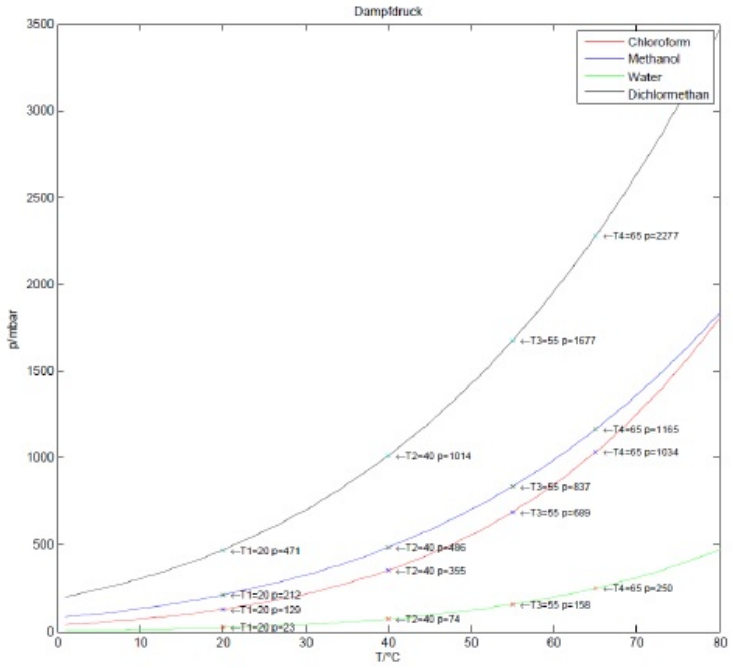

Figure 2.2: The relation between temperature and evaporation pressure for Chloroform, Methanol, Water and Dichlormethan according to the equation 2.1 [33].

2.2 NMR controlling

After RSE, the organic solvent should be completely evaporated. In order to verify our samples are free of organic solvent, they were investigated with nuclear magnetic resonance spectroscopy (NMR). Each sample was dissolved in d6-DMSO (CD3)2SO to detect trace resonances of methanol (CH3OH) and chloroform (CHCl3). $^1H - NMR$ spectra were collected on an Avance III 300 MHz spectrometer (Bruker, Billerica, MA) using Bruker TopSpin acquisition software, and analyzed with TopSpin 3.2. A standard ^1H pulse sequence with a 30° flip angle and 1 s delay time was employed to collect 32-256 transients at 21 °C. $^1H - NMR$ data were processed with a line-broadening parameter of 1 Hz.

The lack of any MeOH or CHCl3 peaks in the sample spectra meant that if the solvents were present, they were more dilute than 1 part in 1000 (very conservative). The detection limit is close to 1 ppm.

2.2.1 Basics of nuclear magnetic resonance spectroscopy (NMR)

Nuclear magnetic resonance spectroscopy (NMR) is one of the precise methods to find the chemical and physical properties of materials. In this method the sample is solved in deuterated solvents at least 2 mg of sample is required. The sample stock is put under high magnetic field. The magnetic radiation cause change in energy state nuclei and the outgoing photon after this process is detected. Magnetic resonance caused a change in frequency of the outgoing beam. At the end of this process, the intensity versus frequency graph appears on the screen (Figure 2.3). There are some peaks on this graph which are called as chemical shifts. Each peak related to the certain element, therefore, this method can show exactly which elements or chemical groups exist in the sample. This is the reliable approach to finding the purity of the material. However, this is a time consuming and destructive method [25].

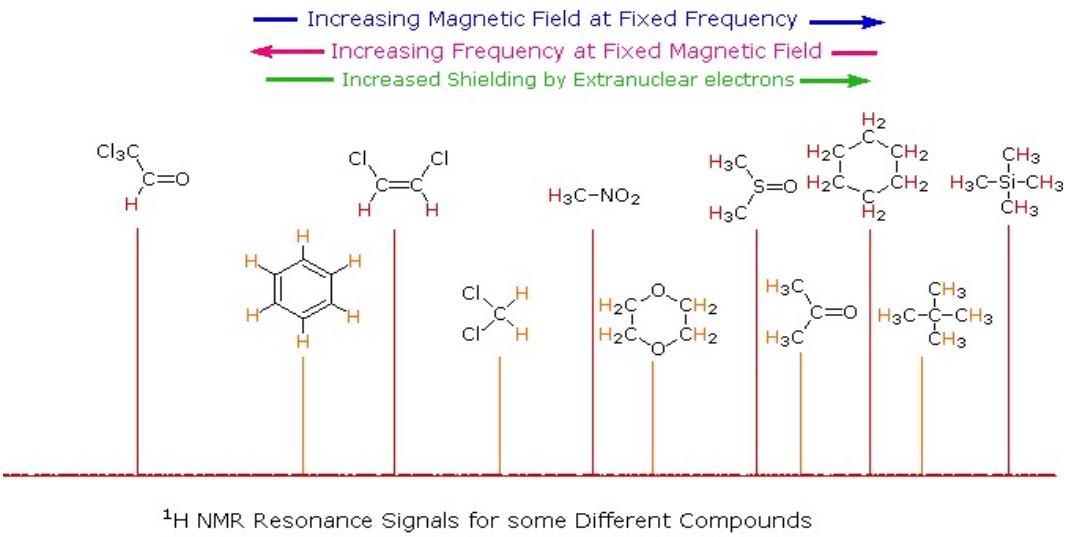

Figure 2.3: An example of chemical shifting spectrum in NMR [26].

2.3 Small angle X-ray scattering (SAXS)

After preparing samples, each sample was checked with small angle X-ray scattering (SAXS) to find information about its structure. In our experiment, the samples had paste like consistency that floated in the aqueous environment. The floating paste was put in the center of paste cell and soaked with the aqueous part of the sample in order to avoid dehydration of the sample under vacuum and high-temperature ranges. The paste cell was placed in SAXS system. We measured each sample at five different temperatures. The measurement time was 1 hour with 10 minutes of equilibration time before each measurement.The scattering patterns were converted to 1-D plots of scattered intensity (I(q)) versus scattering vector (q) by SAXStreat 1.03.006.7324 (Figure 3.2). The I(q) plots were then used to identify peaks that resulted from constructive interference as a result of Bragg's Law.

According to the Bragg's law, lattice parameters were found and, therefore, lattice structure was recognizable (equations 3.3, 3.2).

2.3.1 Basics of small angle X-ray scattering (SAXS)

SAXS is one of the important characterization methods used in soft matter science. In this case, without the need to crystallization the sample, you can find the structural properties of a sample, such as shape, size, lattice structures, phase coexistence, etc. In this method a coherent beam of X-ray illuminates the sample, most of the beam passes through but some are scattered by the sample. The scattered beam is collected by a two-dimensional detector resulting in the scattering pattern observed in Figure 2.4. It is an elastic non-destructive approach to analysis nanomaterials. The wavelength, in this case, is in 0.1 to 0.2 nm and the scattering angles is in 0.1 to 10°.

X-ray sources can be a synchrotron or X-ray tube (as in our case). For two-dimensional scattering pattern beam line collimation can be as a hole in front of X-ray source (Point collimation) or it can come from one split in front of the source (Line collimation). [5]

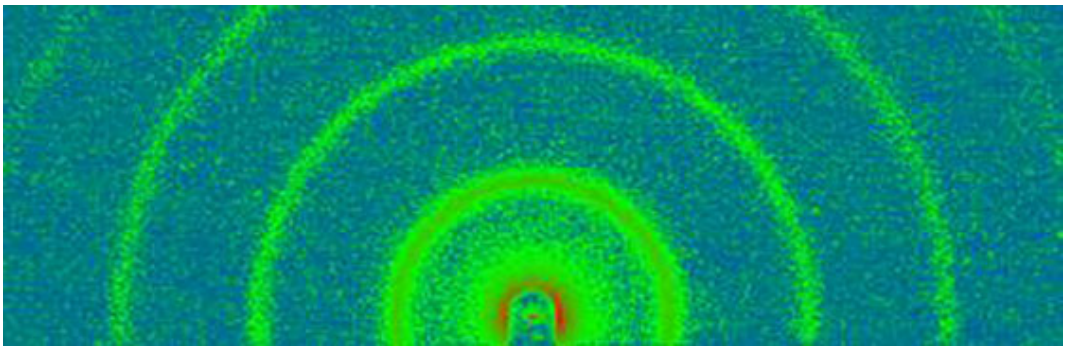

Figure 2.4: The scattering pattern in point collimation method. [6]

2.3.2 SAXS instrument

The SAXSpace instrument was used during our experiments. It is a measuring system for analyzing nano-soft materials with small angle X-ray scattering (SAXS) or wide angle X-ray scattering (WAXS). It is made by Anton Paar Company (Austria). It is equipped with a Pilatus 100K-S detector system (Dectris, Swiss) with a pixel size of 172 x 172 μm^2 and a total amount of 94965 pixel. The q range in the small angle configuration reaches from 0.3 to 10.86 nm^{-1} with a step width of 0.032 nm^{-1}. The X-ray source is a sealed X-ray tube. Cu Kα (1.54 $\AA$) radiation is supplied by a Genix 3D microfocus tube (Xenocs, France) with a power consumption of 30W. The sample temperature is controlled by the TC Stage 150 (Anton Paar, Austria). All samples were contained in a paste cell holder (Anton Paar, Austria). The SAXSpace device can investigate materials in the range of 1 to 200 nm in the temperature range of -150°C to 500°C. Small angle X-ray scattering is an elastic scattering method, thus the energy of the incident photon is equal to the scattered. The distance between sample and detector (SDD) is 308 nm for SAXS mode in this device.

Normally each SAXS apparatus consists of five different parts: the X-ray source, the collimation system, the sample holder, the beam stop, and the detector. In this section, you can find some brief information about each part of this instrument.

The X-ray source

There are different kinds of the X-ray sources such as sealed X-ray tubes, rotating anodes, micro sources and synchrotron radiation. In our system (SAXSpace), the sealed X-ray tube was applied as an X-ray source. This tube consists of a filament (wire) and anode (target) inside of the evacuated box. The filament is warmed up by passing electrical current through it and causes the emission of electrons from the filament. Applying the high voltage (around 30-60 kV) between the filament and the anode caused an acceleration of the emitted electrons into the anode. The electrons lose their acceleration after hitting the anode and according to the Bremsstrahlung principle, they cause X-ray emission. This produces an X-ray spectrum with different wavelengths, but their energies are not higher than the applied voltage i.e. if the applied voltage is 40kV, the energy of X-ray beam is maximum around 40 keV. The fraction of electrons causes expel electrons from atoms of the anode. [46] Then remain electrons inside the anode atoms rearrange themselves that causes the fluorescence radiation. The wavelength of this radiation depends on the anode component element.

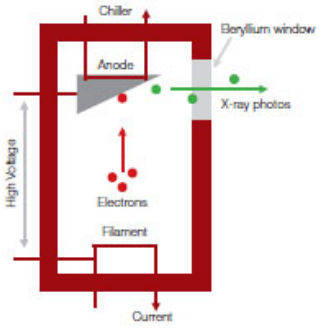

Figure 2.5: A schematic view of the X-ray tube. [46]

In this method, the X-ray density is controllable by changing the electrical current which passes trough anode. Copper is used as the anode in our system. This kind of tubes operates at 2 kW with a high voltage and electron current set as 40 kV and 50 mA, respectively.

The collimation system

In SAXS, the scattering angle is smaller than 0.1°. Therefore, it is difficult to distinguish between incoming beam and scattered beam, especially because the scattered beam is always less intense than the incident beam. Using collimation system helps to avoid this problem. This system consists of a many splits that the beam goes through. For making the narrow beam, narrow slits are required. The use of slits causes a decrease of intensity of the outgoing beam. Normally the X-rays produced by the source consists of photons with different wavelengths i.e. they are polychromatic. In this case, photons with different wavelength are scattered in a different direction (wavelength smearing). Only the beams which are scattered in angles smaller than 0.1°, are favorable for us. To avoid wavelength smearing phenomena, a monochromator was used to make a monochromatic beam. The monochromator diffracts X-rays with certain wavelengths related to the Bragg's law. The Bragg's d spacing, in this case, is about 4 nm. There are two main collimation systems for SAXS instrument: Point collimation and line collimation. We have used the point collimation system during our experiments. In this case, the pinholes convert the beam into the small circular or elliptical spot. In this approach, only the small area of the sample is illuminated by the beam (around $3 \times 3\ mm^2$). Therefore, the scattering is centrosymmetric and the 2D scattering pattern shows the concentric circles around the primary beam. The slit smearing is neglectable in this case. When the sample volume is very small, the scattered beam intensity is low. This problem can be solved by increasing the distance between sample and detector. When this distance is in meter range then the measurements take few hours. The point collimation system is favorable for studying of very small samples or find their surface properties. [46]

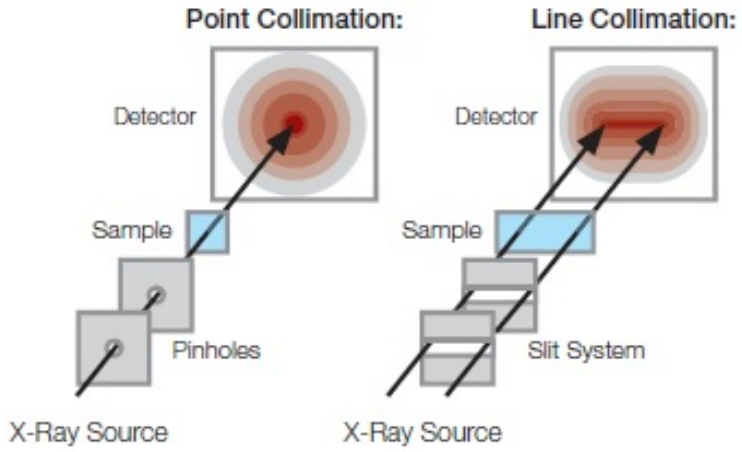

Figure 2.6: Two main collimation systems in SAXS instrument. [46]

The sample holder

The sample holder is one of the most critical parts of the SAXS. Because our group use different kinds of samples with different property and sensitivity. For instance, some samples cannot stand under vacuum, but the vacuum is necessary to keep low scattering background [46]. Sometimes a change in the environment causes a change in sample structure. For example, some samples are structurally more sensitive to change the temperature, pressure, strain, humidity and some other things. In our case, we have chosen paste cell sample holder because our samples had a paste consistency.

The paste sample is sensitive to vacuum. Its sample holder consists of two removable windows. These windows should be transparent to X-ray and also should not scatter the beam. These windows should be made of material that has no chemical interaction with paste material and have the resistance against a high range of temperatures. Normally Kapton films are used as the window in paste cell [46].

Figure 2.7: The paste cell [47].

Beam stop

If the direct incoming beam passes through the detector, the scattering pattern will be unclear because of overshadowing. The intensity of the incoming beam is much higher than scattered beam and in some sensitive detectors, this intensive beam causes destructions to the detector. There are two kinds of beam stop system. One of them made from electron dense materials like as Lead and can block the direct beam completely. The other beam stop systems made of transparent materials which can change the intensity of the direct beam to the reasonable intensity for the detector. If the transparent beam stop is used, the monitoring of the direct beam and scattered pattern at the same time is possible. Therefore, the eventual drifts of generator intensity can be controlled by normalization the beams with the same intensity. Also the extra experiments in order to find the position of the direct beam and its properties are not required [46]. But it should be noted that transparent beam stop can add extra signals to the background signals.

The detector

There are different kinds of detectors: wire detectors, CCD detectors, imaging plates and solid state (or CMOS) detectors. We have used one kind of solid state detectors during our experiments. This type of detector consists of Silicone-diode to record the X-ray photons directly. This semiconductor diode produces the countable ion pairs after illumination by X-ray. Applying additional circuits help to count only pulses which are higher than threshold energy. Because *Si* can not absorb beam with a low wavelength, the quantum efficiency decreases for beams with a wavelength smaller than *Cu* wavelength. This kind of detector can be stable even at high radiation

doses and their linearity is stable even for beams with intensity near to the initial X-ray beam (2 kW). However, illumination high-intensity beam for a long time can damage solid state detector [46]. The exposure time, a number of frames, temperature ranges and other experiment variables related to exposure are aligned manually in SAXSdrive software before starting the experiment.

2.4 Hexagonal phase

One of the liquid crystal structures made from mixing amphiphilic lipids and water is the Hexagonal phase. This structure consists of long tubes which array beside each other making a hexagonal lattice. Now a day, this kind of lipid structures are subject of studies such as drug delivery, gene transport and nanotechnology [34, 35]. There are two kinds of hexagonal phase structure: normal hexagonal phase (H_I) and inverse hexagonal phase (H_{II}). (See figure 2.8)

H_I is the less common of the hexagonal structures. The highly polar lipids or lipids with very large headgroups are suitable to form this structure. In this case, the outer part of cylinders consists of heads and inside of them filled with hydrocarbon chains.(See Figure 2.8)

H_{II} consists of water filled cylinders, that means the inside of the cylinders are hydrophilic and made by head groups. Therefore the outside of the cylinders are covered with carbon chains. Tight packing of the hydrophilic part of lipids reduces their connection with aqua phase. One of the most important lipids that form the H_{II} is PE. The diameter of cylinders is a function of temperature, pressure, type of lipid and pH of the environment. By changing the balance between lipid's head and tail to the longer hydrocarbon chains and smaller head group, the probability of making inverse hexagonal phase is increasing. Also, it is possible to go from a lamellar phase at high temperatures to the H_{II} phase [14, 27].

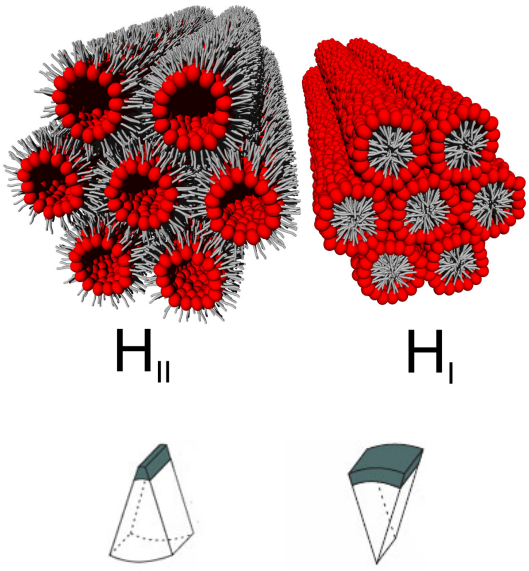

Figure 2.8: Normal hexagonal H_I and inverse hexagonal H_{II} structures with their wedge shape phospholipid molecules. [7, 36]

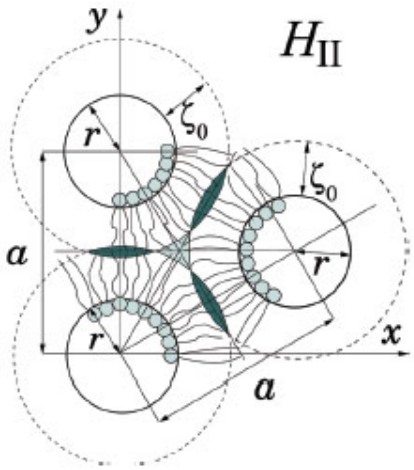

Figure 2.9: Schematic cross section of inverse hexagonal phase. r, ζ_0 and a denote the tube radius, equilibrium length of hydrocarbon chains and lattice parameter, respectively. [42]

As you can see in figure 2.9, the hydrocarbon chain length is not constant

in H_{II} structure. The equilibrium length of hydrocarbon chains is ζ_0. At the point that tubes are tangency point with each other, the hydrocarbon length is smaller than the equilibrium length because of compressing near each other. The highest length of hydrocarbons related to the chains near the voids region. In this case because of stretching force, they have the maximum length.

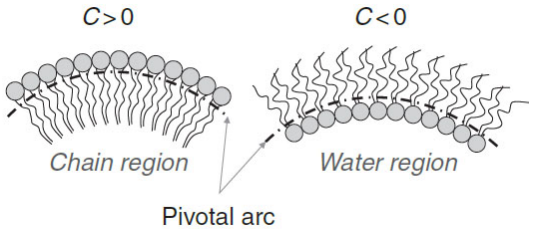

Figure 2.10: Schematic conditions of positive and negative monolayer related to pivotal plane bending [36].

The long cylinders in hexagonal structure actually form monolayer lipid structures. In this case, if the pivotal plane bends towards the hydrocarbon chains, its curvature is positive ($C > 0$). In versa if the pivotal plane of lipid monolayer bends toward the head group (water region), the curvature is negative ($C < 0$). The pivotal plane is located at the joint point of heads and tails of lipid. In this area, the stretching and bending energy are in equilibrium and the lipid per area ratio does not change during applying bending moment in this plane [37].
The cylindrical plane has high anisotropy i.e. there is a huge difference between their two principle curvatures [36].

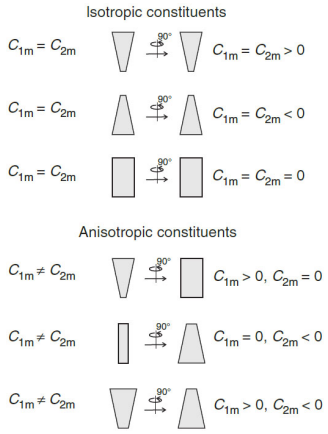

Figure 2.11: Different categories of isotropic and anisotropic structures depend on lipid intrinsic curvatures $C_{m1} and C_{m2}$ [36].

Because of the intrinsic shape of wedge phospholipids, they cannot make the planar structure, but in the aqueous environment, they self-assemble as the cylindrical monolayers. Therefore, the membrane curvature depends on the intrinsic shape of its constituent lipids. The definition of intrinsic curvature is the tendency to curve the shape of the monolayer in the absence of any external force or torque [27, 36]. Same as the membrane principal curvatures, there are two intrinsic principal curvatures too (C_{m1}, C_{m2}). If these two curvatures are equal, the lipid is isotropic and in another case we have an anisotropic lipid molecules. One example for anisotropic lipid molecule is hexagonal phase. For inverted a hexagonal shape lipids we have $C_{m1} = 0, C_{m2} < 0$.

Geometrically, the inverted hexagonal phase is the simplest non-planar structure [38]. This structure belongs to the liquid-crystal phase. The recent studies show, the nonlamellar biological structure such as inverted hexagonal phase can play a role in setting up the protein function. Also, membrane fusion occurs in highly curved structures. Some bacteria have this kind of structures [36]. Therefore, it is important to understand the properties of this kind of structures.

2.5 Data analysis

After making a sample with RSE and finding its scattering pattern with SAXS, the next step is finding structural information of sample like lattice parameters to find the real lattice structure of the sample and other characteristic information about that.

2.5.1 Scattering basics

The small angle X-ray scattering principles are based on Bragg's law. During SAXS, the coherent planar X-ray beam is irradiated on the sample. This process is elastic, i.e. the wavelength of the X-ray beam and the wave vector $|\vec{k}| = \frac{1}{\lambda}$ are conserved during this process. The incoming X-ray beams are scattered by lattice electrons. As you can see in figure 2.12, the incoming wave can be scattered with two different electrons in the lattice, in this case, the distance between positions of these two electrons is shown as $\vec{r}$. If we consider the incoming and scattering wave vectors as $\vec{k_i}$ and $\vec{k_s}$, respectively, then their phase difference describes as

$$\Delta\phi = 2\pi \ \vec{r} \cdot \left(\vec{k_s} - \vec{k}_i\right) = 2\pi \ \vec{r} \cdot \vec{R} \tag{2.2}$$

which is related to the destructive (if r and R be perpendicular) or constructive (if r and R be parallel) interferences of scattered waves.

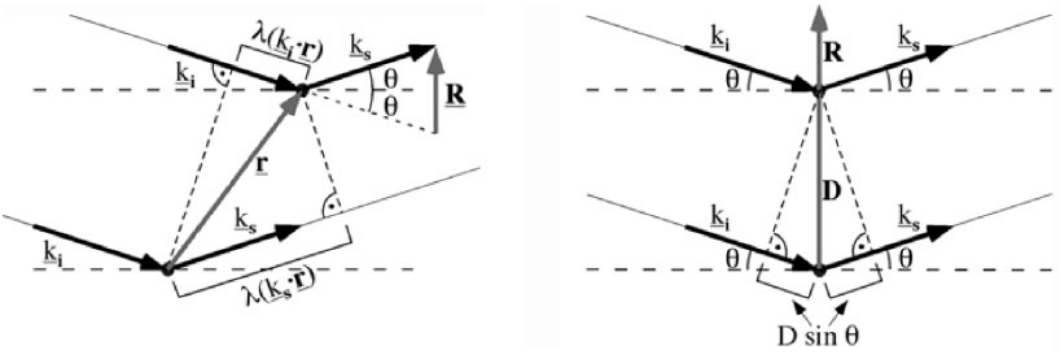

Figure 2.12: Scattering by two points (left) and by two planar surfaces (right) [40].

According to the figure 2.12 and geometry principles, it is clear that $\vec{R}$ is proportional to half of the scattering angle θ.

$$|R| = 2sin\theta/\lambda \tag{2.3}$$

For two planes with distance D, the Bragg's diffraction follows the bellow equations

$$\vec{r} \cdot \vec{R} = |\vec{r}| \cdot |\vec{R}| = 2D \cdot \frac{sin\theta}{\lambda} = n \text{ with } n = 1, 2, 3, ... \text{ and } |\vec{r}| = D \tag{2.4}$$

Because of this fact that $\vec{R}$ belongs to the spatial reciprocal vector ($|\vec{R}| = \frac{n}{D}$), then it is possible to find the electron density (ρ) from the structure factor function (F(R)).

$$F(\vec{R}) = \int_{\vec{r}} \rho(\vec{r}) exp(2\pi i \vec{r} \cdot \vec{R}) d\vec{r} \tag{2.5}$$

For membrane studies, if the membrane is considered as a plane in y-z axes, then the distribution of electrons can happen only in the perpendicular axis to this plane i.e. x-axis. Thus, structure factor will be as equation 2.6.

$$F(R) = \int_x \rho(x) exp(2\pi i x R) dx \tag{2.6}$$

As you can see, the structure factor is the Fourier transformation of electron density distribution. Therefore, with applying inverse Fourier transform, we can easily find the electron density function $\rho(x)$.

$$\rho(x) = \int_R F(R) exp(-2\pi i x R) dR \tag{2.7}$$

For the multilayer lamellar, this function is periodic.

During the scattering process, the intensity of scattered waves can be found from the below equation.

$$I(R) = F^*(R)F(R) = |F(R)|^2 \tag{2.8}$$

One disadvantage of scattering is that we cannot find the phase direction from this method. The only thing we find directly from scattering is the amplitude of structure function. Therefore, in order to find the electron

distribution, we need some extra equations.
For a symmetric membrane, the center of symmetry is considered as the center of the membrane. Then the structure factor for isolated membrane is

$$\begin{aligned} F_u(R) &= \int_{-D/2}^{+D/2} \rho(x) exp(2\pi i R x) dx \\ &= \int_{-D/2}^{+D/2} \rho(x) \cos(2\pi R x) dx + i \int_{-D/2}^{+D/2} \rho(x) \sin(2\pi R x) dx \end{aligned} \tag{2.9}$$

In this case, the imaginary part is equal to zero because of the symmetry and, therefore, the structure factor has only the real part.

$$F_u(R) = |F_u(R)| \cdot \exp(i\alpha) = |F_u(R)| \cdot \cos(\alpha) + i|F_u(R)| \cdot \sin(\alpha) \tag{2.10}$$

This imaginary part of above equation is zero if the sin function is zero, i.e. $\alpha = n\pi$. Therefore, the real term has $\pm$ sign because of cos function. Experimentally, we need many scattering measurements in order to have a reasonable guess about the structure factor sign.

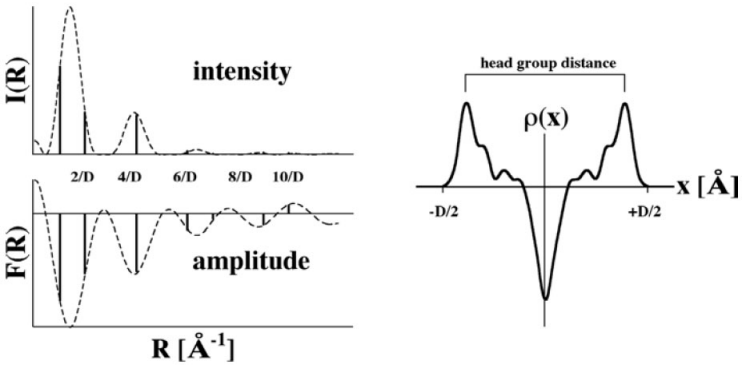

Figure 2.13: Scattering intensity and structure function amplitude graphs and estimated electron density of them for a multilamellar membrane with the repeat spacing D [40].

As you can see in figure 2.13, the electron density is higher in the outer part of the membrane.

The diffraction of inverse hexagonal phase has a different periodic pattern in comparison to the multilamellar structure. In this case, the scattered

waves positions (q) follow the below relations

$$q_{hk} = \frac{4\pi\sqrt{h^2 + k^2 + hk}}{\sqrt{3}a} \tag{2.11}$$

where h and k are miller indexes of two dimensional lattice and a is the lattice parameter which is actually the distance between the center of two neighbor tubes of H_{II} structure [41]. The position of Bragg peaks are multiple of $1, \sqrt{3}, 2, \sqrt{7}, 3, \ldots$. In figure 2.14, one can see the two main diffraction layer of H_{II} structure. As it is shown in the picture, the first two diffraction peaks come from position 1 and $\sqrt{3}$ related to (1,0), (1,1)plane respectively.

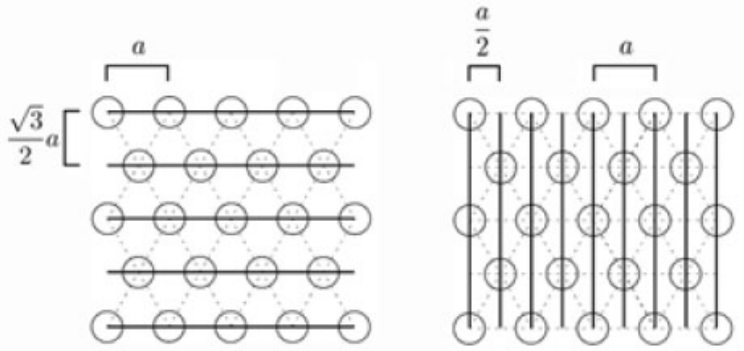

Figure 2.14: The first and second diffraction layers in inversed hexagonal lattice [40].

The inversed hexagonal phase occurs at high temperatures because the packing cylindrical structure needs to disorder the chains.

The Fourier transform in two dimensions is

$$F(u,v) = \int_{-\infty}^{\infty}\int_{-\infty}^{\infty} f(x,y)exp(-j2\pi(ux+vy))dxdy \tag{2.12}$$

$$f(x,y) = \int_{-\infty}^{\infty}\int_{-\infty}^{\infty} F(u,v)exp(j2\pi(ux+vy))dudv \tag{2.13}$$

where u and v are the spatial frequencies in x and y directions. The 2D spectrum of f(x,y) is F(u,v). The inverse Fourier transform is actually the f(x,y) which is the linear combination of complex exponentials $exp(j2\pi(xu + yv))$ with complex weights F(u,v). If the complex weight is written in polar form the amplitude and phase are achievable

$$F(u,v) = F_r(u,v) + jF_i(u,v) = |F(u,v)|\, exp(j\angle F(u,v)) \tag{2.14}$$

where the amplitude and the phase are defined by $|F(u,v)|$ and $\angle$ F(u,v) respectively [51].

$$\begin{cases} |F(u,v)| = \sqrt{F_r(u,v)^2 + F_i(u,v)^2} \\ \angle F(u,v) = tan^{-1}\left[F_i(u,v)/F_r(u,v)\right] \end{cases} \tag{2.15}$$

According to the mathematical rules of polar coordination, we can write frequency as w=$\sqrt{u^2+v^2}$ and direction as $\theta = tan^{-1}(v/u)$. The unit vector along direction (u,v) is $\vec{n} = (\frac{u}{w}, \frac{v}{w})$ and $\vec{r} = (x,y)$ is a vector in (x,y) direction. Therefore $\vec{r} \cdot \vec{n}$ gives the projection of a spatial point (x,y) in $\vec{n}$ direction. In order to find 2D electron density, we can write form factor function as equation 2.16 and then, according to the favorable phases, the electron density can be found for each point by equation 2.17 [50].

$$F(h,k) = \int_{\text{unit cell}} \rho(X,Y) \exp(-2\pi i(X,Y)\cdot(h,k)) dXdY \tag{2.16}$$

$$\rho(X,Y) = \int F(h,k) \exp(2\pi(X,Y)\cdot(h,k)) dhdk \tag{2.17}$$

where X=x/a and Y=y/a and a is lattice parameter.

The distance between two nearest planes with the same miller indexes is called d-spacing or interplanar spacing (for 2D lattice d_{hk}). For two-dimensional hexagonal lattice, this element is

$$d_{hk} = \frac{\sqrt{3}}{2} \frac{a}{\sqrt{h^2+hk+h^2}} \tag{2.18}$$

where a is lattice parameter and h, k are miller indexes. The d-spacing has the constant amount for all of the nearest planes, but during analyzing the scattered pattern, it is more important to know the calculated d-spacing by Bragg's law is related to which certain planes in the lattice. Finding the same d-spacing for different miller indexes during X-ray scattering is called multiplicity.

The multiplicity factor shows how many family planes with the same d spacing is in the certain lattice. The multiplicity factor for 2-dimensional hexagonal lattice is defined in table 2.1.

The diffraction peak is proportional to the multiplicity

$$I(hkl) = |S(hkl)|^2 \times M_{hkl} \times LP(\theta) \times TF(\theta) \tag{2.19}$$

Table 2.1: The multiplicity value for different plane families in 2D hexagonal lattice [49].

Plane	Multiplicity factor
(h h)	6
(h k)	12
(h 0)	6
(0 k)	6

where $S(hkl), M_{hkl}, LP(\theta)$ and $TF(\theta)$ are respectively the structure factor, multiplicity, Lorentz and polarization factor and temperature factor [48].

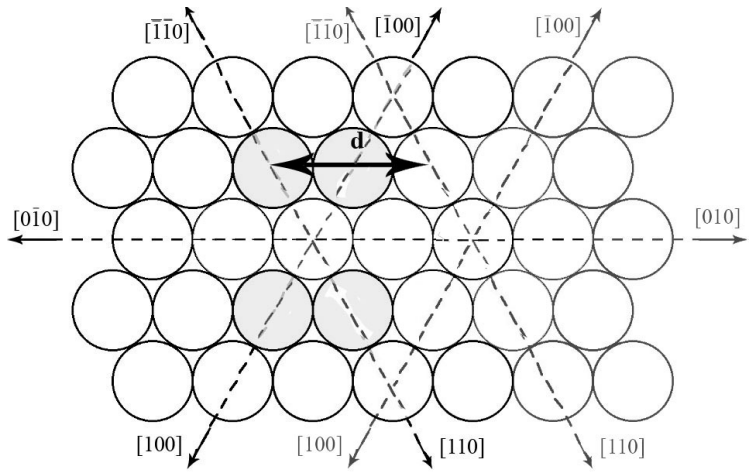

Figure 2.15: The schematic view of d-spacing between two similar planes in a hexagonal lattice.

2.5.2 X-ray data analysis

For analyzing the X-ray data, we used the home source Matlab scripts. The investigation in this program is based on the determination of lattice parameter and then calculating the electron density map of H_{II}. As you can see in figure 2.16 this program fitted the scattering pattern of DOPE according to Lorentzian fit and linear background. Normally, each inverse hexagonal scattering pattern consists of five or seven clear peaks. After

choosing the first peak manually, the program distinguishes other Bragg peaks of lattice automatically by vertical lines. If the vertical lines are near the scattering pattern peaks, the sample is really H_{II} and we can start to fit other peaks too. After fitting, at least, five peaks, the electron density map can be generated [8].

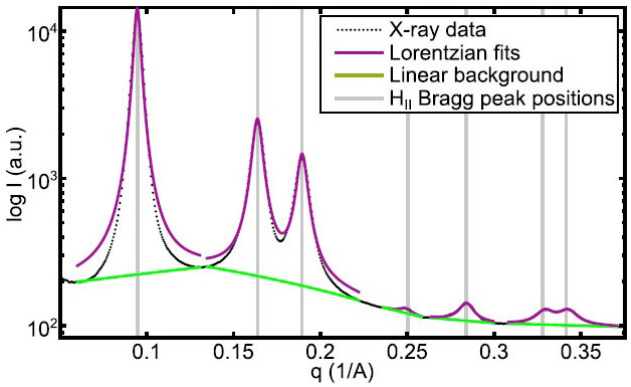

Figure 2.16: Fitting DOPE by Matlab. [8]

Estimations of this program are based on a formula which is described by Rappolt [9]. According to reflection law, the lattice parameter of inverse hexagonal phase (a) follows the equation 2.20

$$\frac{\sqrt{3}aq_{h,k}}{4\pi} = 1, \sqrt{3}, 2, \sqrt{7}, ... \tag{2.20}$$

where a is the lattice parameter, $q_{h,k}$ is scattering vector related to the (h,k) plane in the lattice and h, k are miller indexes. According to the Rappolt [9] formula, equation 2.20 and expanding Fourier series, electron density in real space is formulated in equation 2.21.

$$\rho(\vec{r}) = \sum_{h,k} \alpha_{h,k} \sqrt{\frac{I_{h,k}(q_{h,k}^2)}{m_{h,k}}}.cos(2\pi\vec{q}_{h,k} \cdot \vec{r}) \tag{2.21}$$

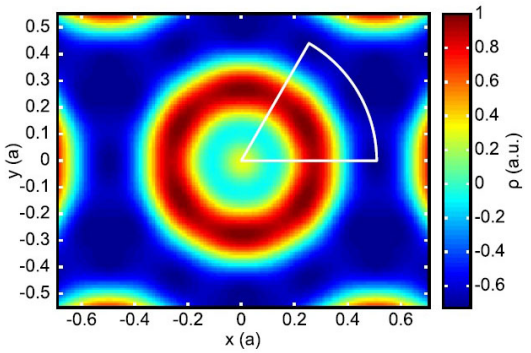

Figure 2.17: Electron density of DOPE made with Matlab. [8]

where $\alpha_{h,k}$ is the phase (± 1 for centrosymmetric structures as in this work), $I_{h,k}$ is intensity and multiply of this with quadratic scattering vector $q^2_{h,k}$ is called Lorentz correction, $m_{h,k}$ is the multiplicity of the equivalent diffraction planes (6 for (1,0), (1,1), (3,0)...; 12 for (2,1), (3,1), (3,2)...) [8].

2.5.3 Finding spontaneous curvature

The aim of our experiments is finding the spontaneous curvature of lipids from their electron density map. In order to estimate this parameter, it is necessary to find the radius of the neutral plane (R_0) first. The neutral plane is located where the bending and stretching energies are decoupled [39]. There is only 10% difference between the neutral plane and pivotal plane position [16]. According to former researches, we considered the position of the neutral plane at the glycerol backbone place [8, 16, 17, 43–45](See Figure 2.18). In this case we used the equation 2.22

$$R_0 = R_p + d_{H1} \tag{2.22}$$

where R_p is radius of the lipid head group and d_{H1} is the distance between head group and glycerol backbone of lipids. [8, 16, 17]

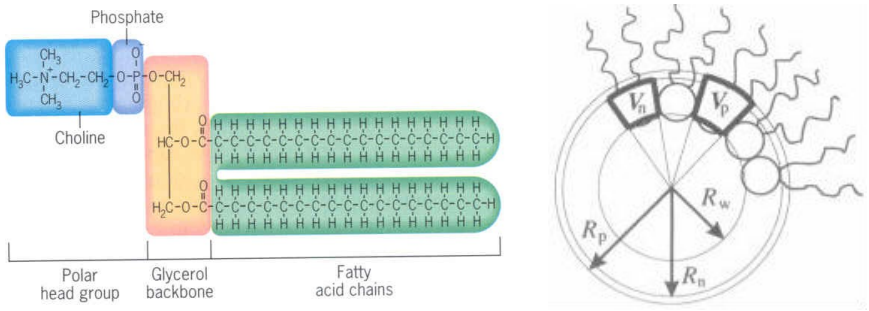

(a) (b)

Figure 2.18: (a)Schematic view of phospholipid [28].
(b)R_n, R_p and R_w are related separately to the radius of neutral plane, radius of pivotal plane and radius of water inside cylinder. V_n and V_p are related to the neutral and pivotal unit volumes respectively [39].

In order to find the R_p, our program uses the Gaussian fitting of the maximum peak in the electron density plot. d_{H1} was previously determined. [10–13] In our program, the average value of d_{H1} is a constant.($d_{H1} = 0.44 \pm 0.05$)

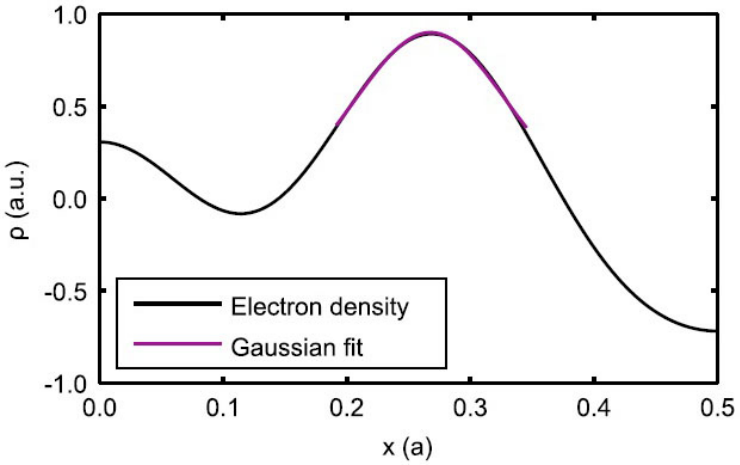

Figure 2.19: Gaussian fit of head group in a radial cross section of electron density. [8]

After these calculations, spontaneous curvature (J_0) could be derived from

neutral plane radius.(equation. 2.23) [14, 15]

$$R_0 = \frac{-1}{J_0} \tag{2.23}$$

In order to find the accurate spontaneous curvature for lipid monolayers, it is necessary to remove stress from the lipid structure. In our case, 9-cis-Tricosene mixed to our lipid structure to decrease the stress in the inverse hexagonal phase. Because Tricosene fills the interstitial regions among the inverse hexagonal structure and causes reduced packing frustration energy of acyl chains to a stress-free state. [15]

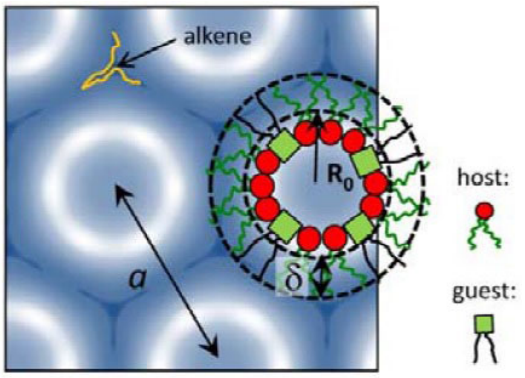

Figure 2.20: The position of Tricosene (alkene) in inverse hexagonal structure. [15]

Some lipids such as PCs are bilayer forming lipids, therefore, it is impossible to find the spontaneous radius of curvature in a pure system. In order to find the spontaneous curvature of this kind of lipids, they are mixed as a host with monolayer making lipids such as PEs. According to the equation 2.24 it is possible to find the monolayer spontaneous curvature for bilayer lipid. χ in this equation related to concentration of guest lipid. [8]

$$J_0^{mix} = \chi J_0^{guest} + (1-\chi) J_0^{host} \tag{2.24}$$

2.5.4 Extrapolation

One of the methods to find the monolayer spontaneous curvature of bilayer lipids is to mix them as the guest lipids in one monolayer forming lipid

host structure. During this process, the spontaneous curvature of a mixture of lipids changes compared to the spontaneous curvature of the pure host structure. This difference is a function of guest lipid concentration. Then the extrapolation helps to find the monolayer spontaneous curvature of the bilayer lipid. Normally the inversed hexagonal phase is used as the lipid host template for finding monolayer spontaneous curvature of the bilayer forming lipids [52]. Actually, this method predicts monolayer spontaneous curvature of the guests according to the change's of spontaneous curvature of some different samples with different mole fractions.

$$J_0^{min} = \sum_i \chi i J_0^i \tag{2.25}$$

where χ^i and J_0^i are mole fraction and spontaneous curvature of the i-th sample.

3 Results

This research was based on making inverse hexagonal phase with RSE method. After determining the suitable lipid, an alkene was added to this lipid to generate a stress-free structure. Then, some guest lipids were added to the base lipid to find the guest lipid's monolayer spontaneous curvature. This chapter consists of more information about each level of our experiments.

3.1 DOPE

DOPE or 1,2-dioleoyl-sn-glycero-3-phosphoethanolamine is a non-bilayer forming lipid which can make the hexagonal structures. In the first level of our experiment, we wanted to determine if the inverse hexagonal phase of DOPE can be generated with RSE? In Table 3.1, you can find the RSE parameters used in this experiment.

In our case, the DOPE was dissolved in an organic solvent to a 30 mg/ml concentration. Chloroform/Methanol with ratio [9:1] was used as our organic solvent. The ratio of water/organic solvent was 1:1 in each sample. The same amount of water was injected into the test tube and put in the oven in the 45°C (same as RSE temperature). After four minutes the test tube was removed from the oven and lipid stock was injected into it and was placed for five minutes in RSE device. After RSE the sample looked like a white paste floating in an aqueous environment.

Table 3.1: The RSE parameters for making H_{II} of DOPE.

Temperature (°C)	Pressure (mbar)	Vortex speed (rpm)	Argon flow (ml/min)
45	200	1800	61

We checked each sample by SAXS, to find their structures. The paste part of the sample was put in the center of a paste cell and soaked with the aqueous part. The sample was exposed to X-rays at 25°C for small angle scattering X-ray spectroscopy. A representative scattering pattern can be seen in Figure 3.1. The SAXStreat program converted the 2-D scattering pattern to the intensity versus scattering vector graph. Figure 3.2 shows the first peak is the most intense peak. Also, there are two peaks near each other and some other small peaks are at the short distance from them. This kind of pattern seems to be related to the hexagonal structure, but, it was necessary to find the lattice parameter and unit cell to know for sure. It is possible to find the lattice parameter (a) from scattering vector (q) using equation 2.20. In this case, we have found the lattice parameter for the pure DOPE as 7.38 nm which is a reasonable value when compared to reference. [18]

In this experiment, the SAXSpace instrument was used. It is a measuring system for analyzing nano-soft materials with small angle X-ray scattering (SAXS) or wide-angle X-ray scattering (WAXS). It is made by Anton Paar Company (Austria). It can investigate materials in the range of 1 to 200 nm in the temperature range of -150°C to 500°C. The detection system can be aligned analog or digital to find 2D or 1D scattering pattern.

The final paste sample was put in the paste cell sample holder and placed in SAXS machine. The temperature and SDD (sample to detector distance) were 25°C and 308 nm respectively for all of the samples. The exposure time for each sample was about one hour.

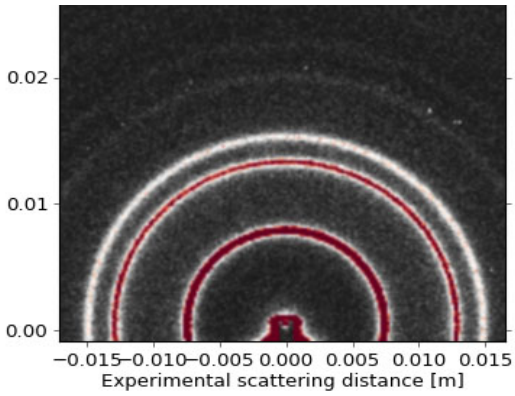

Figure 3.1: The scattering pattern of DOPE after SAXS measurement.

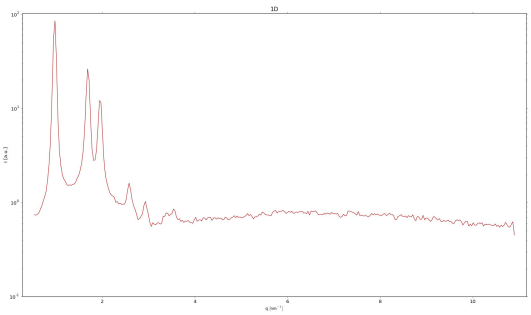

Figure 3.2: The intensity (I) versus scattering vector (q) made by SAXStreat.

After analysis of the DOPE data it was clear that we were able to make the inverse hexagonal phase of DOPE with RSE.

3.2 DOPE-Tricosene mixture

The next step of our experiments was finding the spontaneous curvature of some bilayer making lipids by mixing them into the DOPE lattice. In this case, the mixture stocks of DMPC, DPPC, DSPC, SM, and Ceramide in DOPE were made with the participation of 9-Cis-Tricosene. The exact information about these experiments is available in this section.

3.2.1 Alkene

Alkene is an unsaturated hydrocarbon chain with at least one carbon double bond. There is no chemical functional group in the alkene and they are soluble in an organic solvent. The chemical formula of this organic element is C_nH_{2n} [29].

3.2.2 9-Cis-Tricosene

9-Cis-Tricosene is an alkene, which works as a fly sex hormone and a bee communication chemical in nature. [19] Its chemical formula is $C_{23}H_{46}$. As described in 2.5.2, adding Tricosene in inverse hexagonal phase decreased the packing frustration by reducing the stretch force of lipid hydrocarbon chains in void regions.

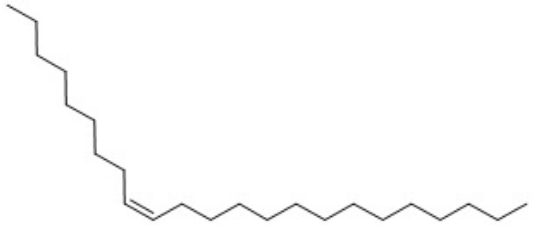

Figure 3.3: The schematic chemical structure of Tricosene. [20]

After determining the inverse hexagonal phase of DOPE can be made with RSE, different weight fraction of 9-Cis-Tricosene was added to DOPE, to find the best lattice structure with RSE.

The experimental Tricosene weight fractions were: 2.5%, 5%, 7.5%, 10%, 11%, 12%, 12.5%, 13%, 14%, 15% WT. Normally the weight fraction ratio (WT%) is used for measuring exact concentration of one element in another element mixture. In our case, we have found the concentration of Tricosene in DOPE with this method according to the equation 3.1, where $W_{Tricosene}$and W_{DOPE} are Tricosene and DOPE masses respectively. For making each lipid solution stock, DOPE with concentration 30 mg/ml was dissolved in C/M [9:1] and Tricosene with 10 mg/ml concentration was dissolved in C/M [9:1]. The water/organic solvent ratio was considered 1:1 for each stock. The water was put in the test tube and preheated for four minutes in the oven at 45°C. Then the DOPE and Tricosene solutions were added to the water respectively. After that, the test tube consisting of this mixture was put in the RSE for five minutes under 45°C temperature, 200 mbar pressure, 1800 rpm of the vortex and 61 ml/min of Argon flow.

$$WT\% = \frac{W_{Tricosene}}{W_{Tricosene} + W_{DOPE}} \times 100 \tag{3.1}$$

After RSE, samples were separately measured with SAXS for one hour at 25°C. As described in section 3.1 finally the lattice parameter of H_{II} for each sample was calculated and summarized in Table. 3.2

Table 3.2: Lattice parameter (a) for different weight fractions of Tricosene in DOPE.

Weight fraction WT %	Lattice parameter (a±Δa) [nm]
0	7.43 ±0.05
2.5	7.64 ± 0.05
5	7.81 ± 0.05
7.5	7.91 ± 0.05
10	7.99 ± 0.05
11	8.00 ± 0.05
12	8.04 ± 0.05
12.5	8.10± 0.05
13	8.05 ± 0.05
14	8.03 ± 0.05
15	8.10 ± 0.05

After fitting the SAXS data with Matlab, the spontaneous curvature (J_0) and electron density pattern were found.

The X-ray scattering patterns were analyzed by SAS Data Analysis and Origin 7 SR4. One of the properties of hexagonal phase is that the peak positions of intensity (I) versus scattering vector (q) follow the $1, \sqrt{3}, 2, \sqrt{7}$,... ratios. As you can see in Figure 3.4, the scattering pattern for each sample has a hexagonal phase shape, i.e. one high peak at the beginning and two other smaller peaks near each other. Therefore, the samples seem to be in hexagonal phase. However, as you can see in the X-ray diffraction pattern related to 15 WT%, there is a small peak that emphasized by a black arrow in Figure 3.4 ($q_2^{'} = 1,25\ nm^{-1}$), which suggests this sample was in another phase or in coexisting phases in this regime. The other small peak (pointed with red arrow) in $q_1^{'} = 0,82\ nm^{-1}$ shows that $q_2^{'}$ peak was not related to lamellar phase because it is not double of $q_1^{'}$. Therefore, more experiments are need to explain the reason of appearing these unknown peaks.

According to the peak positions, the lattice parameter (a) and hexagonal repeat spacing position (d_{hex}) are computable. These values were calculated by equations 3.2 and 3.3,

$$q = 2\pi / d_{hex} \tag{3.2}$$

$$a = \frac{2}{\sqrt{3}} d_{hex} \tag{3.3}$$

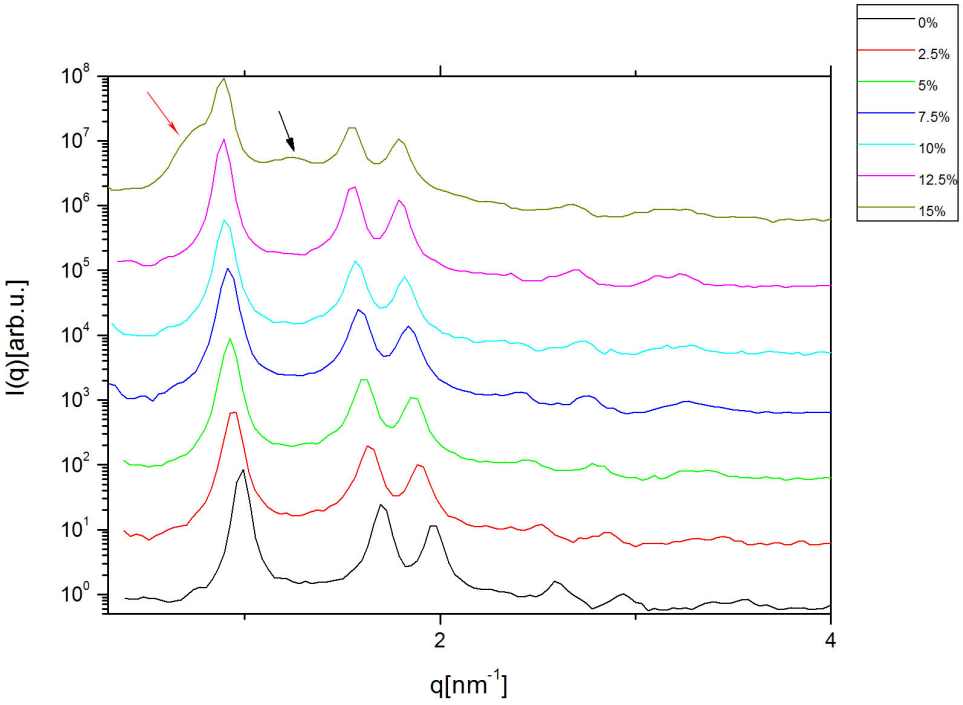

Figure 3.4: The intensity versus scattering vector for DOPE-tricosene samples with different weight fraction. The red and black arrows in the graph of 15% WT sample show coexisting or phase interference.

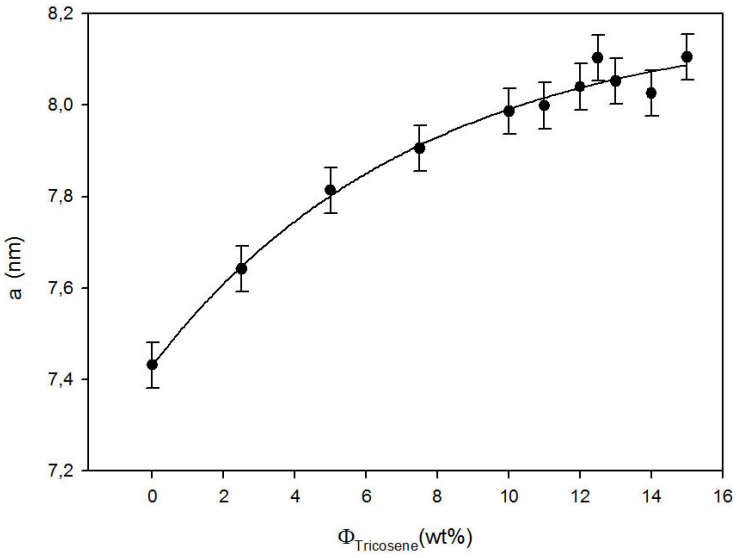

Figure 3.5: The lattice parameter (a) versus weight fraction for DOPE-Tricosene samples.

Figure 3.5 shows the lattice parameter after 12%WT goes to the plateau. After the 12% WT sample, we can see some disorder in length of lattice parameter according to figure 3.5. Therefore, we have chosen DOPE-Tricosene 12% WT as our base host environment for our further experiments.

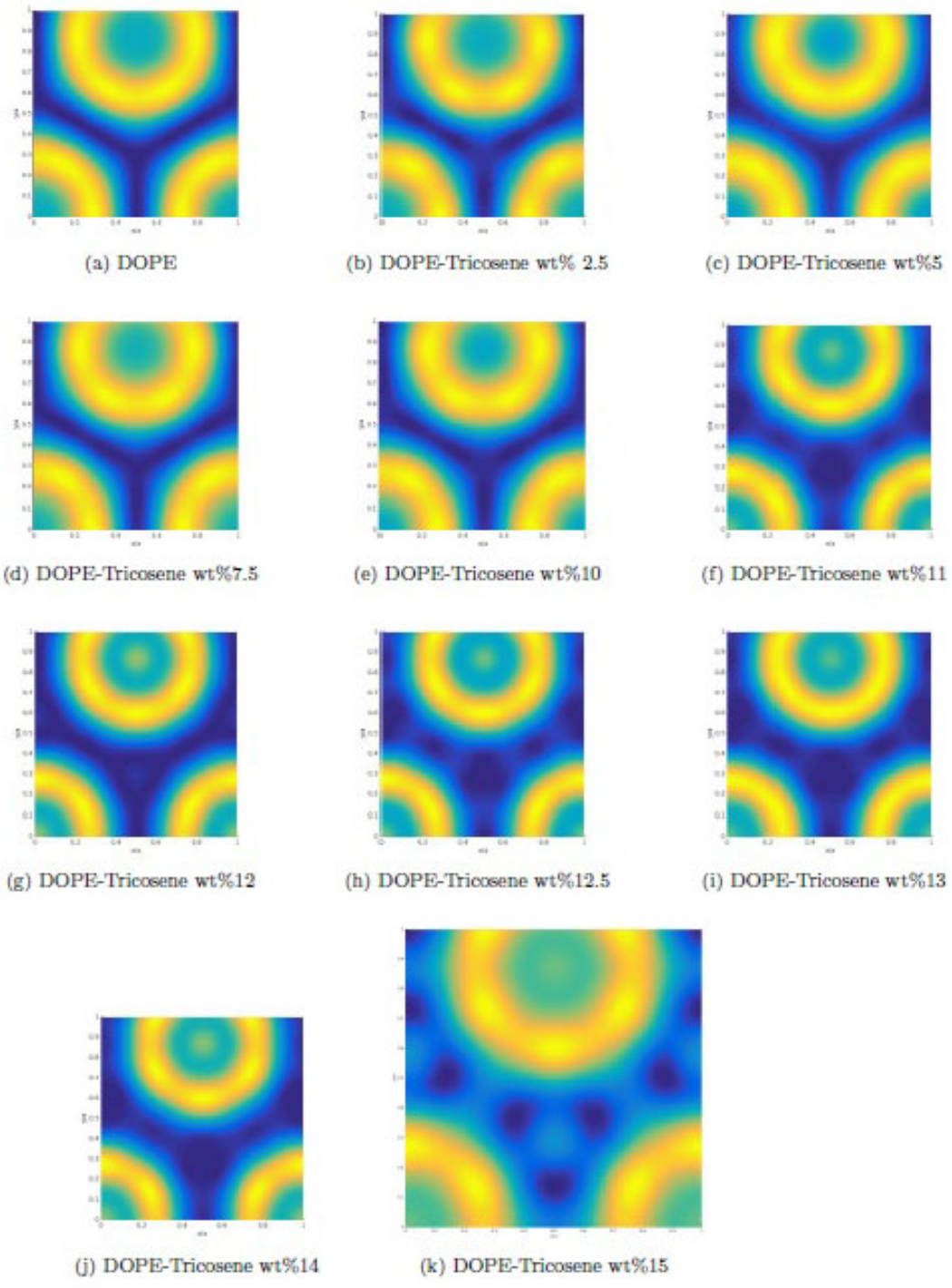

(a) DOPE (b) DOPE-Tricosene wt% 2.5 (c) DOPE-Tricosene wt%5

(d) DOPE-Tricosene wt%7.5 (e) DOPE-Tricosene wt%10 (f) DOPE-Tricosene wt%11

(g) DOPE-Tricosene wt%12 (h) DOPE-Tricosene wt%12.5 (i) DOPE-Tricosene wt%13

(j) DOPE-Tricosene wt%14 (k) DOPE-Tricosene wt%15

Figure 3.6: The electron density map for different weight fractions of DOPE-Tricosene samples.

3.3 Mixing different lipids with DOPE-Tricosene 12 wt%

Finding the spontaneous curvature of the bilayer making lipids is possible only when they are added as a guest to the monolayer making lipid structure. In our case, DMPC, DPPC, DSPC, and SM were added to the DOPE-Tricosene 12 wt%. You can find further information in this section.

3.3.1 DOPE-DMPC-Tricosene 12 wt%

Firstly, 30 mg/ml concentration of DMPC was dissolved in C/M [9:1]. Also, DOPE with 30 mg/ml was dissolved in C/M [9:1]. The concentration of 9-Cis-Tricosene was 10 mg/ml in C/M [9:1]. The weight fraction of Tricosene in DOPE was 12 wt%. The water/organic solvent in each sample was 1:1.

For forming a favorable mixture of different lipids, the first step is finding mole fraction which means the amount of a constituent divided by the total amount of all constituents in the mix. [21] Here the mole fraction of DMPC as a guest on DOPE as a host was found from equation 3.4

$$mol\% = \frac{\frac{m_{DMPC}}{M_{DMPC}}}{\frac{m_{DMPC}}{M_{DMPC}} + \frac{m_{DOPE}}{M_{DOPE}}} \times 100 \tag{3.4}$$

where m_{DMPC} is the mass of DMPC and M_{DMPC} is the molecular weight of DMPC and m_{DOPE} is the mass of DOPE and M_{DOPE} is the molecular weight of DOPE. In our case, the total lipid mass for each stock was 7.5 mg. For making the sample, first, the required amount of DOPE and DMPC were measured, then separately lipids were dissolved in the organic solvent. One test tube was filled with water and put in the oven at 45°C for four minutes. The quantity of water and the organic solvent was equal in each lipid stock.According to the mole fraction of DMPC, the suitable amount of DOPE and DMPC solutions was mixed in separate vials. 10, 20, 30, 40, 50 mol% samples were made. Lipids and tricosene solutions were added to warmed water and put in the RSE device to make a sample. The RSE process took five minutes. Table 3.3 shows the parameters.

After Making samples in RSE, they were checked with SAXS. Each sample was examined with SAXS for different temperatures (20°,30°,40°,50°C) and each temperature took approximately one hour. The scattering pattern of

Table 3.3: The RSE parameters for making H_{II} of DOPE-DMPC-Tricosene 12 wt%.

Temperature (°C)	Pressure (mbar)	Vortex speed (rpm)	Argon flow (ml/min)
45	220	1800	61

SAXS was used to find the lattice parameter and spontaneous curvature, after fitting with Matlab. Figure 3.7 shows the lattice parameter (a) versus different mole fractions of DMPC. These graphs indicate that the lattice parameter increases with increasing the DMPC mole fraction. This increasing is approximately linear. That means with increasing the mole fraction, the radius of the lipid tubes increases. That means increasing ratio of DMPC caused more DMPC goes into the lattice structure. This kind of lipid has a larger headgroup compared to DOPE. Of course, the increased amount of this bilayer-making lipid, inside of inverted hexagonal structures hosted by DOPE, caused larger lipid tube radius and, therefore, a bigger distance between the center of tubes. As a consequence a larger lattice parameter is observed compared to the pure DOPE lattice parameter amount.

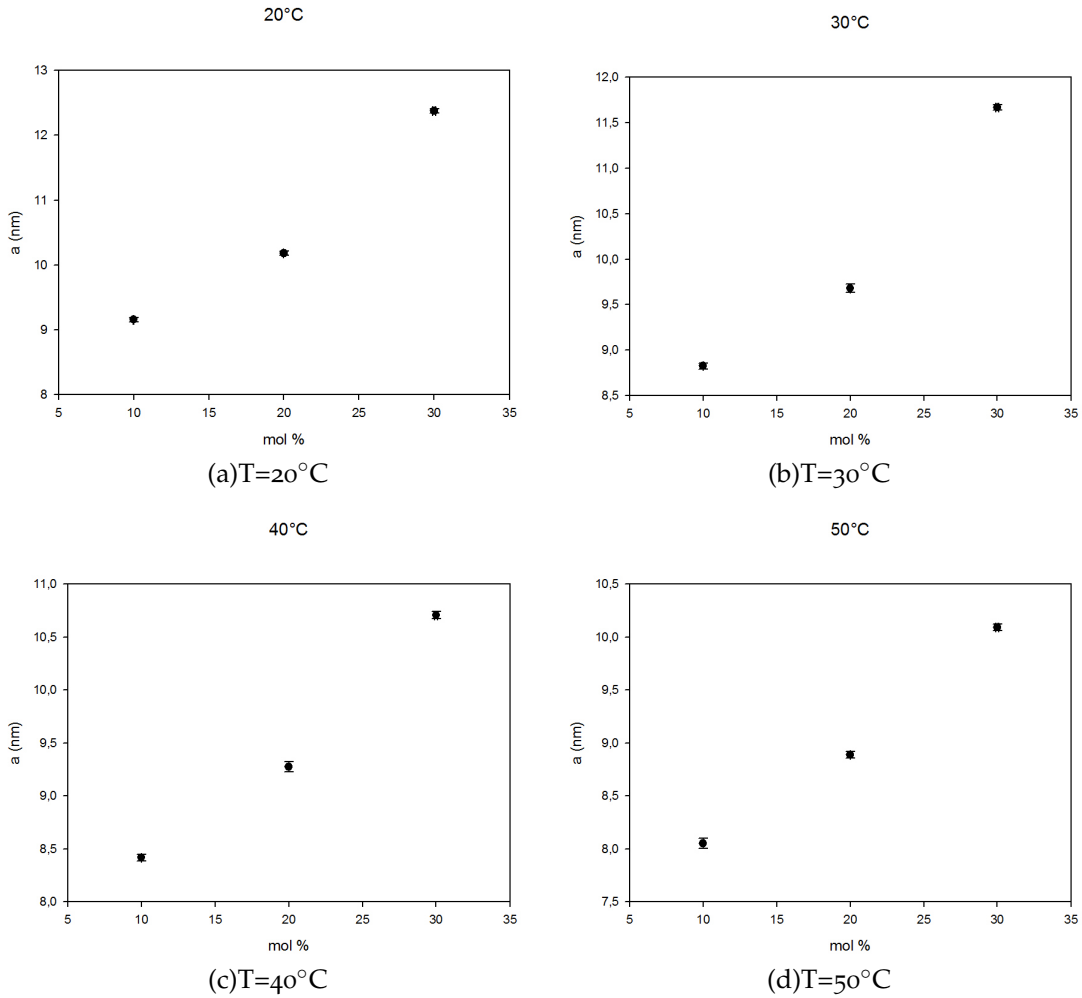

(a)T=20°C (b)T=30°C

(c)T=40°C (d)T=50°C

Figure 3.7: Lattice parameter versus mole fraction in different temperatures for DOPE-DMPC-tricosene 12wt%.

Figure 3.8 indicates the change in lattice parameter of DOPE-DMPC-tricosene 12 wt% with changing of temperature. For each mole fraction, the lattice parameter decreases linearly with increasing temperature. This information tells us that for the certain mole fraction, increasing the temperature caused a rise in mobility of hydrocarbon chains. Therefore, they occupied more space causing pressure on the hydrophilic part of the structure. That means lipid head groups sit close to each other. The radius of

hexagonal rods decreases and the distance between the center of neighbor rods decreases too. That caused a decreasing of lattice parameter.

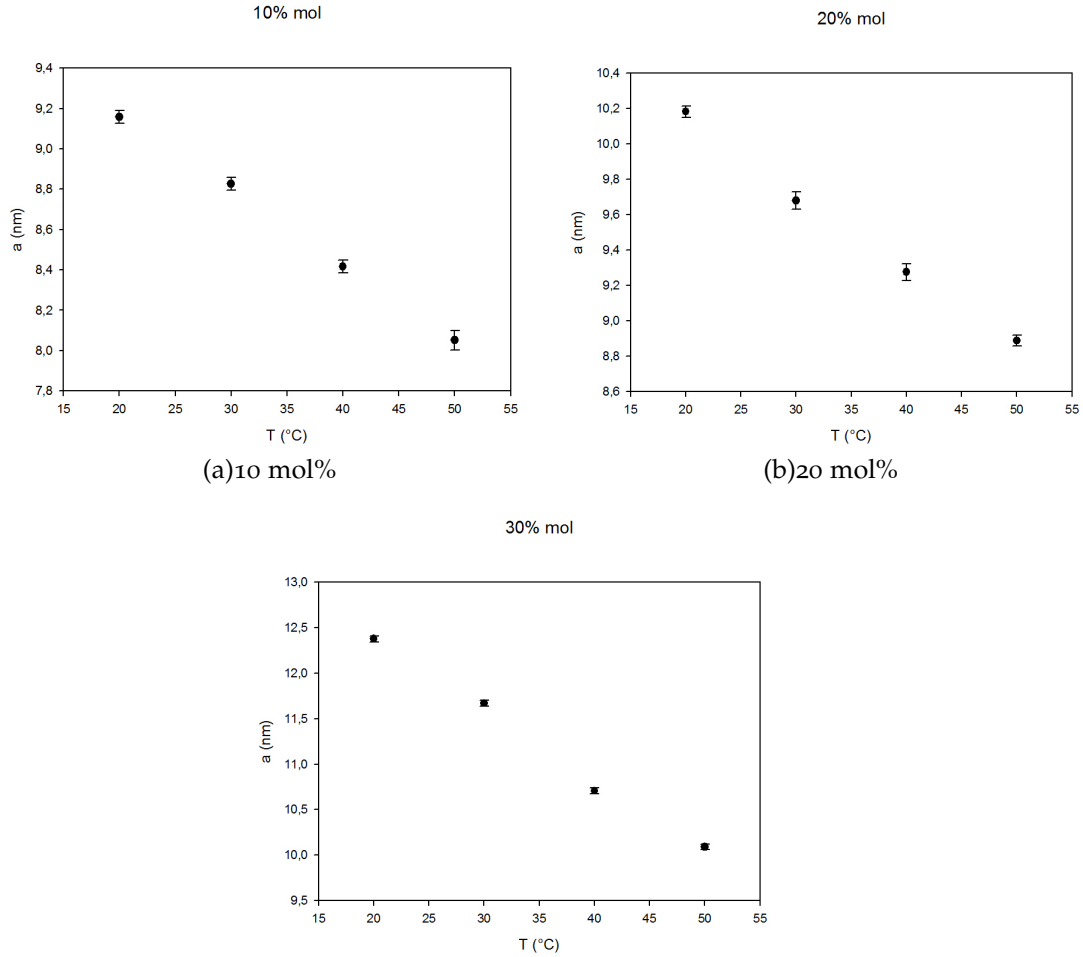

(a)10 mol% (b)20 mol%

(c)30 mol%

Figure 3.8: Lattice parameter versus temperature for different mole fractions of DOPE-DMPC-tricosene 12wt%.

In figure 3.9 you can find how the spontaneous curvature of DMPC changed with increasing the mole fraction. In this case, there is linear increasing. With increasing mole fraction, the amount of DMPC guests increases in the DOPE host structure. That means the amount of lipids with

positive intrinsic curvature increases in comparison to negative intrinsic curvature lipid host. Therefore, J tends to be more positive with increasing mole fraction value.

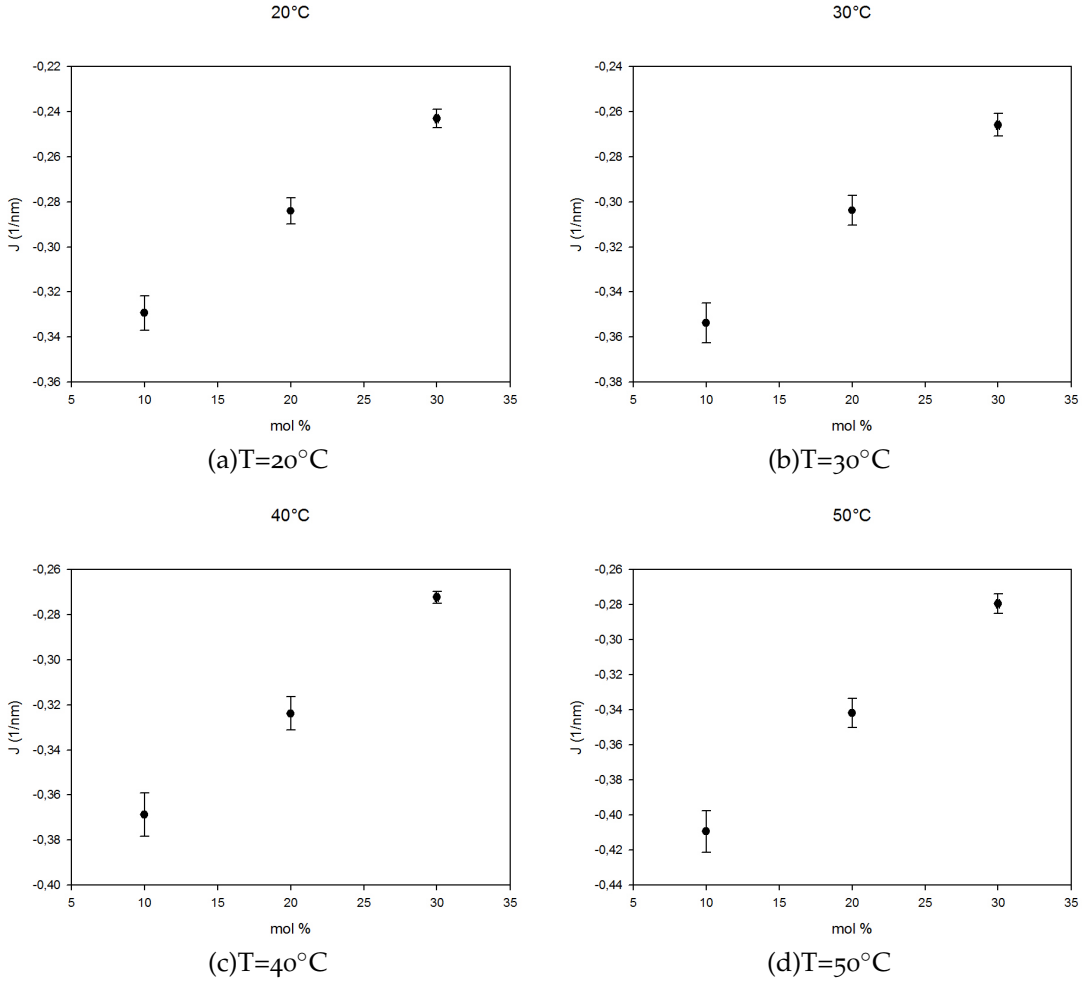

(a)T=20°C (b)T=30°C

(c)T=40°C (d)T=50°C

Figure 3.9: Spontaneous curvature (j) versus different mole fractions of DOPE-DMPC-tricosene 12wt%.

According to figure 3.10, it is understandable that with increasing temperature for each mole fraction, the spontaneous curvature decreases. Because the increasing temperature in a certain mole fraction causes increased mobility of carbon chains and, therefore, making close packed in head parts.

That cause smaller rod cross section and, therefore, the more negative spontaneous curvature of the surface.

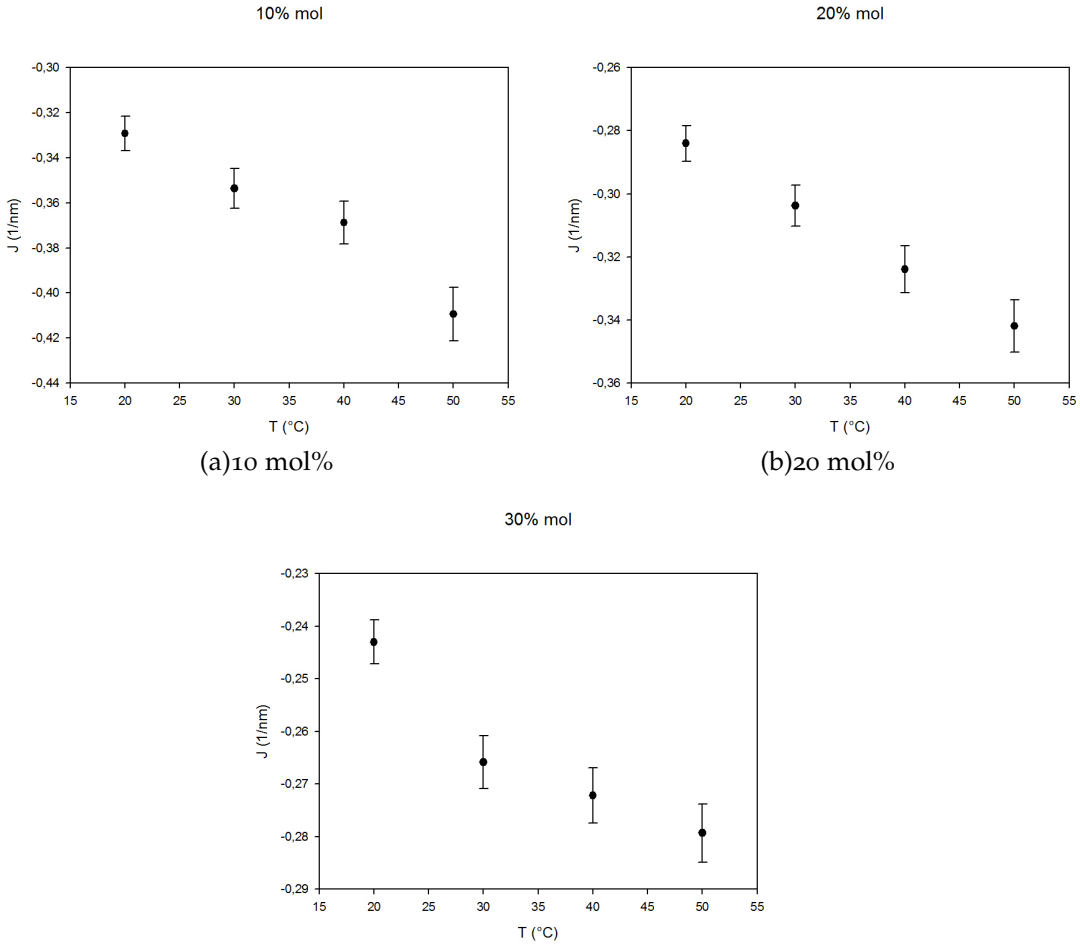

(a)10 mol%

(b)20 mol%

(c)30 mol%

Figure 3.10: Spontaneous curvature (j) versus different mole fractions of DOPE-DMPC-tricosene 12wt%.

As described in section 2.5.4, after extrapolation we can find the value of spontaneous curvature for pure DMPC monolayer. Figure 3.11 indicates the extrapolation of spontaneous curvature of DMPC in DOPE-tricosene 12% WT. The value of monolayer spontaneous curvature of DMPC is near zero.

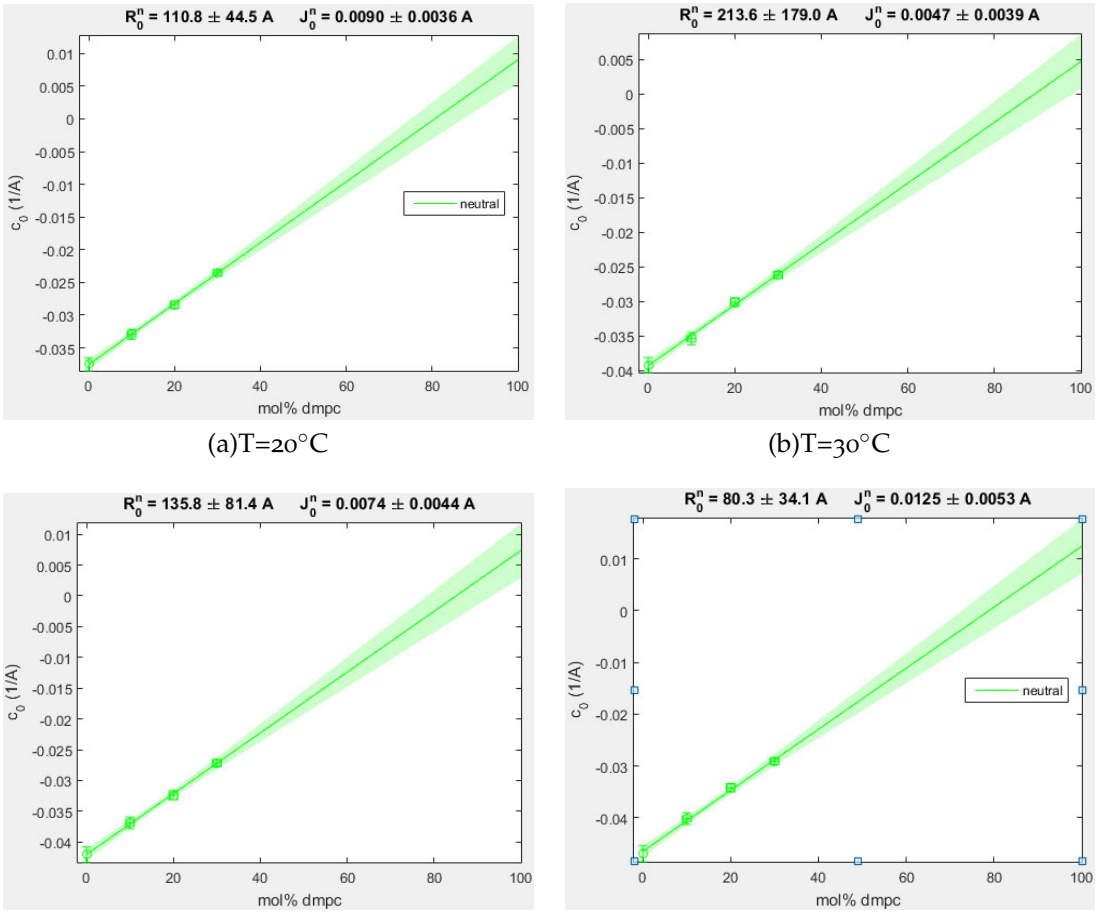

(a)T=20°C (b)T=30°C

(c)T=40°C (d)T=50°C

Figure 3.11: The extrapolation graphs of DMPC in DOPE-tricosene 12%WT in different temperatures.

3.3.2 DOPE-DPPC-Tricosene 12 wt%

Similar to the last section, DOPE and DPPC with concentration 30 mg/ml were dissolved separately in C/M [9:1] and 9-Cis-Tricosene was solved with 10 mg/ml concentration in C/M [9:1]. The weight fraction of Tricosene in DOPE was considered as 12 wt% and different mole fractions of DPPC in DOPE were made:10, 20, 30, 40, 50 mol%. For finding the exact amount of DPPC for each lipid stock, the equation 3.4 was used. In table 3.4 you can

find the RSE parameters for this experiment.

Table 3.4: The RSE parameters for making H_{II} of DOPE-DPPC-Tricosene 12 wt%.

Temperature (°C)	Pressure (mbar)	Vortex speed (rpm)	Argon flow (ml/min)
45	220	1800	61

After making samples with RSE, they were checked with SAXS in different temperature ranges from 20°C to 50°C to find their lattice structure properties.

Figure 3.12 shows the lattice parameter increases with an increasing mole fraction of DPPC in any temperature, but there is not any ordered pattern for this increasing. In additional, increasing of mole fraction of DPPC caused an increasing of the radius in cross section of the lipid tubes. Therefore the difference between the center of the nearest neighbor tubes increased, that caused increasing of the lattice parameter. Increasing of mole fraction means raising the amount of bilayer-making lipids (DPPC) and decreasing the amount of monolayer-making host lipid (DOPE). Therefore, the intrinsic curvature of a mixture of these lipids structure tended to be more positive.

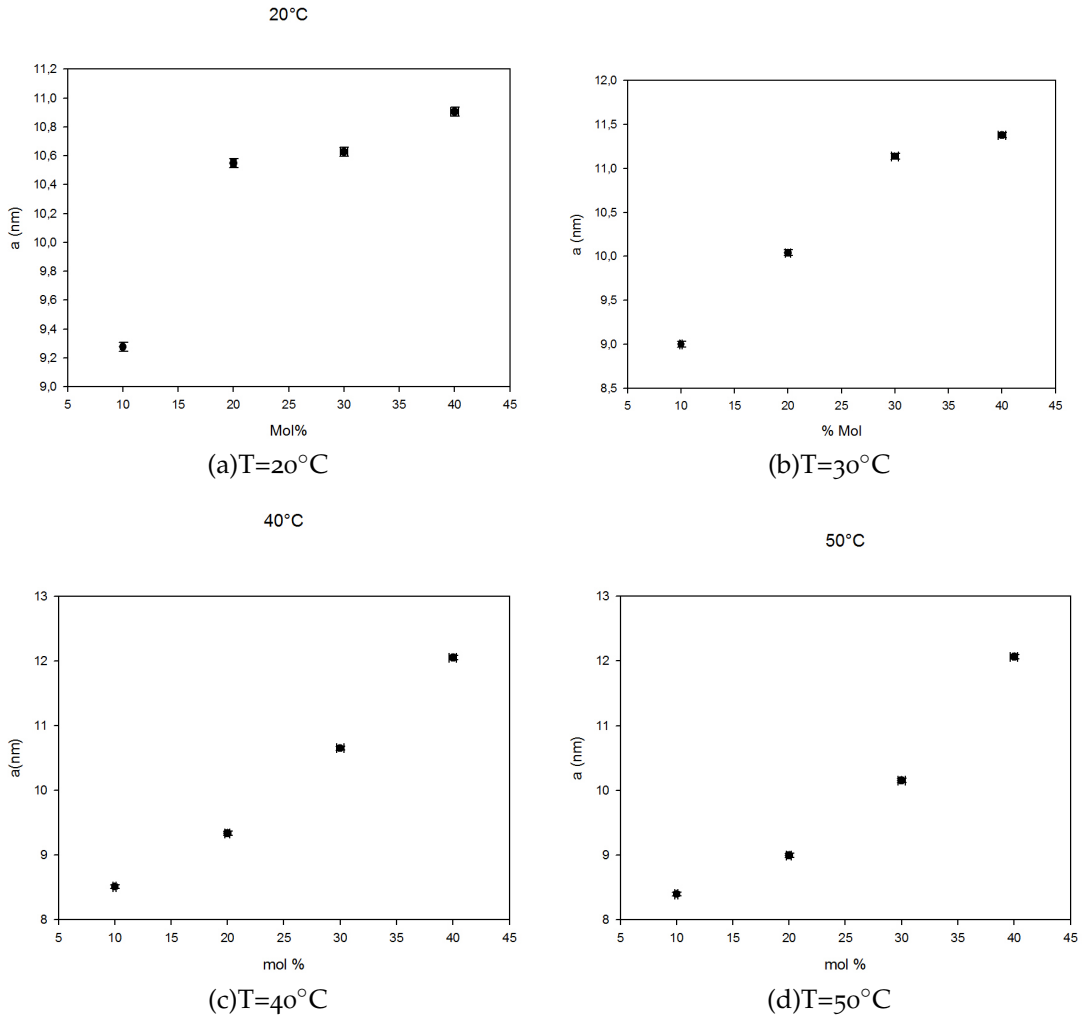

(a)T=20°C (b)T=30°C

(c)T=40°C (d)T=50°C

Figure 3.12: Lattice parameter (a) versus mole fraction for DOPE-DPPC-tricosene 12wt% in different temperatures.

In figure 3.13, one can see the lattice parameter versus temperature for various mole fractions of DPPC in DOPE-tricosene 12% wt. For 10,20 % mole fraction samples, increasing of temperature caused decreases in lattice parameter. This information suggests that for a certain mole fraction increasing the temperature caused an increased mobility of hydrocarbon chains. Therefore, they occupied more space that caused pressure on the

hydrophilic part of the structure. That means lipid head groups sit close to each other. Then the radius of hexagonal rods decreases and the distance between the center of neighbor rods decreases too. That caused a decrease of the lattice parameter. However, according to graphs c and d in figure 3.13, the 30 and 20 % mole fraction samples do not follow the same order. Maybe a change in phase structure was starting from 30 % mol or a coexisting phase happens in these two different mole fractions.

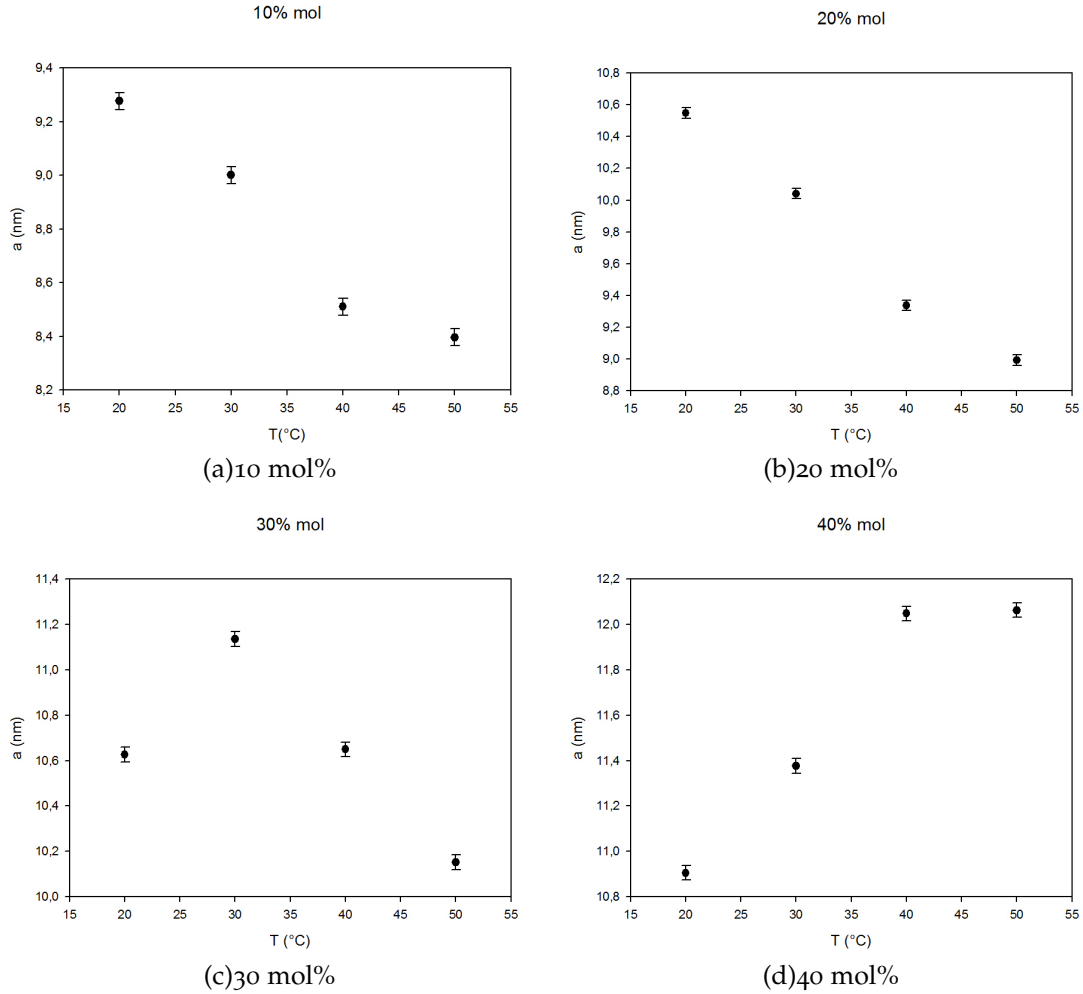

(a)10 mol% (b)20 mol%

(c)30 mol% (d)40 mol%

Figure 3.13: Lattice parameter (a) versus temperature for different mole fractions of DOPE-DPPC-tricosene 12wt%.

In figure 3.14, one can see the spontaneous curvature versus mole fraction of DOPE-DPPC-tricosene 12% wt for different temperature ranges. In addition, spontaneous curvature increased with increasing mole fraction in this case. With increasing mole fraction, the number of DPPC guests increase in DOPE host structure. That means the amount of lipids with positive intrinsic curvature increases in comparison to negative intrinsic curvature lipid host. Therefore, J tends to be more positive with increasing mole fraction value. In figure 3.15, one can find the change of spontaneous curvature (J) from the change in temperature for certain mole fractions of DOPE-DPPC-tricosene 12% wt. For 10, 20% mol samples, J decreased dramatically with increasing the temperature. Increasing temperature in a certain mole fraction causes increased the mobility of carbon chains and therefore making the headgroups closely packed. That causes smaller rod cross section and, therefore, the more negative spontaneous curvature of the surface. For 30, 40% mol samples, there is not any meaningful order for spontaneous curvature versus temperature. Maybe in these samples, change in phases or coexisting phases occurred or maybe there was some problem with making these samples which caused incompleted solvation of DPPC in DOPE-tricosene 12% wt.

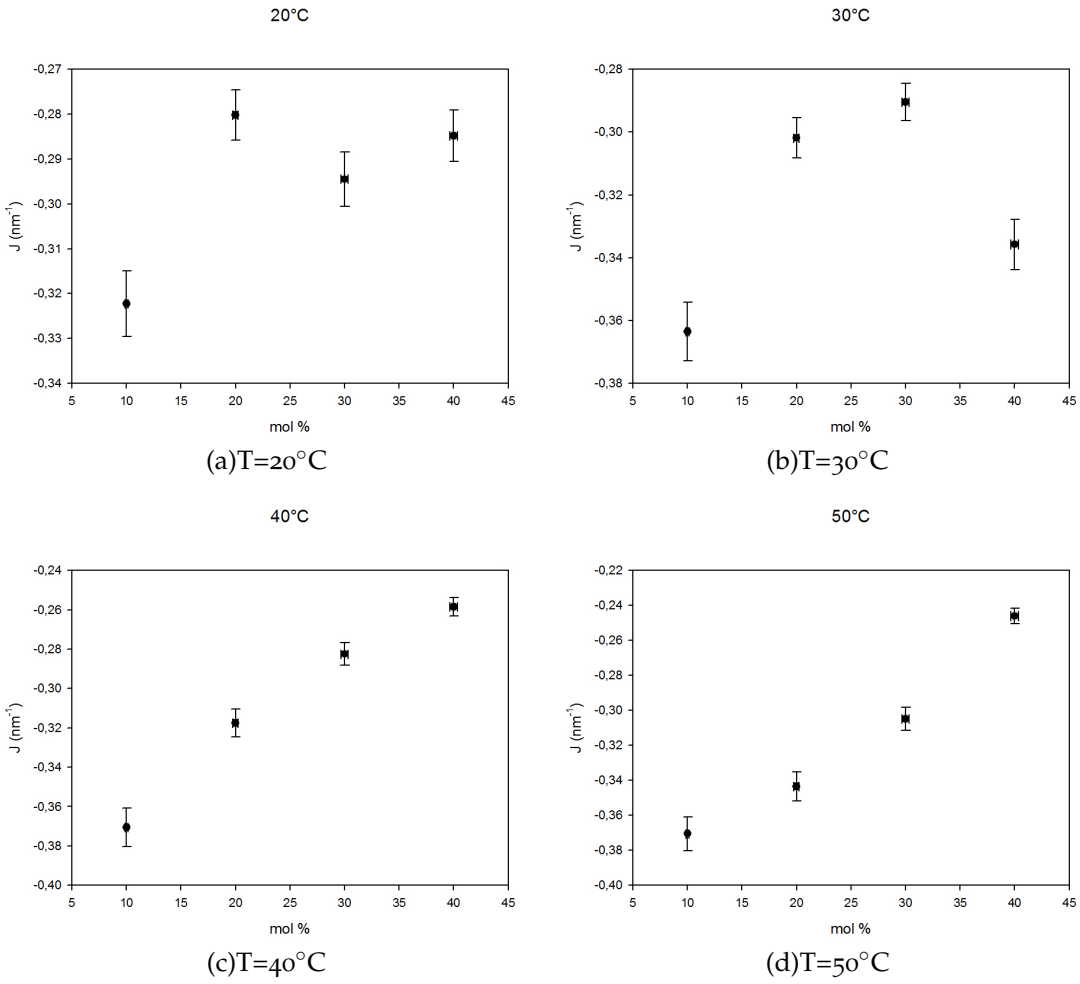

(a)T=20°C (b)T=30°C

(c)T=40°C (d)T=50°C

Figure 3.14: Spontaneous curvature (j) versus the mole fraction of DOPE-DPPC-tricosene 12wt% for different temperatures.

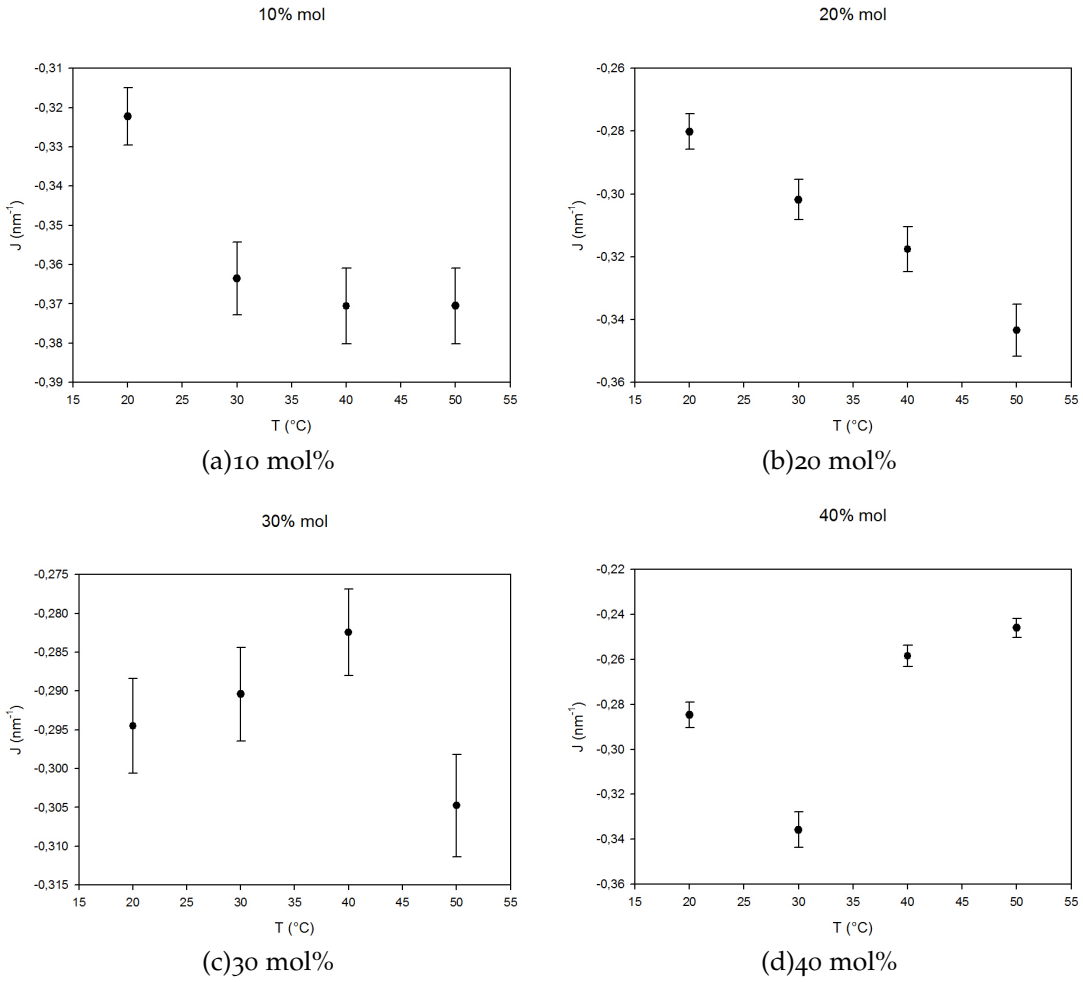

(a)10 mol% (b)20 mol%

(c)30 mol% (d)40 mol%

Figure 3.15: Spontaneous curvature (j) versus temperature for different mole fraction DOPE-DPPC-tricosene 12wt%.

One can find extrapolation of spontaneous curvature of DPPC in DOPE-tricosene 12% WT in figure 3.16. The value of monolayer spontaneous curvature of DPPC is near to zero.

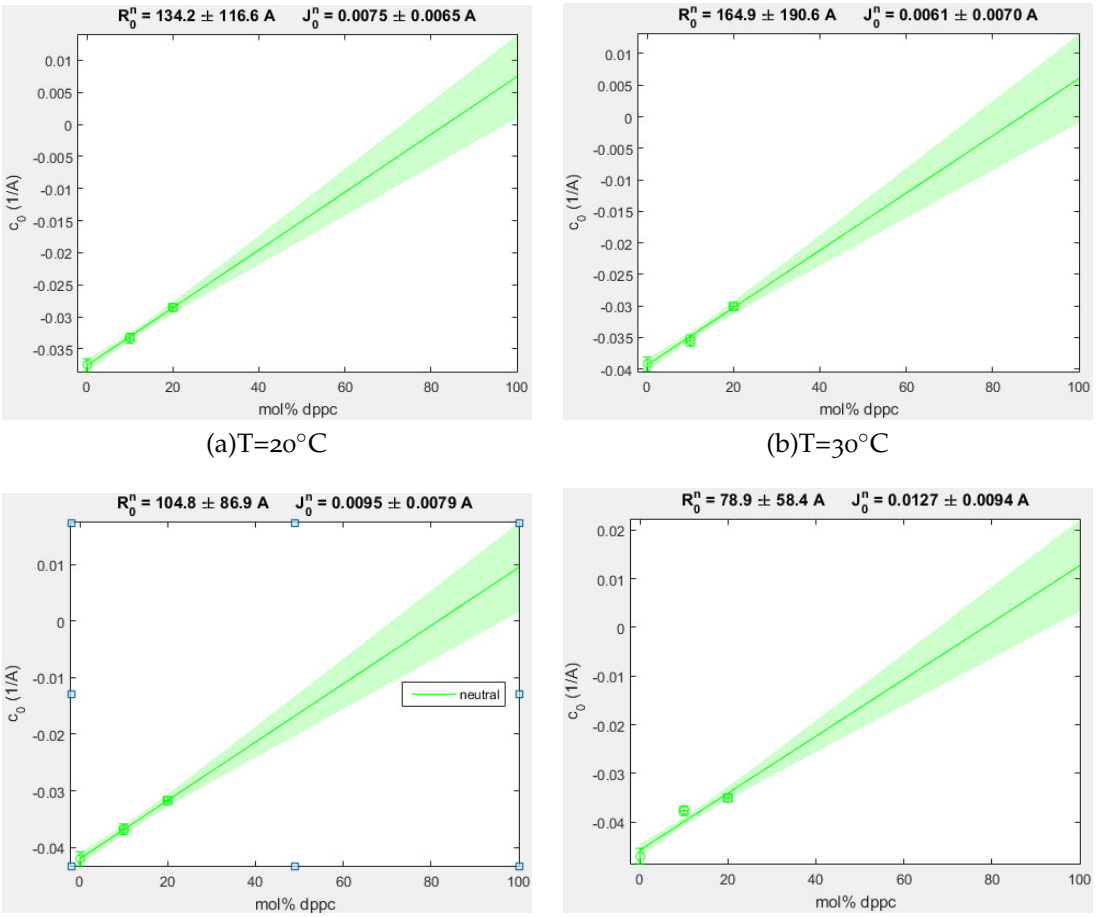

(a)T=20°C (b)T=30°C

(c)T=40°C (d)T=50°C

Figure 3.16: The extrapolation graphs of DPPC in DOPE-tricosene 12%WT in different temperatures.

In this case, we checked our samples with optical polarizing microscopy technique to see if the liquid part of the samples was in a non-isotropic phase. As seen in figure 3.17, the liquid part of our sample, texture is optically isotropic that means the lipid concentration in this part is very low. The picture related to paste part of the sample shows smooth birefringence texture which indicates that the paste part has non-isotropic phase. However, the texture is not good enough to determine fine details about the structure.

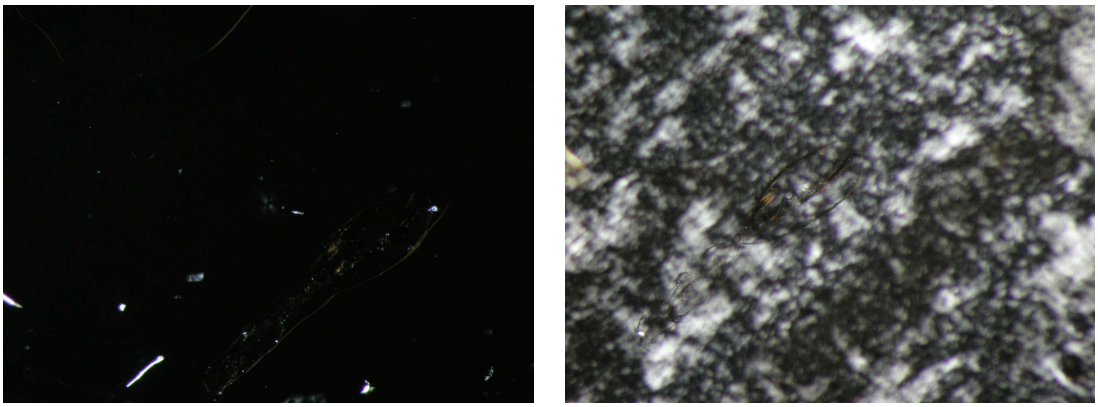

(a)Liquid part of the sample (b)Paste part of the sample

Figure 3.17: The polarization microscopy results of DOPE-DPPC-Tricosene 10% mol 12% wt.

3.3.3 DOPE-DSPC-Tricosene 12wt%

In this experiment, 30 mg/ml of DOPE and DSPC were dissolved separately in C/M [9:1] and 9-Cis-Tricosene with concentration 10 mg/ml was solved in C/M [9:1]. The samples with 12 wt% of Tricosene and 5,7.5,10,15,20% mole fraction of DSPC in DOPE were made with RSE. Table 3.5 gives more information about RSE parameters in this case. After making the sample in RSE, they were checked by SAXS to determine their lattice properties.

Table 3.5: The RSE parameters for making H_{II} of DOPE-DSPC-Tricosene 12 wt%.

Temperature (°C)	Pressure (mbar)	Vortex speed (rpm)	Argon flow (ml/min)
60	350	1800	61

After making samples with RSE, they were checked with SAXS at different temperatures from 20°C to 50°C to find their lattice structure properties. Figure 3.18 shows in additional, at 20, 30, 40°C, the lattice parameter increases with an increasing mole fraction of DSPC at any temperature, but there is no ordered pattern for this increasing. In additional, increasing of

mole fraction of DSPC caused increasing of the radius in cross section of tubes. Therefore the difference between the center of the nearest neighbor lipid tubes increased, that caused increasing of lattice parameter. The increasing of mole fraction means increasing of the number of bilayer-making lipids (DSPC) and decreasing the amount of monolayer-making host lipid (DOPE). Therefore, the intrinsic curvature of a mixture of these lipids structure tended to be more positive.
Figure 3.18 shows at 50°C there is increasing in lattice parameter up to 15% mole fraction sample and after that, there is a sudden drop in lattice parameter for 20% mol sample. According to figure 3.19, we can see the changes in the diffraction pattern of 20% mole sample at 50°C. It seems there is a phase separation of this sample at this temperature.

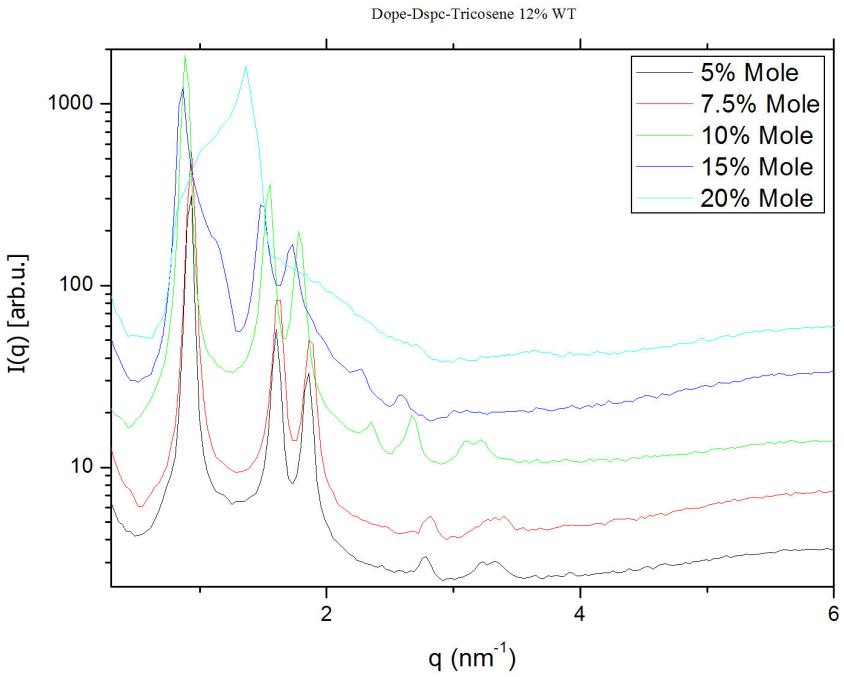

Figure 3.19: The comparison of lattice parameter (a) versus scattering vector (q) for 5, 7.5, 10, 15, 20% mole fractions of DOPE-DSPC-Tricosene 12% wt at 50°C.

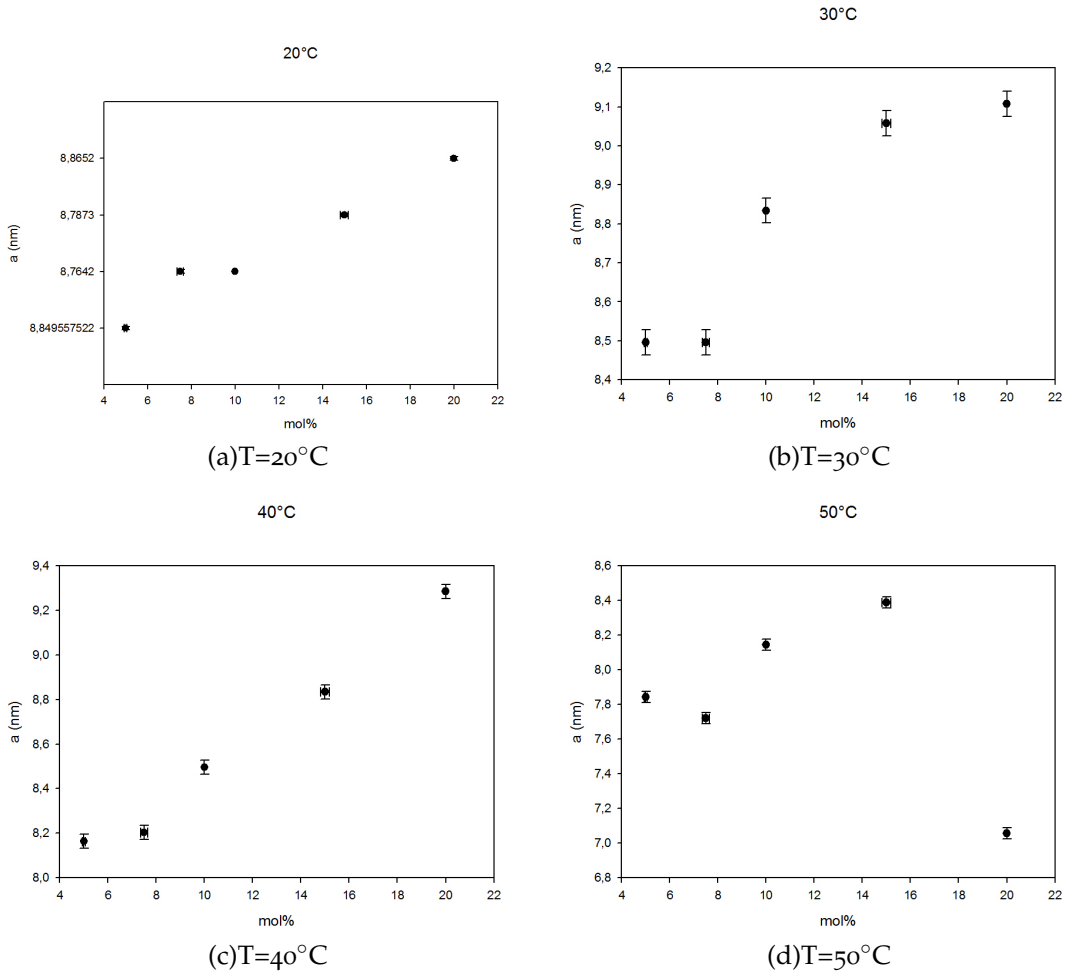

(a)T=20°C (b)T=30°C

(c)T=40°C (d)T=50°C

Figure 3.18: Lattice parameter (a) versus different mole fractions of DOPE-DSPC-tricosene 12wt%.

In figure 3.20, one can see the lattice parameter versus temperature for the different mole fractions of DSPC in DOPE-tricosene 12% wt. For 7.5, 10, 15, 20 % mole fraction samples, increasing the temperature caused a decrease in the lattice parameter. This information tells us that for the certain mole fraction increasing the temperature caused increased mobility of hydrocarbon chains, therefore, they occupied more space and that caused pressure on the hydrophilic part of the structure. That means lipid head groups sit near each other. Then the radius of hexagonal rods decreases and the distance between the center of neighboring rods decreases too. That caused a decrease of lattice parameter. However, according to the graph (a) in figure 3.20, the 5% mole fraction sample does not follow the same order. Maybe a change in phase structure or a coexisting phase exists at this mole fraction. The problem in miscibility can be another reason for this odd relation between lattice parameter and temperature for 5% mole sample.

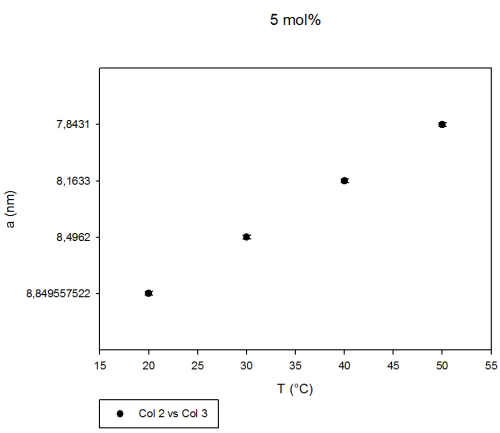

(a)5 mol%

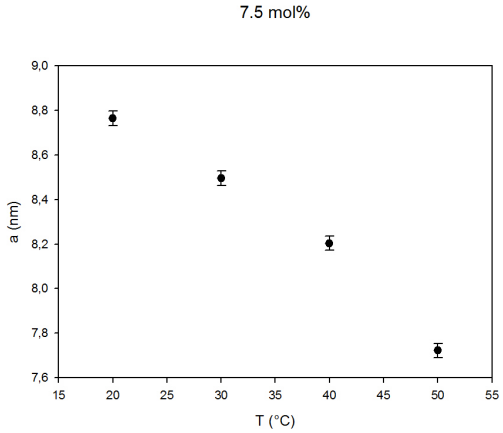

(b)7,5 mol%

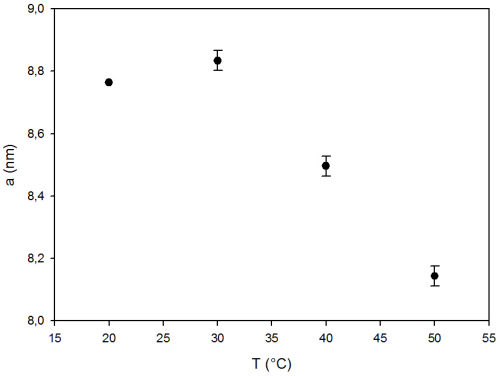

(c)10 mol%

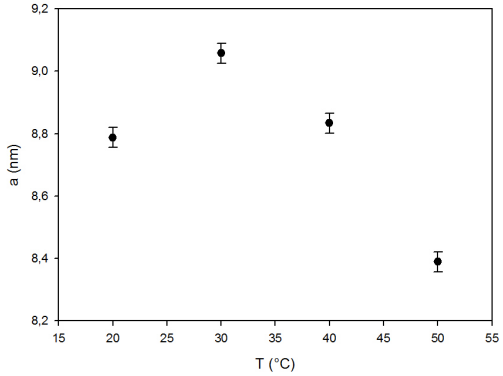

(d)15 mol%

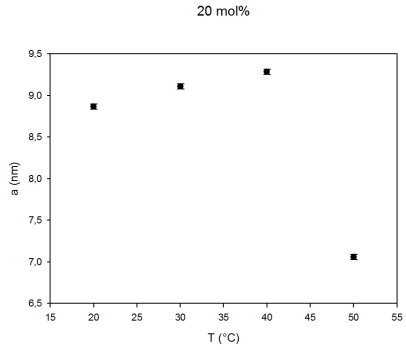

(e)20 mol%

Figure 3.20: Lattice parameter (a) versus temperature for different mole fractions of DOPE-DSPC-tricosene 12wt%.

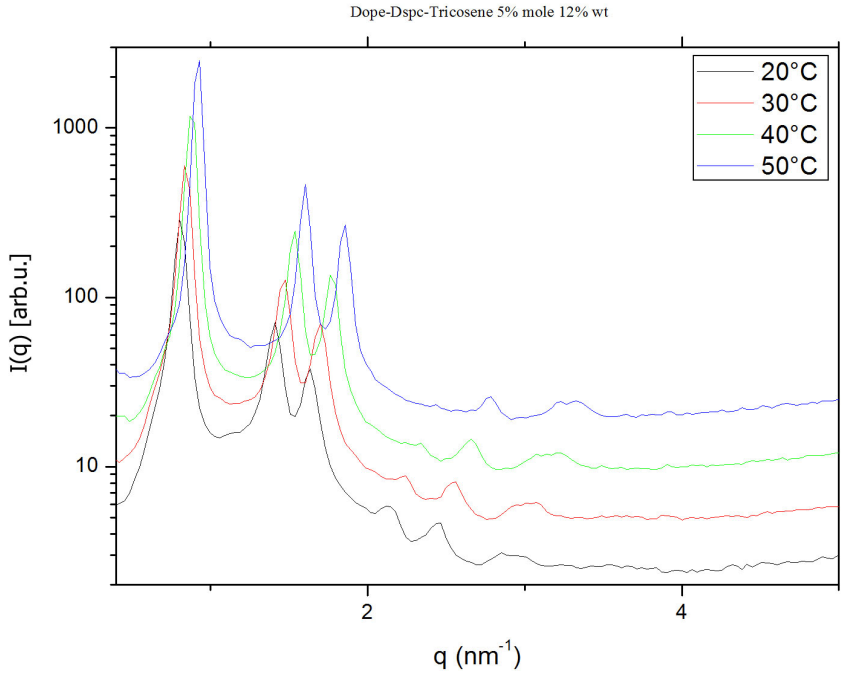

Figure 3.21: The scattering pattern of DOPE-DSPC-Tricosene 5% mol 12% wt at four different temperatures.

Figure 3.22 shows the spontaneous curvature versus mole fraction of DOPE-DSPC-tricosene 12% wt for various temperatures. At 40 and 50°C, spontaneous curvature increased with increasing mole fraction. In this case, the amount of DSPC guests increases in DOPE host structure with increasing mole fraction. That means the amount of lipids with positive intrinsic curvature increases in comparison to negative intrinsic curvature lipid host. Therefore, J tends to be more positive with increasing mole fraction value. At 20 and 30°C, the spontaneous curvature does not follow any particular order according to the change in mole fraction.

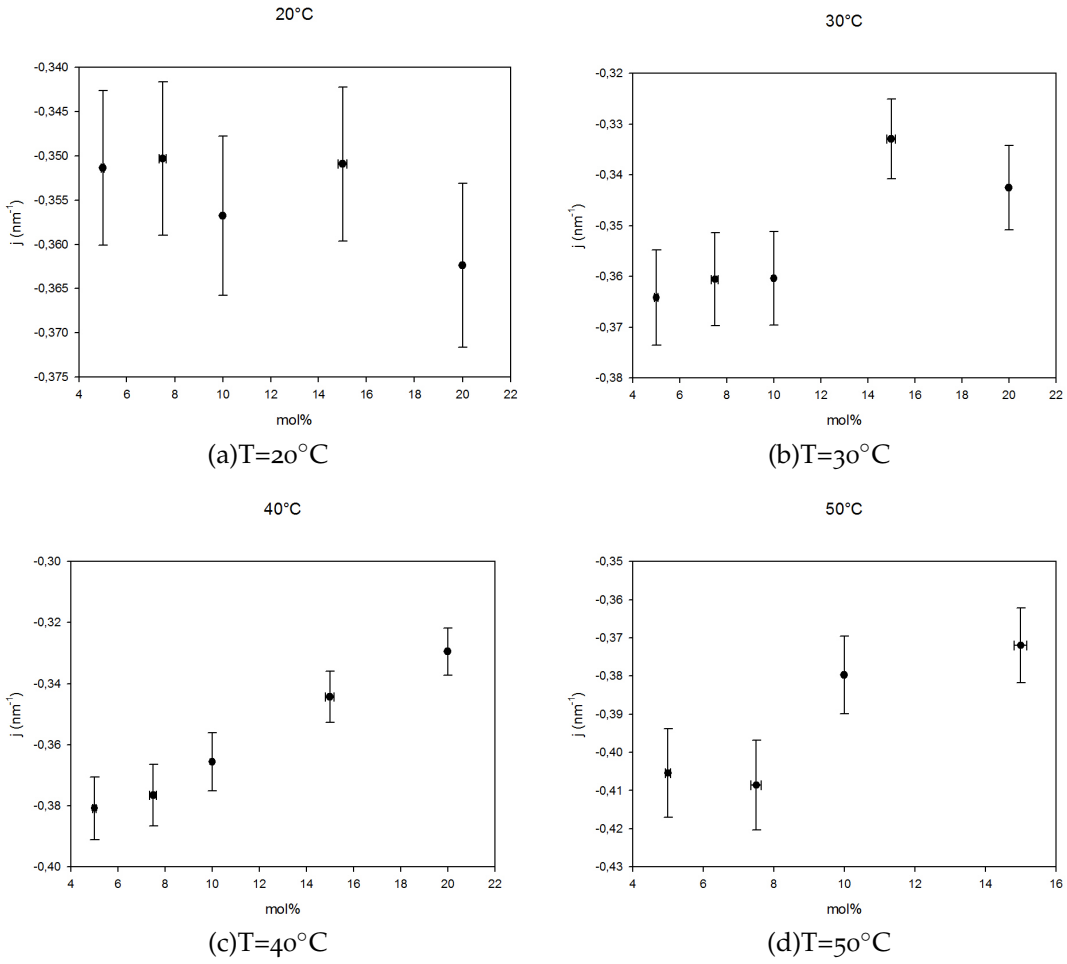

(a)T=20°C (b)T=30°C

(c)T=40°C (d)T=50°C

Figure 3.22: Spontaneous curvature (j) versus mole fraction of DOPE-DSPC-tricosene 12wt% for different temperatures.

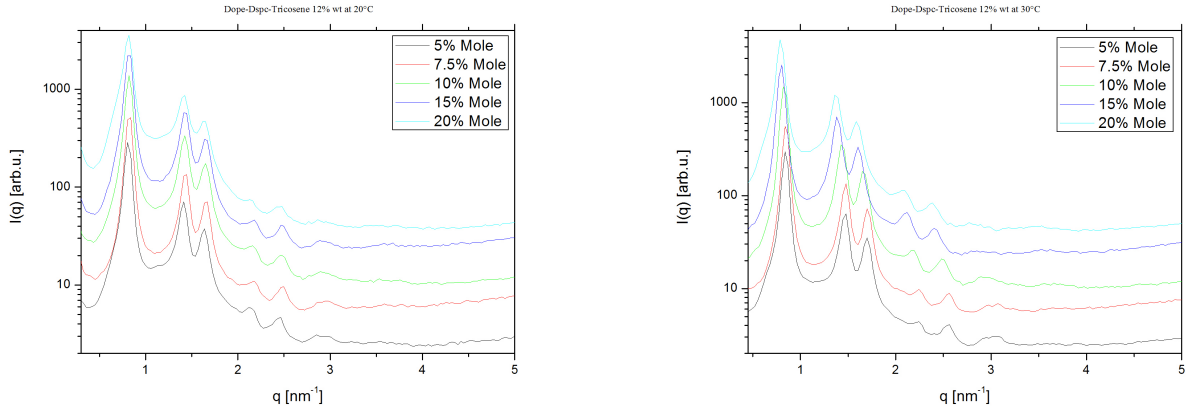

(a)T=20°C (b)T=30°C

Figure 3.23: The scattering pattern of DOPE-DSPC-Tricosene 12%wt in different mole fractions at 20°C (a) and 30°C (b).

In figure 3.24, one can find the change of spontaneous curvature with the change in temperature for certain mole fractions of DOPE-DSPC-tricosene 12% wt. Since 5, 7.5, 10% mol samples, j decreased dramatically with increasing temperature. Increasing temperature in a certain mole fraction causes increased the mobility of carbon chains and, therefore, making closely packed headgroups. That causes smaller rod cross section and, therefore, the more negative spontaneous curvature of the surface. For 15 and 20% mol samples, there is not a significant order for spontaneous curvature versus temperature. Maybe in these samples, change in phases or coexisting phases occurred. Another explanation is due to a problem with making these samples which caused incomplete solvation of DSPC in DOPE-tricosene 12% wt. As you can see in figure 3.25, at higher temperature changes in the scattering patterns for both samples is clearly evident. That means, the phase transition at higher temperatures occurs and caused a change in spontaneous curvature.

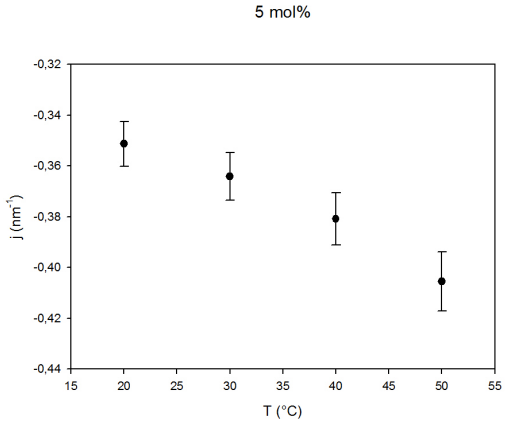

(a)5 mol%

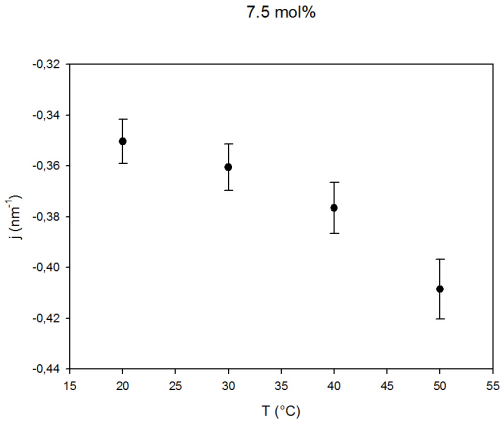

(b)7,5 mol%

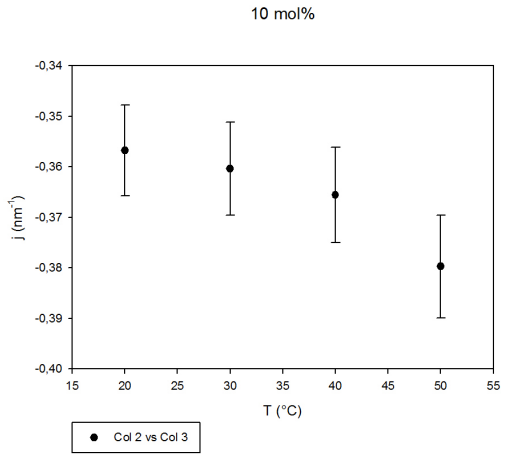

(c)10 mol%

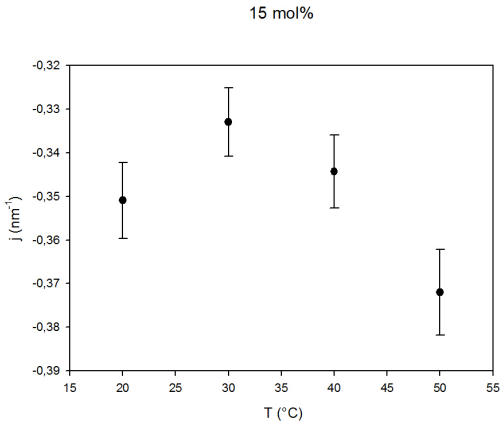

(d)15 mol%

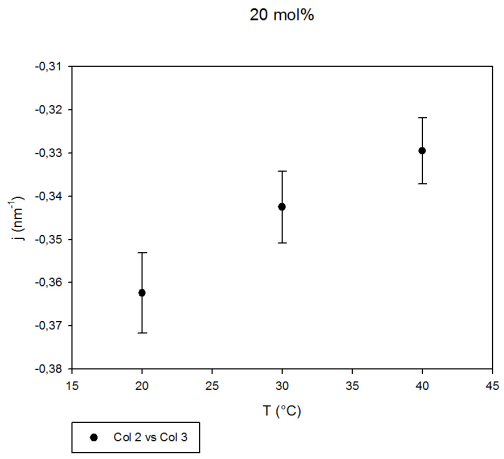

(e)20 mol%

Figure 3.24: Spontaneous curvature (j) versus temperature for different mole fractions of DOPE-DSPC-tricosene 12wt%.

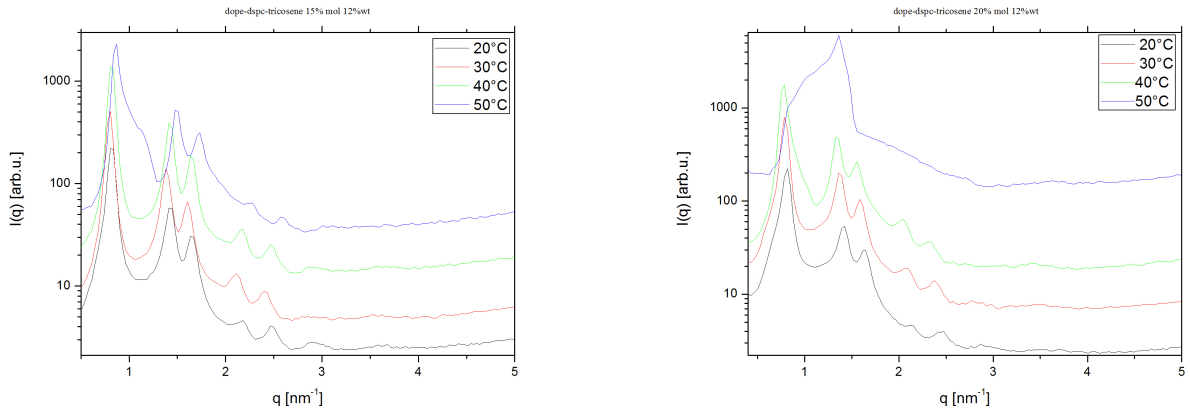

(a)15% mol (b)20% mol

Figure 3.25: Scattering pattern of (a) DOPE-DSPC-tricosene 15% mol 12% wt and (b) DOPE-DSPC-tricosene 20% mol 12% wt at different temperatures.

One can find extrapolation of spontaneous curvature of DSPC in DOPE-tricosene 12% WT in figure 3.26. The value of monolayer spontaneous curvature of DSPC is near to zero.

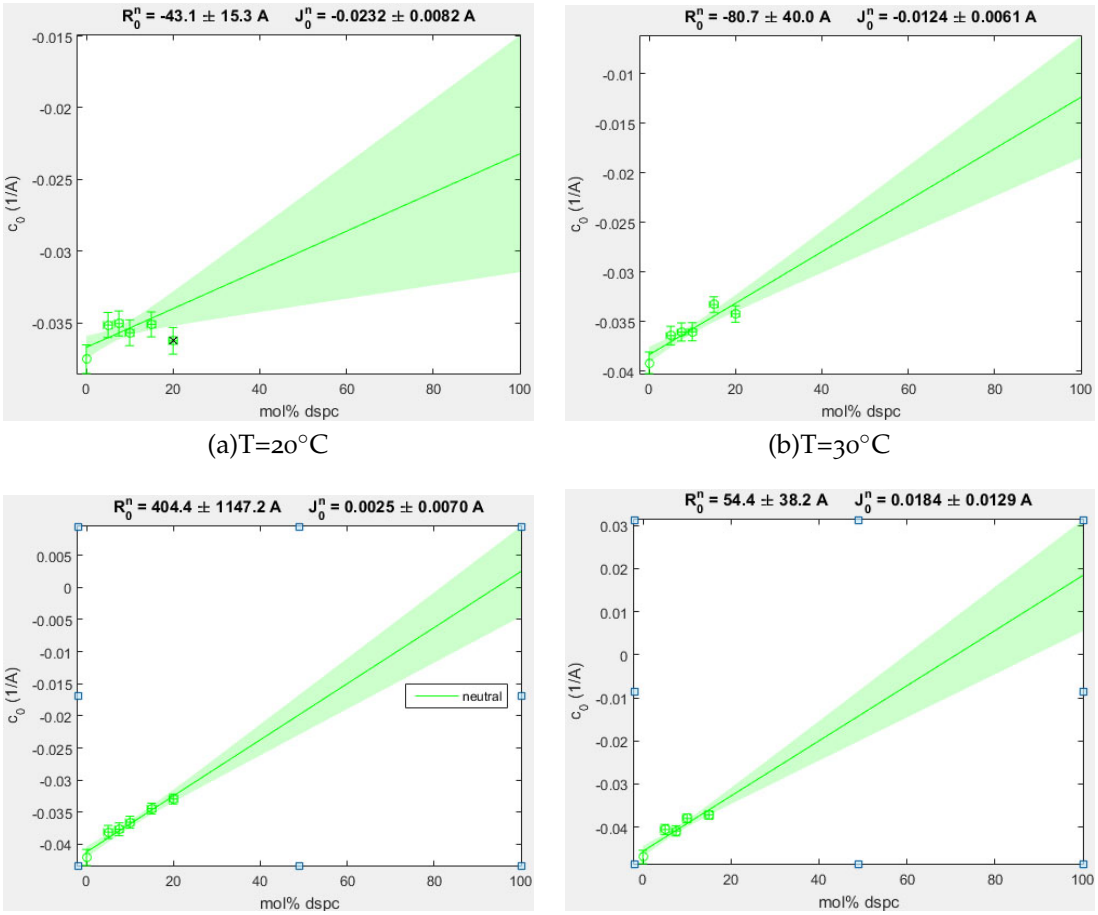

(a)T=20°C (b)T=30°C

(c)T=40°C (d)T=50°C

Figure 3.26: The extrapolation graphs of DSPC in DOPE-tricosene 12%WT at different temperatures.

3.3.4 DOPE-SM-Tricosene 12wt%

This time, 30 mg/ml of DOPE and SM were dissolved separately in C/M [9:1]. Also, 9-Cis-Tricosene with concentration 10 mg/ml was dissolved in C/M [9:1]. The samples with 12 wt% of Tricosene and 10, 20, 30, 40, 50% mole fraction of SM in DOPE were made with RSE. You can find more information about RSE parameters for this experiment in Table 3.6. After making the sample with RSE, they were checked by SAXS to determine

their lattice properties.

Table 3.6: The RSE parameters for making H_{II} of DOPE-MS-Tricosene 12 wt%.

Temperature (°C)	Pressure (mbar)	Vortex speed (rpm)	Argon flow (ml/min)
45	220	1800	61

After making the samples with RSE, they were checked with SAXS in different temperature ranges from 20°C to 50°C to find their lattice structure properties.

Figure 3.27 shows all temperatures (20, 30, 40, 50°C). The lattice parameter increases with an increasing mole fraction of SM dramatically. That means, increasing of mole fraction of SM caused increasing of the radius in cross section of the lipid tubes. Therefore, the difference between the center of neighboring tubes increased, that caused increasing of lattice parameter. Increased mole fraction means increasing of a number of bilayer-making lipids (SM) and decreasing the amount of monolayer-making host lipid (DOPE). Therefore, the intrinsic curvature of a mixture of these lipids structure tended to be more positive.

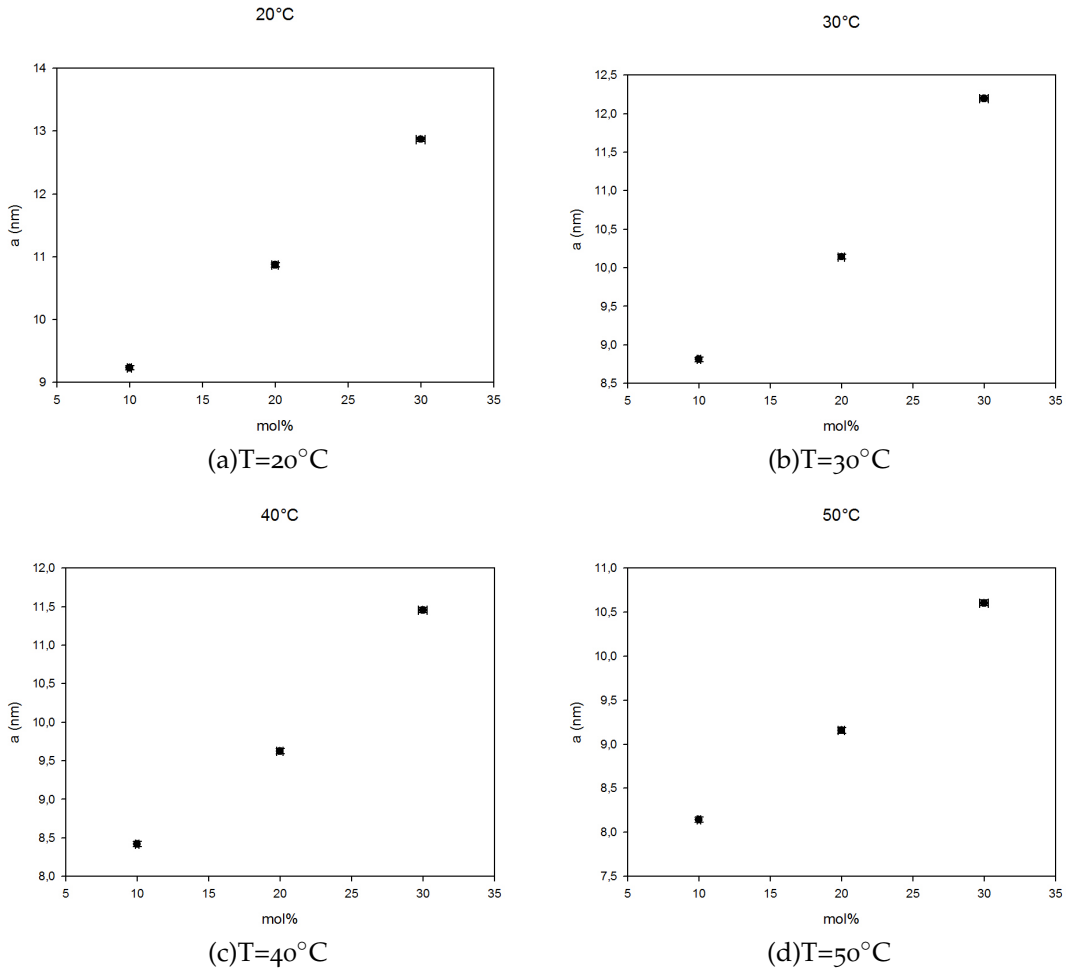

(a)T=20°C (b)T=30°C

(c)T=40°C (d)T=50°C

Figure 3.27: Lattice parameter (a) versus different mole fractions of DOPE-SM-tricosene 12wt%.

In figure 3.28, one can see the lattice parameter versus temperature relation for different mole fractions of SM in DOPE-tricosene 12% wt. For 20, 30 % mole fraction samples, increasing of temperature caused decreases in lattice parameter dramatically. This information suggests that for the certain mole fraction increasing the temperature caused increasing the mobility of hydrocarbon chains. Therefore, they occupied more space and that caused pressure on the hydrophilic part of the structure. This means lipid head

groups pack tightly. Then the radius of hexagonal rods decreases and the distance between the center of neighbor rods decreases too. That caused decreasing of lattice parameter. However, according to the graph (a) in figure 3.28, the 10% mole fraction sample does not follow the same order. Maybe a change in phase structure occurred or a coexisting phase occurs for this mole fraction. The problem in miscibility can be another reason for this odd relation between lattice parameter and change in temperature for 10% mole sample.

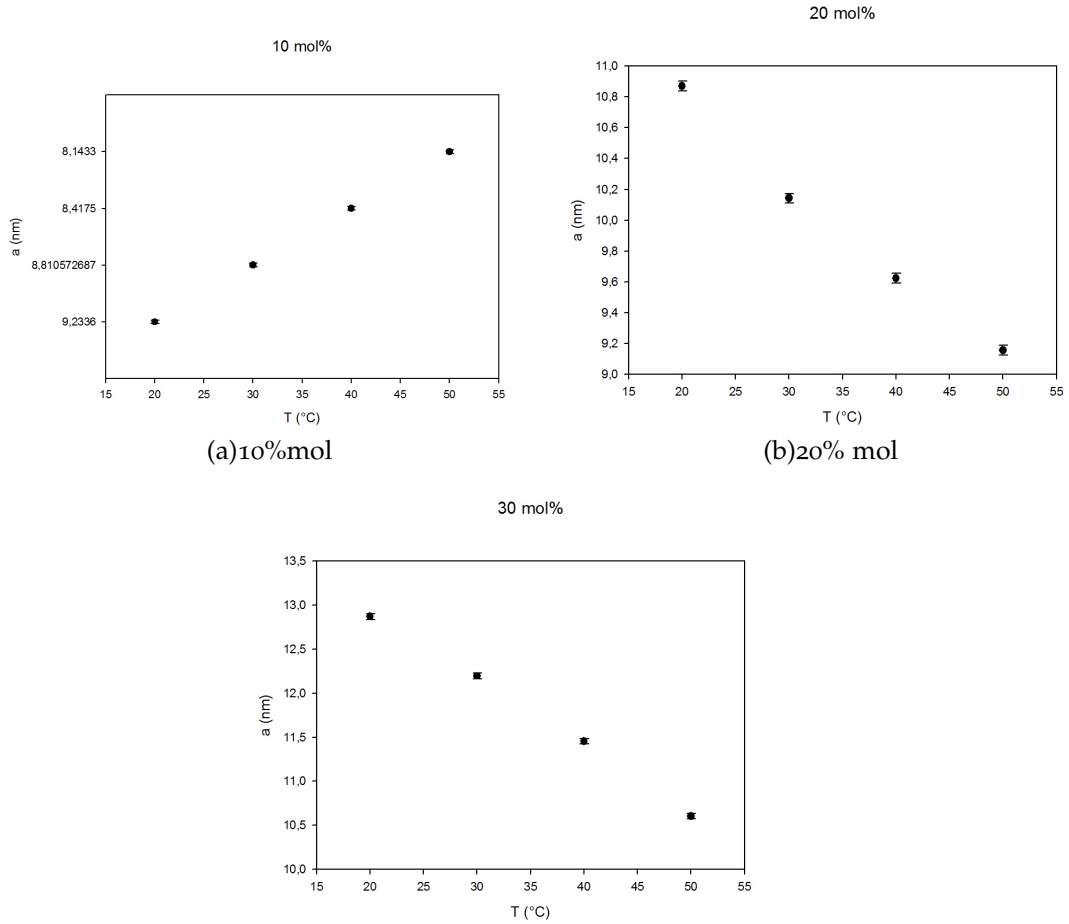

(a)10%mol (b)20% mol

(c)30%mol

Figure 3.28: Lattice parameter (a) versus temperature for different mole fractions of DOPE-SM-tricosene 12wt%.

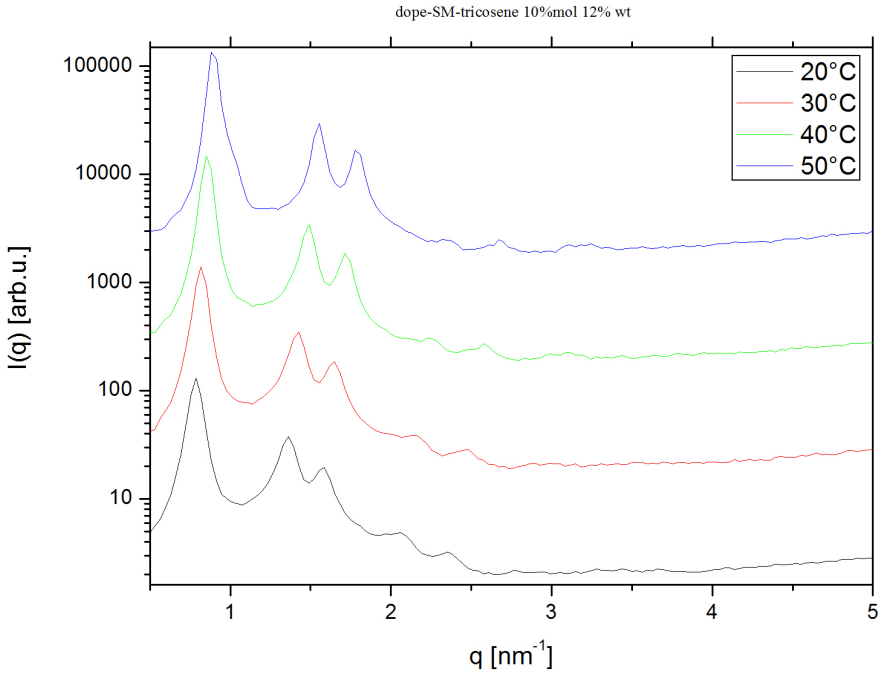

Figure 3.29: Scattering pattern of DOPE-SM-Tricosene 10% mol 12% wt at different temperatures.

In figure 3.30, you can see the spontaneous curvature versus mole fraction of DOPE-SM-tricosene 12% wt for various temperatures. As you know, at all temperatures, spontaneous curvature increased with increasing mole fraction dramatically. In this case, the amount of SM guests increase in DOPE host structure with increasing mole fraction. This means the amount of lipids with positive intrinsic curvature increases in comparison to negative intrinsic curvature lipid host. Therefore, J tends to be more positive with increasing mole fraction factor.

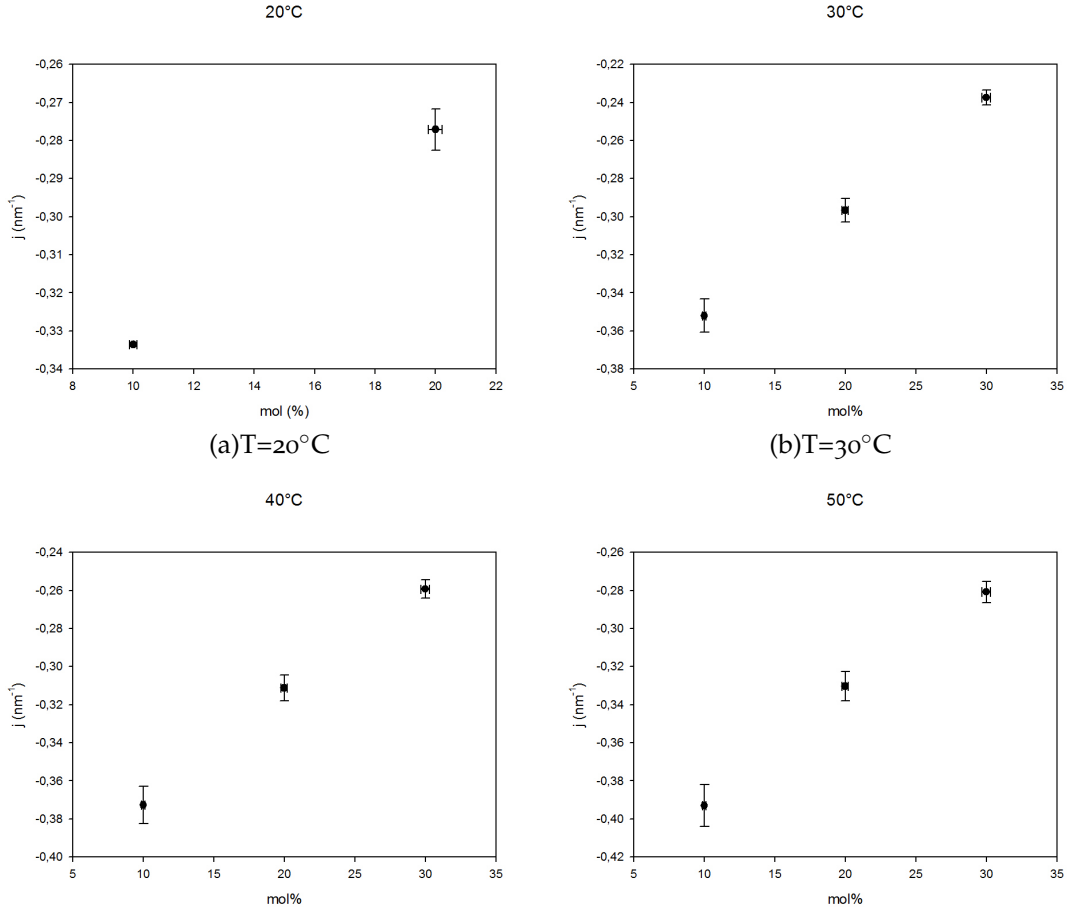

(a)T=20°C (b)T=30°C

(c)T=40°C (d)T=50°C

Figure 3.30: Spontaneous curvature (j) versus the mole fraction of DOPE-SM-tricosene 12wt% for different temperatures.

In figure 3.31, one can find the change of spontaneous curvature (j) with the change in temperature for certain mole fractions of DOPE-SM-tricosene 12% wt. As you can see in all mole fractions, j decreased dramatically with increasing the temperature. Increasing temperature in a certain mole fraction causes increased mobility of carbon chains and, therefore, making closely packed with headgroups. That causes smaller rod cross section and, therefore, the more negative spontaneous curvature of the surface.

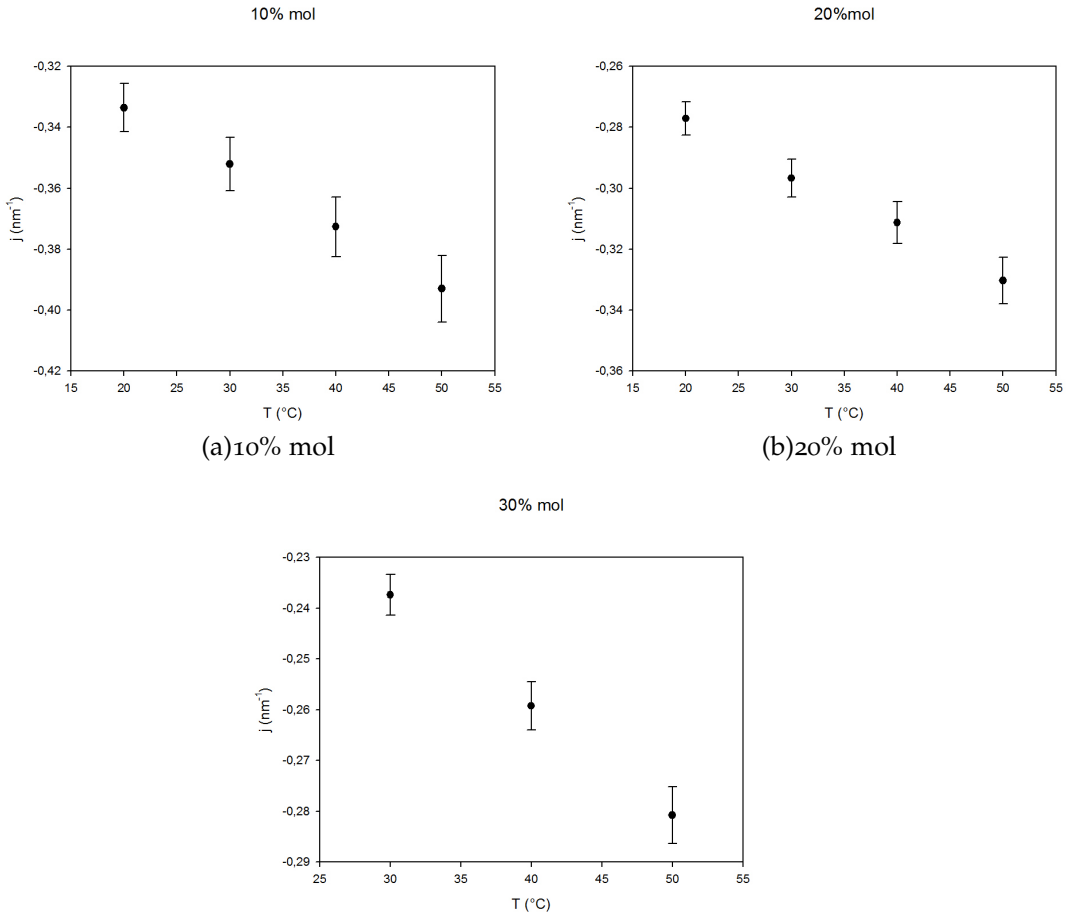

(a)10% mol (b)20% mol

(c)30% mol

Figure 3.31: Spontaneous curvature (j) versus temperature for different mole fractions of DOPE-SM-tricosene 12wt%.

One can find the extrapolation of spontaneous curvature of SM in DOPE-tricosene 12% WT in the figure 3.32. The value of monolayer spontaneous curvature of SM is near to zero.

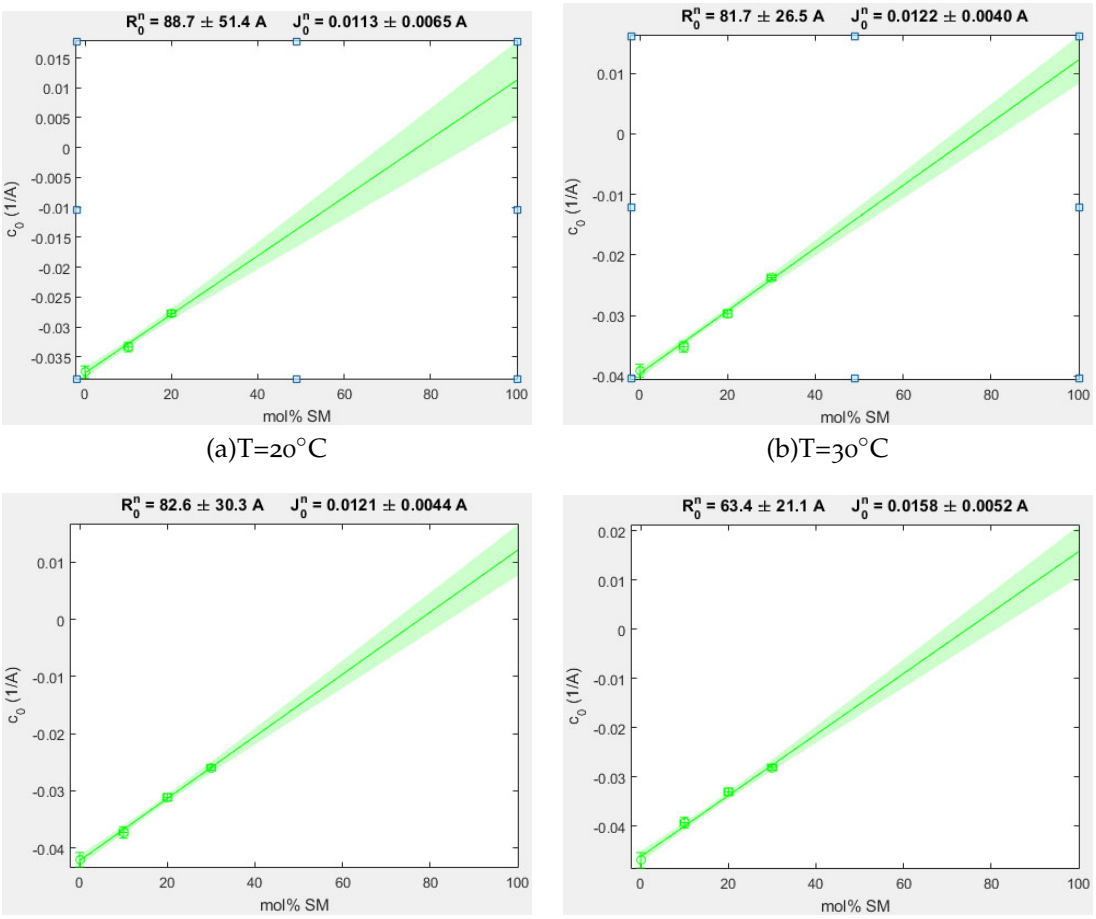

(a)T=20°C (b)T=30°C

(c)T=40°C (d)T=50°C

Figure 3.32: The extrapolation graphs of SM in DOPE-tricosene 12%WT at different temperatures.

3.3.5 DOPE-Ceramide-Tricosene 12wt%

For this experiment, DOPE (dioleoylphosphatidylethanolamine) and 16-ceramide were purchased from Avanti polar lipids and 9-cis-tricosene was bought from Sigma-Aldrich. The samples were prepared with 5%, 10% and 20% mole fractions of 16-Ceramide with RSE(auto)(See Table 3.7). The DOPE and 16-Ceramide concentration were 30 [mg/ml] and for 9-cis-Tricosene was 10 [mg/ml]. Chloroform/ Methanol (C/M [9:1]) was used as an organic

solvent in this process. All of the samples had the 12% weight fraction of 9-cis-Tricosene. The organic solvent/water ratio was 1:1 in each sample.

Table 3.7: The RSE parameters for making H_{II} of DOPE-Ceramide-Tricosene 12 wt%.

Temperature (°C)	Pressure (mbar)	Vortex speed (rpm)	Argon flow (ml/min)
80	800	1800	61

Samples information

The data in this report are related to four samples. You can find information about these samples in Table 3.8.

Table 3.8: Sample notation

A	5% mole fraction of DOPE-16ceramide-tricosene without annealing
B	same 5% mole fraction of DOPE-16ceramide-tricosene without annealing after some days
C	10% mole fraction of DOPE-16ceramide-tricosene after annealing about one hour in 95°C
D	20% mole fraction of DOPE-16ceramide-tricosene after annealing about one hour in 95°C

Figure 3.33 is the scattering pattern of these samples in 25°C. As you can see, there are only hexagonal patterns here.

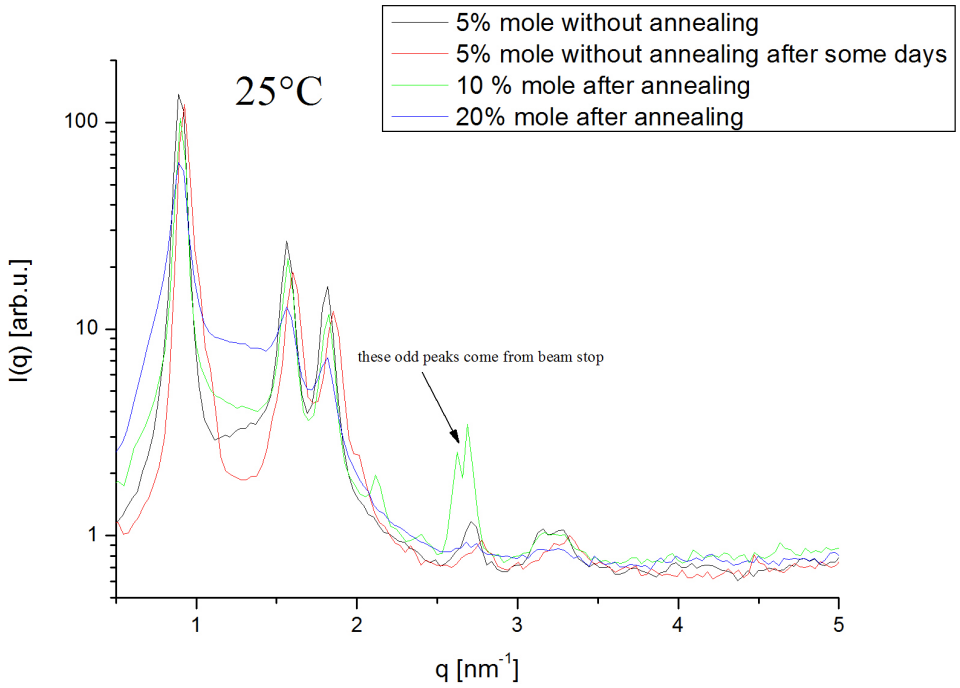

Figure 3.33: Small angle scattering pattern of DOPE-16ceramide-tricosene for different mole fractions in 25°C

3.3.6 Comparison with Ibai's data for DOPE-16ceramide-tricosene in different mole fractions

We had some information about the hexagonal phase structure of DOPE-16Ceramide-Tricosene made by the thin film method. Ibai has made them with 5, 10, 15, 20, 30, 40, 50% mole fractions and found their scattering pattern at different temperatures. Below is the comparison between our results and Ibai's results.

In figure 3.34, there is a comparison between the scattering pattern of sample A and Ibai's data in 20°C and 30 °C. The change in lattice parameter according to the change in temperature is in figure 3.35 for 5% mol samples. In both samples, we can see the increasing temperature caused decreasing of

lattice parameter. Also, our data and Ibai's data followed the same order and they have a good approximation. As we know, for the certain mole fraction increasing the temperature caused increasing the mobility of hydrocarbon chains. Therefore, they occupied more space and that caused pressure on the hydrophilic part of the structure and decreases this. That means lipid head groups sit close to each other. Then the radius of hexagonal rods decreases and the distance between the center of neighboring rods decreases too. That caused a decrease in the lattice parameter.

Similar results are observed in figure 3.36 and figure 3.37 for sample B, in figure 3.38 and figure 3.39 for sample C and in figure 3.40 and figure 3.41 for sample D. As you can see, there is a reduction in lattice parameter (a) with increasing the temperature.

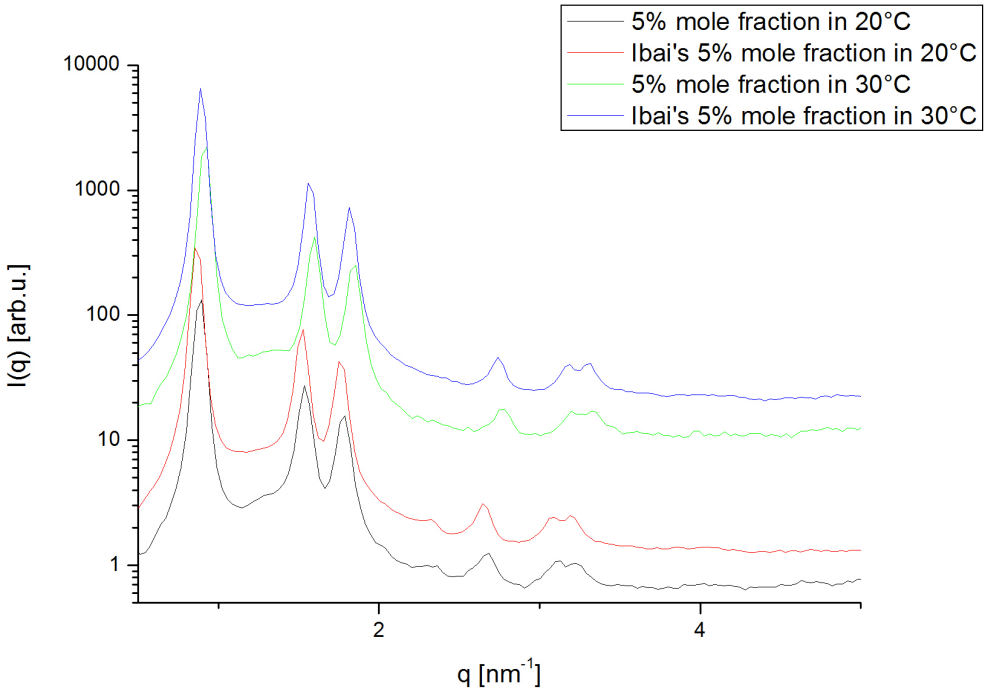

Figure 3.34: Comparison of scattering pattern between sample A and Ibai's data in different temperature ranges

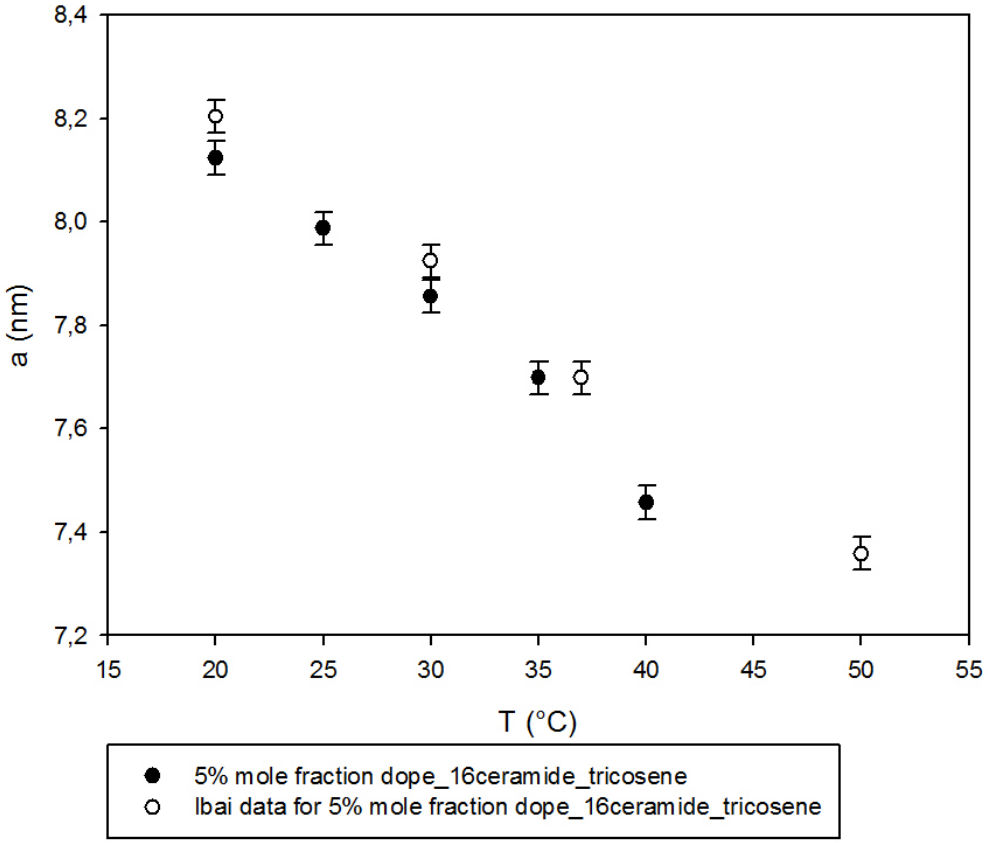

Figure 3.35: Comparison of lattice parameter between sample A and Ibai's data in different temperature ranges

We repeated the SAXS experiments again with same 5% mol sample after some days. As you can see in figure 3.36, there is some change in the scattering pattern of our 5% mol sample. This means this sample is not very stable. To check this sample at the broad temperature range, for preventing the sample dehydration under high vacuum and temperature, this sample was soaked again after 30°C and put again into the SAXS device. In figure 3.37, you can find the change in lattice parameter versus temperature and comparison of our data with Ibai's data. In additional, the main trend of lattice parameter is decreasing according to the increasing the

temperature.

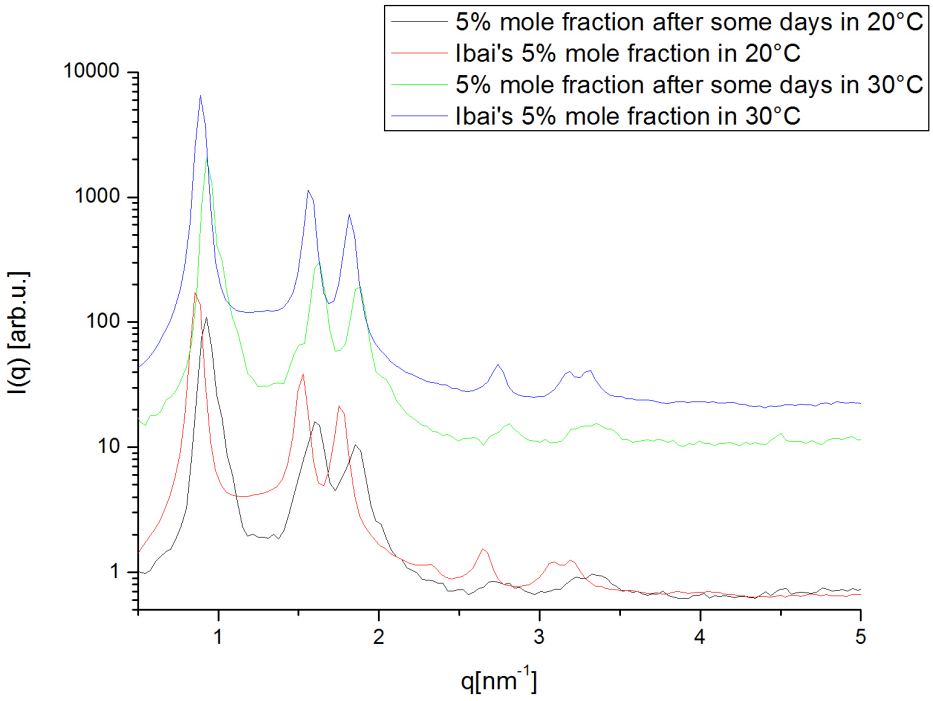

Figure 3.36: Comparison of scattering pattern between sample B and Ibai's data in different temperature ranges

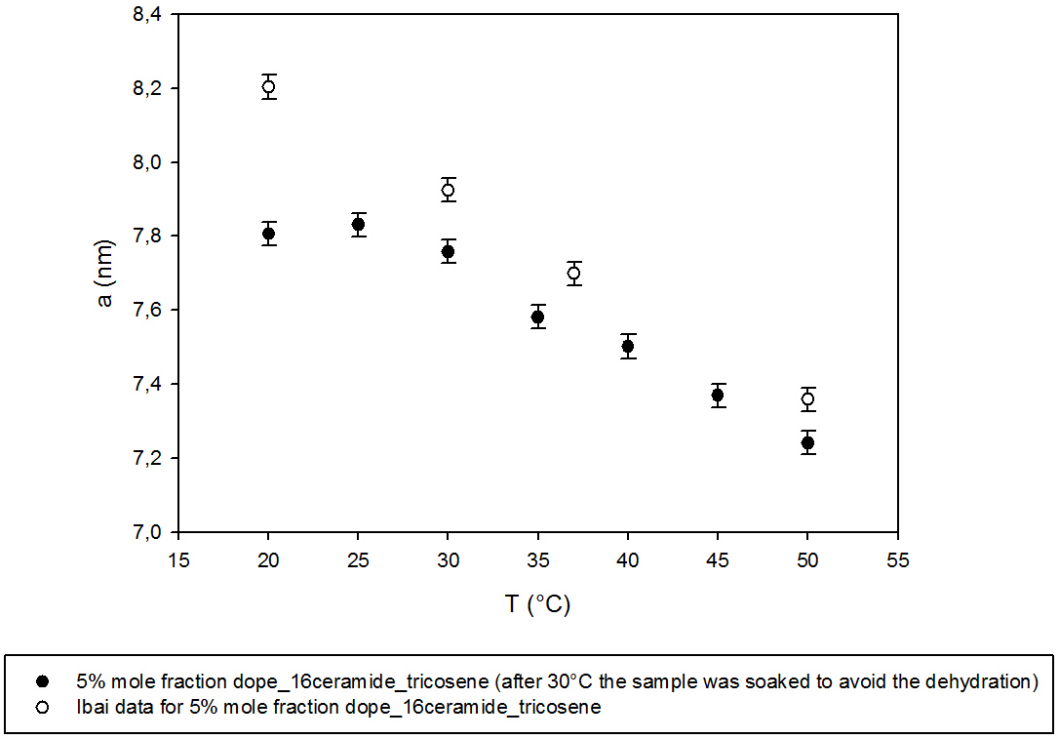

Figure 3.37: Comparison of lattice parameter between sample B and Ibai's data in different temperature ranges

After preparation of the 10%mol sample, we put this in the oven for one hour at 95°C. The annealing process helps to ensure the ceramides are melted and go inside of DOPE structures. Because the melting temperature of 16-Ceramide is around 98°C, a much higher than melting temperature of DOPE, annealing helps to have a more homogeneous mixture. However, to prevent destroying the sample, annealing process should take as minimum time as possible.
In figure 3.38 you can find the comparison of scattering pattern between our DOPE-16Ceramide-tricosene 10% mol 12% wt and Ibai's same sample. We could reach to the pure hexagonal phase only in 25°C. In Ibai's data, an extra lamellar peak after first hexagonal peak is observed, which starts to grow from 20°C. What I can say in this case is, we could achieve a pure hexagonal phase at low temperatures with the RSE method better than thin

film method.

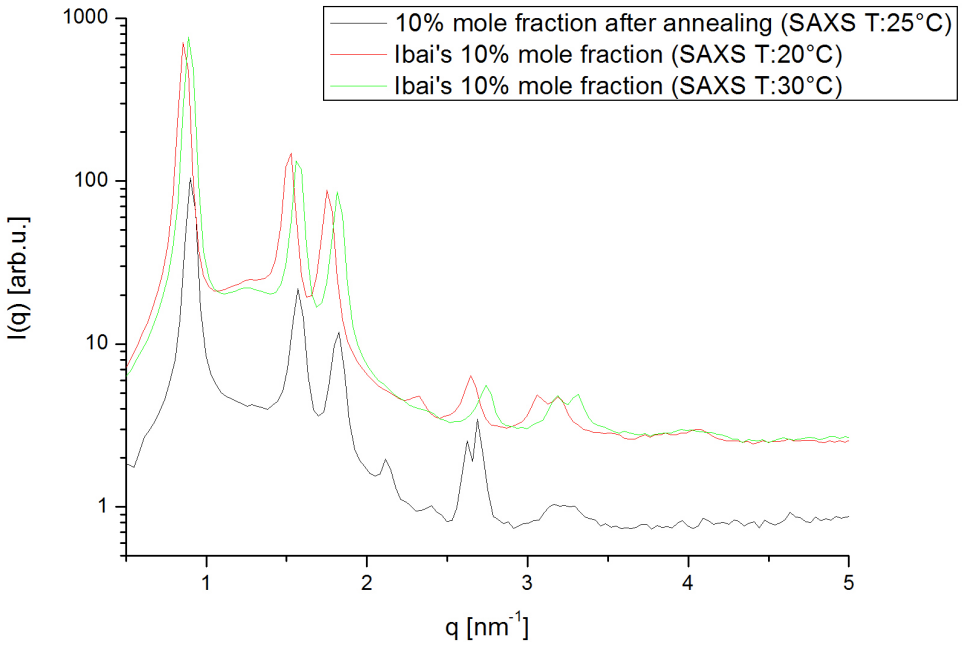

Figure 3.38: Comparison of scattering pattern between sample C and Ibai's data in different temperature ranges

In figure 3.39, there is a comparison of the change in lattice parameter according to the change of temperature in our 10%mol sample and Ibai's sample. In this case, decreasing of lattice parameter is visible again.

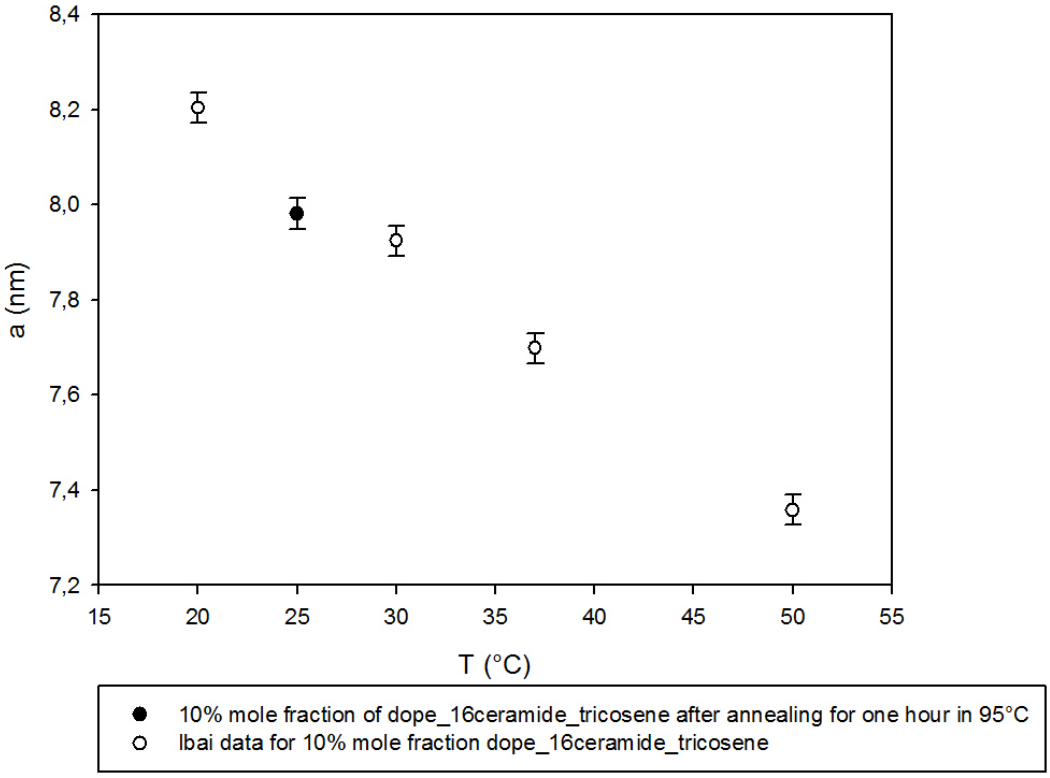

Figure 3.39: Comparison of lattice parameter between sample C and Ibai's data in different temperature ranges

After preparation of 20%mol sample, we put this in the oven for one hour at 95°C. The annealing process helps to be sure that all of the ceramides are melted and go inside of DOPE structures. Because the melting temperature of 16-Ceramide is around 98°C and it is higher than melting temperature of DOPE, annealing helps to have a more homogeneous mixture of these two different lipids. However, to prevent destroying the sample, annealing process should take as minimum time as possible. In figure 3.40 is the comparison of scattering pattern between our DOPE-16Ceramide-tricosene 20% mol 12% wt and Ibai's same sample. We could reach the pure hexagonal phase only at 25°C. In Ibai's data, an extra lamellar peak after first hexagonal peak is observed, which starts to grow from 20°C.

That seems we could achieve to pure hexagonal phase at low temperature with the RSE method better than thin film method.

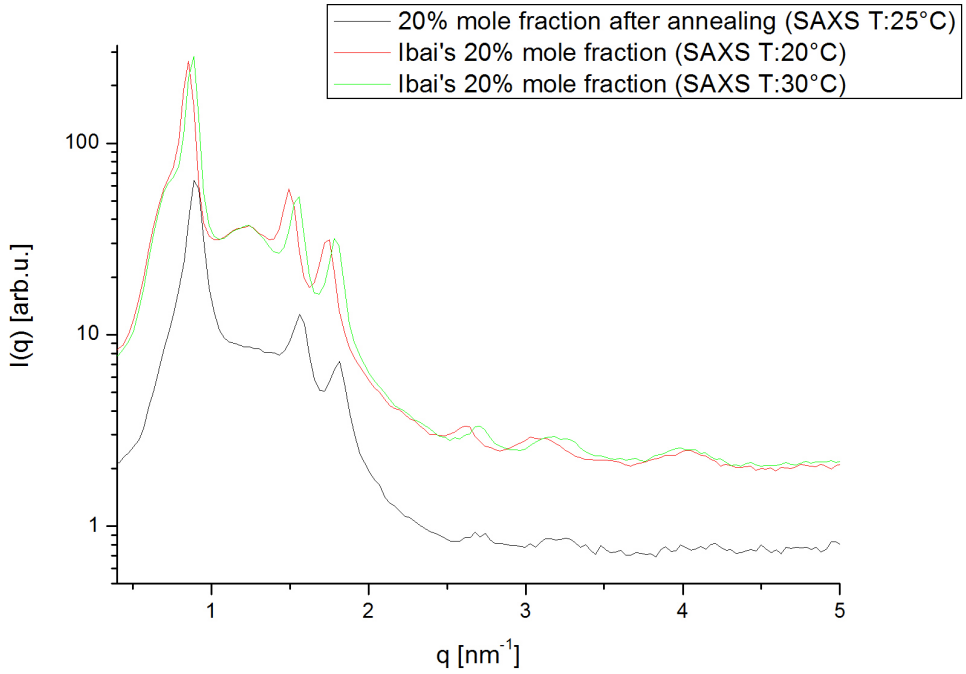

Figure 3.40: Comparison of scattering pattern between sample D and Ibai's data in different temperature ranges

In figure 3.41, there is a comparison of the change in lattice parameter according to the change of temperature in our 20%mol sample and Ibai's sample. In this case, decreasing of lattice parameter is visible again.

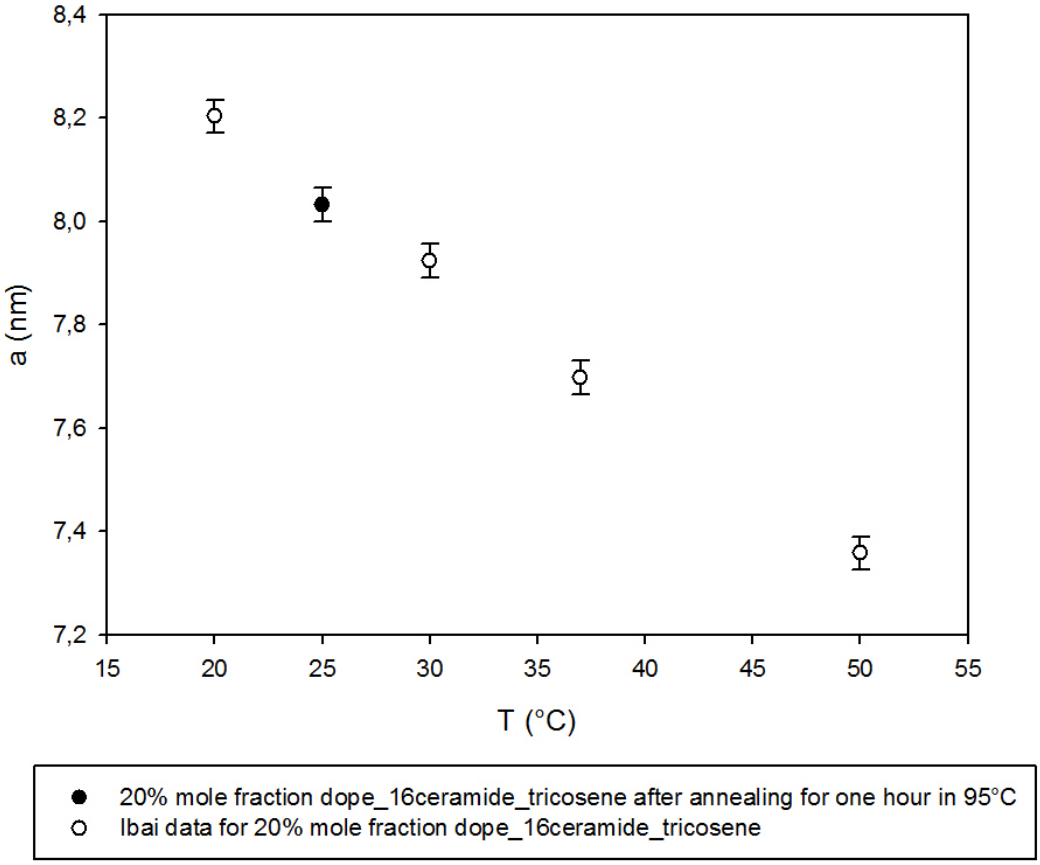

Figure 3.41: Comparison of lattice parameter between sample D and Ibai's data in different temperature ranges

3.3.7 Change in lattice parameter and spontaneous curvature according to change the mole fraction

As you can see in figure 3.42, increasing the mole fraction of 16-ceramide causes an increase in lattice parameter. In figure 3.43 you can find information about the spontaneous curvature (j) as a function of increasing the mole fraction of 16-ceramide. Here, the spontaneous curvature does not follow any logical order.

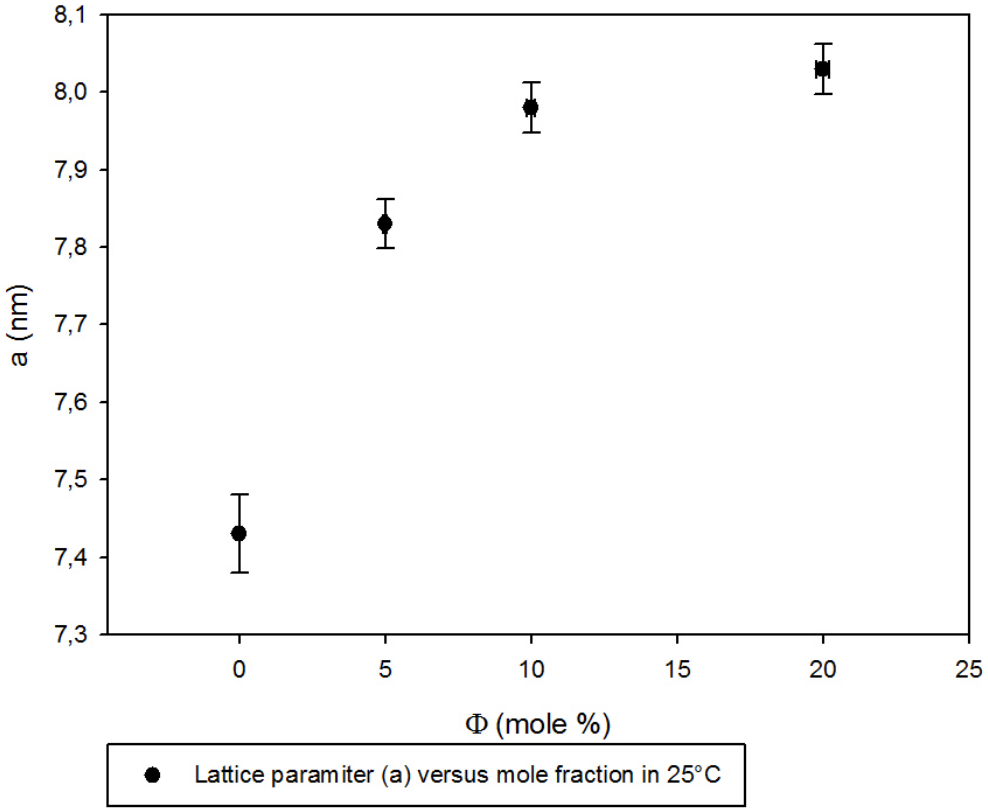

Figure 3.42: Change in lattice parameter during a change in mole fraction of 16-ceramide in 25°C. The 5% point is related to sample B.

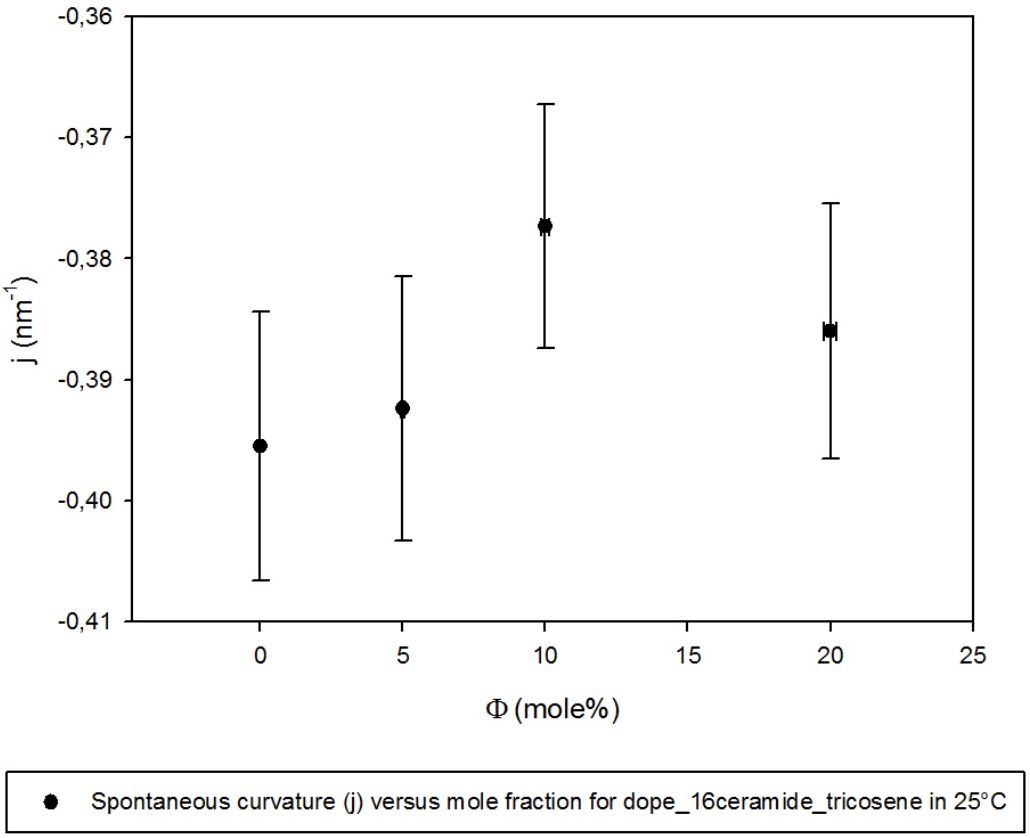

Figure 3.43: Change in spontaneous curvature during a shift in the mole fraction of 16-ceramide in 25°C. The 5% point is related to sample B.

16-Ceramide needs more experiments at very low mole fractions to find a strong view about the properties of DOPE-16Ceramide-tricosene hexagonal phase during a change in mole fraction and temperatures.

3.4 Additional final result

During our experiments, the main purpose was defining the spontaneous curvature of bilayer making lipids after mixing them as the guest lipids in monolayer making lipids. We used DMPC, DPPC, DSPC and SM as the

guest lipid and DOPE as a host lipid. Our guest lipids were monolayer making lipids with different carbon chain lengths. We wanted to see if the length of the carbon chains affected on the value of spontaneous curvature of different lipids?(See figure 3.44)

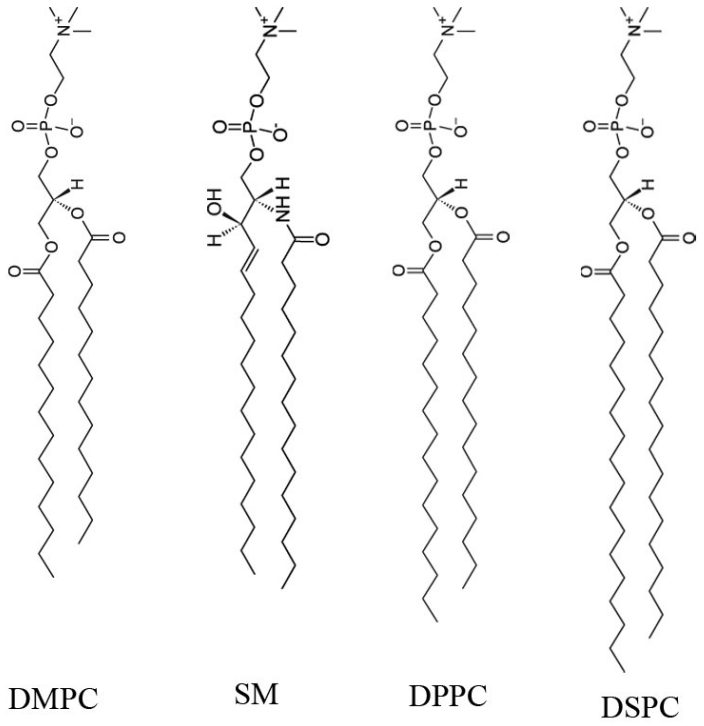

Figure 3.44: Lipids with different carbon chain lengths. DMPC:14, SM:16, DPPC:16, DSPC:18

After making each sample and do SAXS experiments with them, we exploit all favorable data and at the end made an extrapolation calculation in order to find the spontaneous curvature of pure monolayer making lipid. In figure 3.45 you can find the comparison of spontaneous curvature of different pure monolayer making lipids at different temperatures. AS you can see, in each studied temperature J value of all lipids are near zero and it seems there is no correlation between the spontaneous curvature and the length of carbon chains.

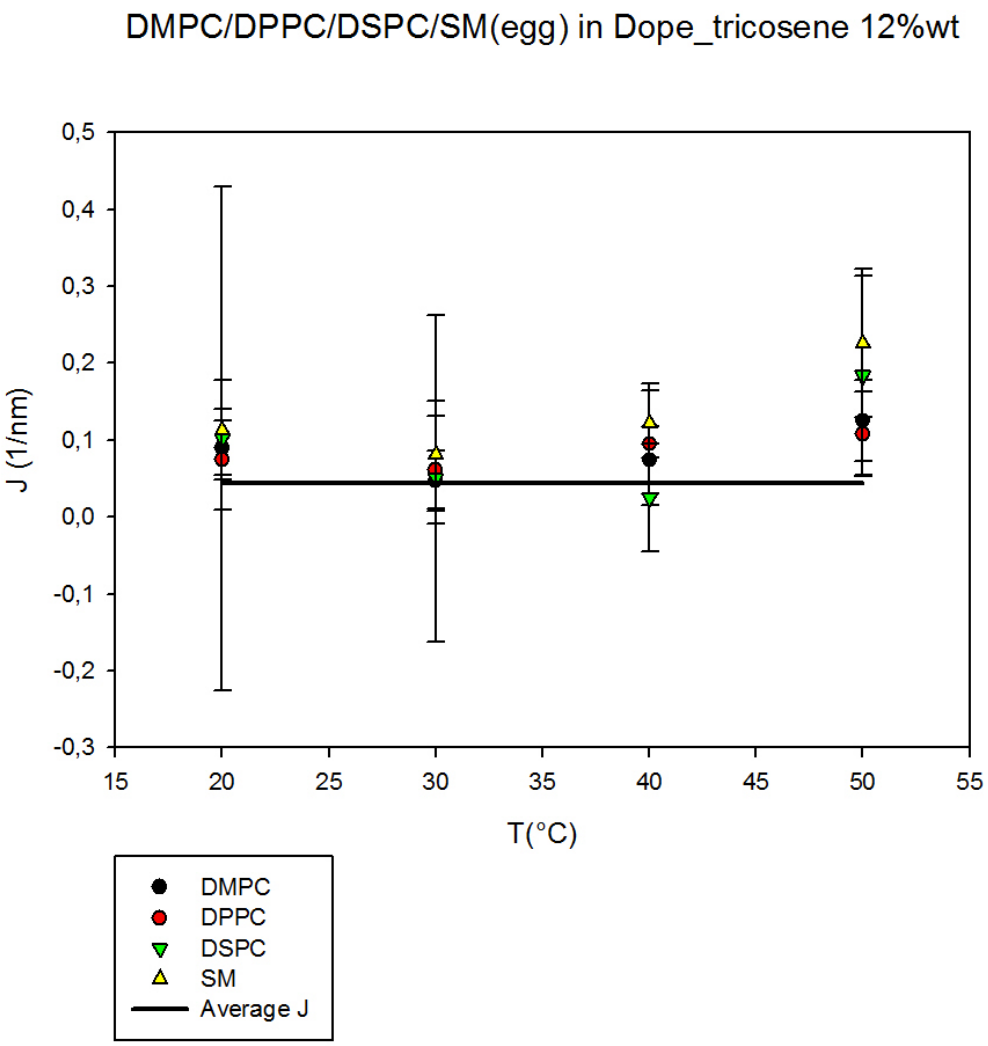

Figure 3.45: Comparison of spontaneous curvatures of pure DMPC, DPPC, DSPC and SM versus different temperatures

4 Summary and conclusion

Our research shows that the RSE method can be employed as a fast and clean method to make the hexagonal phase of monolayer forming lipids or a mixture of monolayer-bilayer forming lipids. Using this method, we can generate hexagonal structure in a few minutes. Adjusting the pressure and the temperature according to the intrinsic property of used lipids, we can increase the probability of the miscibility of guest lipids. We should always choose a convenient vortex speed because very high vortex speed can destroy the hexagonal structure and makes the structures less correlated such as nematic and isotropic phase. Very low vortex speed decreases the mixing rate of the lipids.

During our study, DOPE was used as a monolayer making host lipid and four other bilayer forming lipids with different carbon chain lengths were individually mixed DOPE as the guest lipids separately: DPPC, DMPC, DSPC and SM. We made samples with 16-Ceramide, however, further experiments at lower mole fractions are required.We tried to find how the carbon chain length of guest lipids can affect the spontaneous curvature value of these lipids and if there is any preference in this case? Our results show the spontaneous curvature of each pure guest lipid after extrapolation is near zero and there is no meaningful difference between lipids with different carbon chains. In addition, for each mixture sample, at given temperature, the lattice parameter (a) and the spontaneous curvature (j) increase with increasing of mole fraction of guest lipids. In most cases the increase in spontaneous curvature is linear. At a given mole fraction, the lattice parameter and spontaneous curvature decrease linearly with increasing the temperature. However, in samples with high mole fractions, we lost the pure hexagonal structure and some extra lamellar and coexisting peaks appeared in the scattering pattern.

For optimizing the RSE method, it would be useful if the RSE apparatus isolated the RSE test tube environment completely. Also, the process of dissolving lipids in the organic solvent should be performed as quickly as

possible to avoid of evaporation the organic solvent. Due to improvements of the RSE method, it is necessary to attempt to make lipid structures from lipid mixtures for a variety of purposes.It would also be useful to make a database for the required RSE conditions for each lipid in an attempt to make an automatic RSE device.

Bibliography

[1] Ole G. Mouritsen, Highlight Article Lipids, curvature, and nano-medicine,*Eur. J. Lipid Sci. Technol.*113 ,(2011)1174–1187.

[2] Michael M. Kozlov, Harvey T. McMahon and Leonid V. Chernomordik, Protein-driven membrane stresses in fusion and fission, *Cell* Volume 35, Issue 12,(2010)699–706.

[3] https://universe-review.ca/R15-26-CalabiYau01.htm

[4] http://www.avantilipids.com

[5] Heimo Schnablegger, The Basics of Small-Angle X-Ray Scattering *http://www.anton-paar.com*

[6] *http://www.anton-paar.com*

[7] Guillaume Tresset, The multiple faces of se lf-assembled lipidic systems, *PMC Biophysics* 2:3,(2009)

[8] Benjamin Kollmitzer, Peter Heftberger, Michael Rappolt and Georg Pabst, Monolayer spontaneous curvature of raft-forming membrane lipids *Soft Matter* 9 ,(2013)10877-10884

[9] Michael Rappolt, Andrea Hickel, Frank Bringezu and Karl Lohner, Mechanism of the Lamellar/Inverse Hexagonal Phase Transition Examined by High Resolution X-Ray Diffraction, *Biophysical Journas* 84,(2003)3111–3122.

[10] N. Kučerka, S. Tristram-Nagle and J. F. Nagle, Closer Look at Structure of Fully Hydrated Fluid Phase DPPC Bilayers, *Biophysical Journal.*90, (2006)L83–L85.

[11] N. Kučerka, S. Tristram-Nagle and J. F. Nagle, Structure of Fully Hydrated Fluid Phase Lipid Bilayers with Monounsaturated Chains, *The Journal of Membrane Biology.*208, (2006)193–202.

[12] N. Kučerka, J. F. Nagle, J. N. Sachs, S. E. Feller, J. Pencer, A. Jackson and J. Katsaras, Lipid Bilayer Structure Determined by the Simultaneous Analysis of Neutron and X-Ray Scattering Data*Biophysical Journal.*95,(2008)2356–2367.

[13] N. Kučerka, M.-P. Nieh and J. Katsaras, Fluid phase lipid areas and bilayer thicknesses of commonly used phosphatidylcholines as a function of temperature, *Biochimica et Biophysica Acta.*1808, (2011)2761-2771.

[14] S. H. Alley, O. Ces, M. Barahona and R. H. Templer, X-ray diffraction measurement of the monolayer spontaneous curvature of dioleoylphosphatidylglycerol *Chemistry and Physics of Lipids*154, (2008)64–67.

[15] Beate Boulgaropoulos, Michael Rappolt, Barbara Sartori, Heinz Amenitsch, and Georg Pabst, Lipid Sorting by Ceramide and the Consequences for Membrane Proteins *Biophysical Journal.*102, (2012)2031–2038.

[16] S. Leikin, M. M. Kozlov, N. L. Fuller and R. P. Rand, Measured Effects of Diacylglycerol on Structural and Elastic Properties of Phospholipid Membranes, *Biophysical Journal.*71, (1996)2623-2632.

[17] M. M. Kozlov, S. Leikin and R. P. Rand, Bending, Hydration and Interstitial Energies Quantitatively Account for the Hexagonal-Lamellar-Hexagonal Reentrant Phase Transition in Dioleoylphosphatidylethanolamine, *Biophysical Journal.*67, (1994)1603-1611.

[18] R. Lipowsky, D. Richter, K. Kremer, The Structure and Conformation of Amphiphilic Membranes *Springer*(1992)263.

[19] Corinna Thom, David C. Gilley, Judith Hooper, Harald E. Esch, The Scent of the Waggle Dance, *PLoS Biology.*5, (2007)e228.

[20] `http://www.chemicalbook.com/ChemicalProductProperty_DE_CB0689773.htm`

[21] `http://goldbook.iupac.org/A00296.html`

[22] Fahy, Eoin et al. “Update of the LIPID MAPS Comprehensive Classification System for Lipids.” Journal of Lipid Research 50.Suppl (2009): S9–S14. PMC. Web. 13 Nov. 2015.

[23] Subramaniam, Shankar et al. "Bioinformatics and Systems Biology of the Lipidome." Chemical Reviews 111.10 (2011): 6452–6490. PMC. Web. 13 Nov. 2015.

[24] A:A: Rieder, D: Koller, K. Lohner and G. Pabst, Optimizing rapid solvent exchange preparation of multilamellar vesicles, *Chemistry and Physics of Lipids.*186 (2015)39-44.

[25] Gottlieb, Hugo E., Vadim Kotlyar, and Abraham Nudelman. NMR chemical shifts of common laboratory solvents as trace impurities, *The Journal of organic chemistry.*62.21 (1997)7512-7515.

[26] `https://www2.chemistry.msu.edu/faculty/reusch/VirtTxtJml/Spectrpy/nmr/nmr1.htm`

[27] Ole G. Mouritsen, Life as a matter of fat the emerging science of lipidomics*Springer*(2005)

[28] `http://homepage.smc.edu/wissmann_paul/anatomy2textbook/phospholipids.html`

[29] G.P. Moss, P.A.S. Smith and D. Tavernier, GLOSSARY OF CLASS NAMES OF ORGANIC COMPOUNDS AND REACTIVE INTERMEDIATES BASED ON STRUCTURE,*Pure and App.Chem.*67,(1995)1307-1375.

[30] Jeffrey T. Buboltz, Gerald W. Feigenson, A novel strategy for the preparation of liposomes: rapid solvent exchange,*Biochimica et Biophysica Acta.*1417, (1999)232-245.

[31] Jeffrey T. Buboltz, A more efficient device for preparing model-membrane liposomes by the rapid solvent exchange method,*REVIEW OF SCIENTIFIC INSTRUMENTS.*80, (2009).

[32] `http://www.cheric.org/research/kdb/hcprop/cmpsrch.php`

[33] Alexander Rieder, Aufbau und Optimierung einer Rapid Solvent Exchange Apparatur zur Herstellung künstlicher Zellmembranen, *Graz University of Technology*(2014).

[34] Yaghmur Anan, Peter Laggner, Shuguang Zhang, Michael Rappolt, Tuning curvature and stability of monoolein bilayers by designer lipid-like peptide surfactants, *PLoS One*2, (2007)e479.

[35] G.S. Attard, J.C. Glyde, C.G. Goltner, Liquid crystalline phases as templates for the synthesis of mesoporous silica, *Nature*378, (1995)366–368.

[36] *Šá*rka Perutkov*á*, Matej Daniel, Gregor Dolinar, Michael Rappolt, Veronika Kralj-Igli*ć* and Aleš Igli*č*, Stability of the Inverted Hexagonal Phase. In A. Leitmannova Liu and H.T. Tien, editors: Advances in Planar Lipid Bilayers and Liposomes, Vol. 9, Burlington: Academic Press, (2009), pp. 237-278.

[37] *Šá*rka Perutkov*á*, Matej Daniel, Michael Rappolt, Georg Pabst, Gregor Dolinar, Veronika Kralj-Igli*č* e and Aleš Igli*č*, Elastic deformations in hexagonal phases studied by small-angle X-ray diffraction and simulations, *Phys. Chem. Chem. Phys.*13, (2011)3100–3107.

[38] M. Rappolt, The biologically relevant lipid mesophases as "seen" by X-rays, *Adv. Planar Lipid Bilayer and Liposomes.*5, (2006)253–283.

[39] M. M. Kozlov and M. Winterhalter, Elastic moduli and neutral surface for strongly curved monolayers. Analysis of experimental results, *Journal de Physique II*1.9, (1991)1085–1100.

[40] Thomas Heimburgk, Thermal Biophysics of Membranes, *Wiley-VCH Verlag GmbH und Co. KGaA, Copenhagen*, (2007).

[41] B. E. Warren, X-ray diffraction, *Reading, Mass.: Addison-Wesley Pub. Co.*, (1969).

[42] T. Mareš, M. Daniel, Š. Perutkova, A. Perne, G. Dolinar, A. Igli*č*, M. Rappolt, V. Kralj-Igli*č*, Role of phospholipid asymmetry in the stability of inverted hexagonal mesoscopic phases, *J. Phys. Chem. B.*8, (2008)16575–16584.

[43] S. M. Gruner, V. A. Parsegian and R. P. Rand, Faraday Discuss., (1986), 81, 29–37.

[44] M. W. Tate and S. M. Gruner, Biochemistry, 1989, 28, 4245– 4253.

[45] R. P. Rand, N. L. Fuller, S. M. Gruner and V. A. Parsegian, Biochemistry, 1990, 29, 76–87.

[46] Heimo Schnablegger, Yashveer Singh, The SAXS Guide (Getting acquainted with the principles), 3rd Edition,*Anton Paar GmbH.* June(2013).

[47] SAXSess mc^2 (The Modular Tool for Nanostructure Analysis), *Anton Paar GmbH*.

[48] Lecture in solid state chemistry (X-ray poder diffraction II peak intensities)https://chemistry.osu.edu/~woodward/ch754/lect2003/xrd_peakintensities.pdf

[49] Pr. Em. Charles Kappenstein, POWDER X-RAY DIFFRACTION II – DIFFRACTION ,LACCO, Laboratoire de Catalyse en Chimie Organique, Poitiers, France, http://www.gsc.dicp.ac.cn/down/jx/2011/2011.5.23/2-Diffraction-A.pdf

[50] Tony Phillips, X-ray Crystallography and the Fourier Transform, Stony Brook University, http://www.ams.org/samplings/feature-column/fc-2011-10

[51] http://fourier.eng.hmc.edu/e101/lectures/Image_Processing/node6.html

[52] S. May and A. Ben-Shaul, Spontaneous curvature and thermodynamic stability of mixed amphiphilic layers,*J. Chem. Phys. 103.9*, (1995)3839.

[53] http://www.echelon-inc.com/index.php?module=Products&func=detail&id=787

[54] Jeffrey T. Buboltz, Charles Bwalya, Krystle Williams, and Matthew Schutzer, High-Resolution Mapping of Phase Behavior in a Ternary Lipid Mixture: Do Lipid-Raft Phase Boundaries Depend on the Sample Preparation Procedure?, *Langmuir*.23,(2007) 11968-11971.

Appendix